ROUTE TO DRY OUT FROM ANNULAR FLOW BY APPLICATION OF EXTERNAL HEAT SUPPLY

A DISSERTATION

Submitted in partial fulfilment of the
requirements for the award of degree
of
MASTER OF TECHNOLOGY
in
MECHANICAL ENGINEERING
(With specialization in Thermal Engineering)

By

AVIK SAHA

DEPARTMENT OF MECHANICAL & INDUSTRIAL ENGINEERING
INDIAN INSTITUTE OF TECHNOLOGY ROORKEE
ROORKEE, UTTARAKHAND, INDIA-247667

JUNE, 2019

CANDIDATE'S DECLARATION

I hereby declare that the work carried out in this dissertation entitled, **"ROUTE TO DRY OUT FROM ANNULAR FLOW BY APPLICATION OF EXTERNAL HEAT SUPPLY"** is presented on behalf of partial fulfilment of the requirements for the award of degree of "Master of Technology" in Mechanical Engineering with specialization in Thermal Engineering submitted to the Department of Mechanical and Industrial Engineering, Indian Institute of Technology Roorkee (India), is an authentic record of my own work carried out under the supervision of **Dr. Arup Kumar Das,** Assistant Professor, MIED, IIT Roorkee.

I have not submitted the record embodied in this dissertation report for the award of any other degree or diploma in any other institute.

Date:
Place: IIT Roorkee **(AVIK SAHA)**

CERTIFICATE

This is to certify that the above statement made by candidate is correct to the best of my knowledge and belief.

Date:
Place: IIT Roorkee

Dr. Arup Kumar Das
Assistant Professor
Department of Mechanical and Industrial Engineering
IIT Roorkee

Dedicated to

My Mentor

&

My Parents

ACKNOWLEDGEMENTS

Firstly, I want to thank my supervisor, **Dr. Arup Kumar Das**, Assistant Professor, Mechanical and Industrial Engineering Department, IIT Roorkee. The door to Prof. Das office was always open whenever I ran into a trouble spot or had a question about my research or writing. His passion for science and enthusiasm toward exploration of new physics inspired me a lot throughout the journey. This work would have been impossible without his constant guidance, support and valuable suggestions for making this progress report.

I would also take this opportunity to thank Dr. Ranjan Ganguly, Professor, Department of Power Engineering, Jadavpur University for introducing me to this beautiful world of research, at the time of my graduation. His inspiration later on motivated me for higher study and research.

Also, I am really thankful to my parents. Without their persistent support and encouragement this journey would not have been impossible. I am also thankful to my friends Mr. Saikat Ray, Mr. Tanmoy Moulik, Mr. Joy Ghosh and others for being there and provide me self-belief and courage for this journey.

It has been a great pleasure for me to work in the Two-phase flow and instability laboratory for last one and half years. I really enjoyed the laboratory environment and my interactions with my seniors and colleagues. I would like to thank Dr. Pramod Kumar, Mr. Shadman Hasan Khan and Mr. Digvijay Kumar Singh for their valuable assistance, which smoothened my initial learning phase and allowed me quickly dip into the research work. Also, I express my gratitude toward Mr. Liril D Silvi and Mr. Chandan Swaroop Meena for their assistance in my project work. I am also thankful to the other members of our lab, Mr. Lokesh Rohilla, Mr Darshan Mb, Mr. Vikas Kannojiya, Mr.Rupak Kumar, Mr Prashant Kumar, Mr Mihir Prajapati for their support.

At last but not the least I would like to thank IIT Roorkee and MHRD, India for providing me financial support and other resources which are required to carry on my study.

Date:

Place: IIT Roorkee

Avik Saha

M. Tech (Thermal Engineering)

Enrolment no. 17541005

MIED, IIT Roorkee

ABSTRACT

Numerical study of boiling has been performed around wire and also for internal annular flow inside a pipe in three-dimensional domain with the help of fixed mesh, incompressible, Volume of Fluid solver.

First, to understand the basics of film boiling in presence of external heat supply in the present study pool boiling around a heated wire has been simulated at atmospheric pressure, considering the wire to be at the constant temperature heat source. Film dynamics, bubble nucleation, growth, merging and pinch off has been observed around perfectly smooth and uniform horizontal wire without any nucleation site. Effect of increase of the degree of superheat on boiling rate, measured in terms of vapour generation and bubble population has been studied, next. Similar studies have been made by inclining the wire at different angles (10°, 45°, 60° and vertical), where axial and azimuthal bubble sliding and more efficient bubble merging have been observed. Bubble size and population distribution have been investigated along the length of the inclined wire to link up with corresponding enhancement in boiling rate. For understanding the effect of active and passive neighbour, horizontal boiling around two-wire system has been studied. First horizontal wires have been stacked at the same vertical plane and then different active and passive combination have been simulated. Also boiling from two active wires placed at same horizontal plane has been studied for different wire spacings. For all these cases bubble life cycle has been investigated to understand the role of neighbouring wire. Effect of these neighbouring wires on boiling heat transfer and vapour generation rate has been reported. Ideas of bubble-bubble interaction will be quite helpful for understanding the route cause behind annular flow dryout. Taking queue from the previous effort, an annular flow boiling inside a tube has been also targeted as the next part of this study. Complex interfacial interactions like bubble nucleation, growth and merging underlying the liquid film has been studied beneath the liquid film of annular flow. Simultaneously wave generation, its subsequent deformation and entrainment in between the liquid film and vapor core has been obtained. Bubble bursting and rewetting of the pipe wall has been modelled with care. Due to boiling and bubble bursting liquid film is distorted into lamella and finally dry out has been observed. Azimuthal distribution of

liquid film, bubbles and entrained liquid has also been presented in the cross-sectional view of the pipe at different axial location and temporal instants. Further effect of wall superheat, liquid and vapor velocities on the film evolution and dry out length has been clearly depicted. Dynamics of wavy film has been represented in terms of attractor plot of liquid phase fraction at different axial locations, which gives a better idea about the effect of parametric variations. Finally, axial variation of heat transfer coefficient for different cases has also been compared.

Keywords: Boiling, Merging, Sliding, Annular flow, Rewetting, Interfacial wave.

TABLE OF CONTENT

LIST OF FIGURES

LIST OF TABLES

NOMENCLATURE

C	Specific heat	J/kgK
D	Tube diameter	m
$\vec{g}$	Gravitational acceleration	m/s^2
H_{LG}	Enthalpy of vaporisation	J/kg
k	Thermal conductivity	W/mK
L	Tube length	m
$\dot{m}'''$	Volumetric rate of phase change (+ve for condensation and -ve for boiling)	m^3/s
p	Pressure	Pa
R	Universal gas constant	J/kgK
t	Time	s
T	Temperature field	K
$\vec{U}$	Velocity field	m/s
u	Velocity component	m/s
V	Volume of individual cell	m^3
$\dot{V}''$	Volume flux	m^3/s

Greek Letters

α_L	Liquid phase fraction	-
$\beta_{L,x,t}$	Non-dimensionalised liquid phase fraction with respect to inlet liquid phase	-
κ	Interface curvature	m^{-1}
ρ	Density	kg/m^3
σ	Surface tension	N/m
μ	Viscosity	Ns/m^2

Subscript

b	Boiling
L	Liquid
G	Gas
sat	Saturation

CHAPTER 1 INTRODUCTION

1.1 Preface

Boiling is a highly energy-intensive phenomenon through which heat can be transferred with minimum temperature difference. Due to high heat transfer coefficient, it is one of the prime modes of energy transfer process in power and refrigeration industry where huge amount of heat needs to be dissipated. More recently with development of electronics industry requirement of more effective cooling is in depend and that is pushing electronic industry toward boiling heat transfer. Not only due to its high demand in application, boiling has attracted attention of researchers due to its enriched underlying physics. It is a combination of different complex physical phenomena like fluid mechanics, heat transfer, phase change, two-phase flow and bubble dynamics. Interrelation of all these knowledge sectors makes the whole phenomenon of boiling a more complicated one. Boiling can be observed either by heating the liquid above saturation temperature or by reducing saturation temperature by means of lowering the pressure. Boiling can be classified into two types based on fluidic dynamics namely as pool and flow type.

1.2 Pool Boiling

Pool boiling is the fundamental type of boiling where a stagnant pool of liquid is heated from some solid surface above saturation temperature to initiate phase change. Nukiyama (1966) have identified different regimes of pool boiling based on wall degree of superheat and heat flux. As one can see in Figure 1 there are three major boiling regimes based on interfacial dynamics namely, nucleate, transition and film. For initiation of boiling a small degree of superheat is required, which is known as onset of boiling (point A in Figure 1). Below this degree of super heat only natural convection and evaporation from the interface occurs. Once degree of super heat crosses onset of nucleate boiling, bubble formation on the heated surface starts. In this regimes vapor bubbles are generated from different pores and cavities of the heated

surface, which are more commonly known as nucleation sites. In this stage of boiling, liquid remains in contact with heated surface as bubbles are generated from individual sites only. So, liquid having higher thermal conductivity can readily absorb the heat from the surface and lead to better heat transfer characteristics. But beyond certain heat flux, a continuous film is generated above the surface and bubbles are formed out of that vapour film due to instabilities. This vapor film inhibits heat transfer from the heating surface and as a result sharp rise of temperature has been observed. This is known as film boiling. The maximum heat flux that can be achieved before film formation is called critical heat flux (point C). From point C if we try to increase heat flux further it directly shifts to point E and temperature reaches over metallographic limit of boiling surfaces in majority of applications. On the other hand, in careful lab scale experiment, if heat flux is reduced from the point E then it follows DE path in boiling curve and reaches up to point D to achieve minimum heat flux which is commonly known as Leiden frost point. If heat is further reduced it will shift to nucleate regime directly. In heat flux-controlled experiment CD path of the boiling curve, which is known as transition boiling, cannot be achieved. Only in temperature-controlled experiment by increasing superheat from Point C, one will follow path CD and reach point D, in the boiling curve.

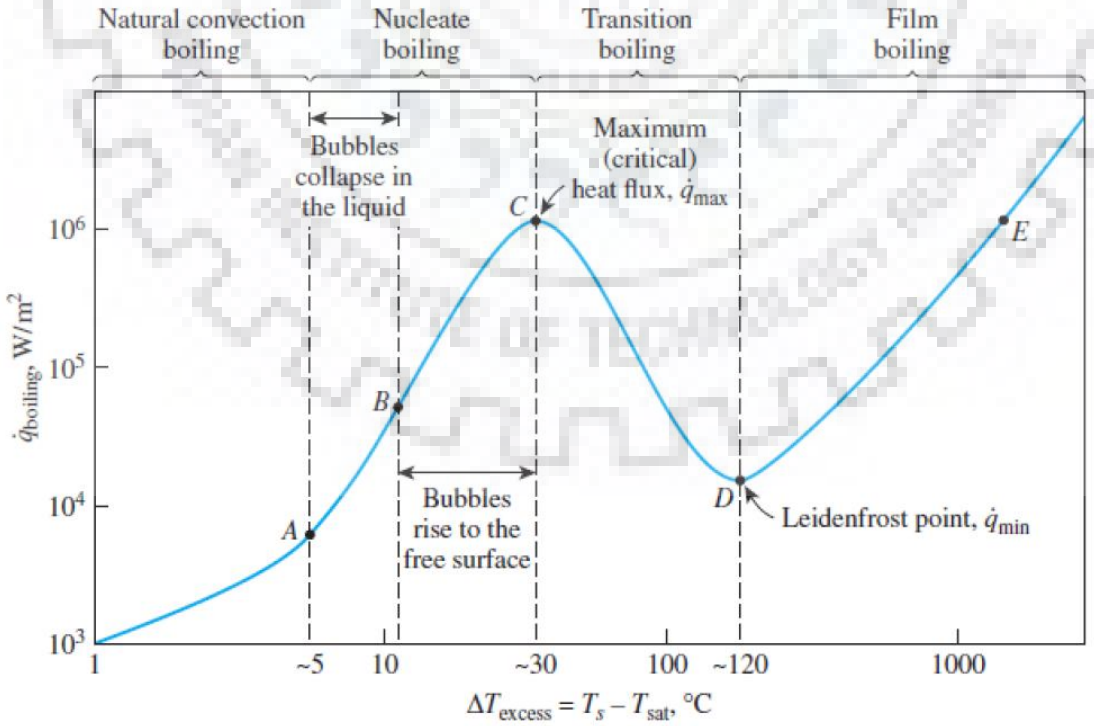

Figure 1.1: Different regimes of pool boiling in boiling curve

1.3 Flow Boiling

Flow boiling is much more complicated compared to pool boiling due to fluidic inertia. In pool boiling vapor generated from the heating surface can easily escape through the liquid pool by virtue of gravity only. But in case of flow boiling the generated vapor propagates along with the flow and its detachment from surface depends on many factors like interplay between inertia, gravity and surface tension. For this reason, in case of flow boiling along with heat flux and wall degree of superheat, phase faction becomes one key parameter. This third parameter converts the boiling curve to a complex boiling surface as we can see in Figure 2(a). Here if we can assume a cut-section of the surface at vapor quality = 0, then it will represent a pool boiling curve. As the quality increases the DNB point gradually comes down signifying reduction in critical heat flux value. For this reason, at higher quality the flow becomes more prone to shift toward liquid deficient regime or dry out even at lower heat flux. For this reason, to avoid dryout, proper understanding of different regimes of two-phase flow need to be studied.

Depending on the pattern of phase association, two-phase flows are classified into different flow regimes. This classification is mainly based on by visual observations depending upon the relative volume fraction of each phase and their distribution inside the pipe, carrying flow boiling. So, it can be difficult to specify with certainty, which regime, a particular flow belongs to. Still it is convenient to classify the various types of interface distribution observed in practice because flow regimes affect different utility parameters, such as pressure drop, rate of evaporation etc. These flow patterns are solely dependent on phase velocities and densities which need to be accurately measured in industrial applications.

Collier and Thome (1994) categorised different flow regimes of upward flow boiling into subcooled, nucleation, bubbly, slug, annular and mist as shown in Figure 1.2. At the bottom, one can see only liquid enters to the pipe. Then due to heating

liquid temperature as well as pipe wall temperature rises. As wall temperature crosses the saturation temperature boiling from the wall starts and they detach from the wall to form bubbly flow. Afterward the smaller bubbles coalesce to form bigger bubble, whose length is even bigger than the pipe diameter. This regime is known as slug flow. Thereafter as these slug bubbles grow further, they merge downstream to create a continuous space for vapour flow in the core of the pipe and at the pipe wall, there will be a liquid film. This regime is popularly known as annular flow. As the flow propagates from bubbly flow to annular flow through slug flow the wall temperature gradually comes down closer to the saturation temperature. But after annular flow the liquid film exhausts and some entrained liquid flow with the vapour flow leading to sharp rise of wall temperature. This flow is known as droplet flow or mist flow. So, we can say annular flow is having lowest possible wall temperature and highest heat transfer coefficient. Next, we discuss annular flow in details.

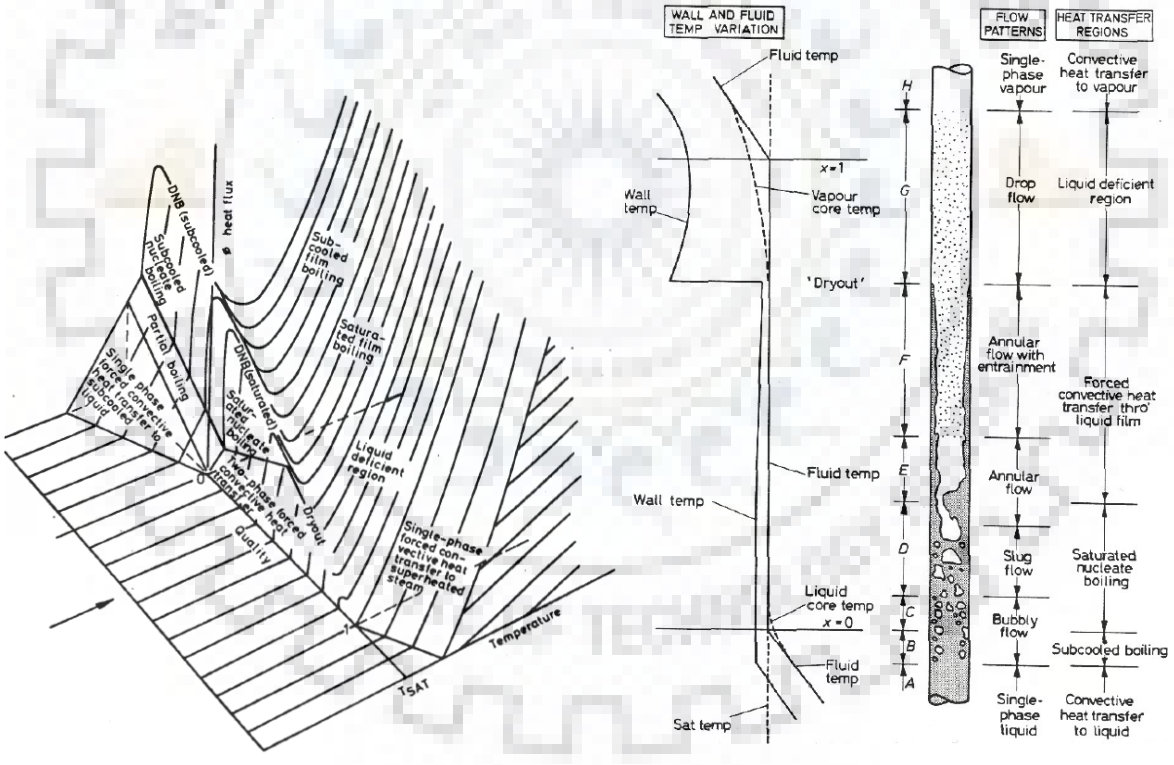

Figure 1.2: (a) Dependence of temperature, heat flux and quality in forced convective boiling, (b) Different flow regimes and heat transfer coefficient in upward flow boiling. (Collier and Thome ,1994)

1.4 Annular flow

The true volumetric gas concentration (void fraction) of the annular flow, ε_G, determined as a fraction of the cross section occupied by the gas phase, is high and, as a rule, exceeds 75-80%. In Figure 1.3, experimental observations at LTCM, EPFL has been shown for boiling channels which generated annular flow pattern. In part (a-d), one can clearly observe the thick liquid film at the periphery and gas core in co-flowing situation.

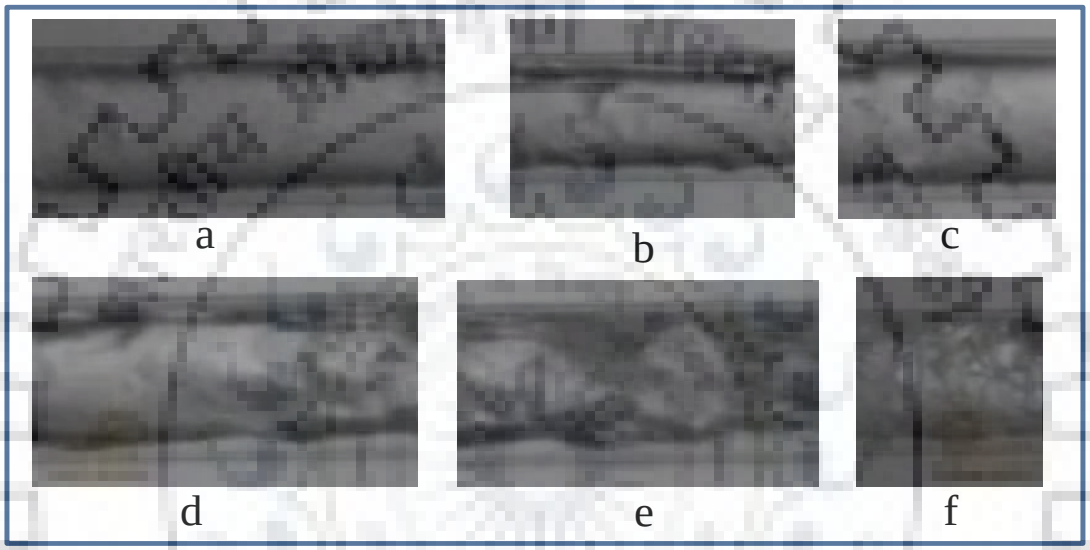

Figure 1.3: Annular and droplet flow in the horizontal channel with phase change (Courtesy: Prof. John Thome, EPFL, Switzerland)

The main objective of studying annular flow with the application of external heat transfer is to predict the dry out condition. In annular flow as the liquid film remains adhered with the cylindrical wall, it helps in cooling and controlling of the heater wall. As because the liquid is having a higher thermal conductivity, it readily absorbs and transfers the heat. But if this liquid film is somehow dried up then in absence of liquid, the wall cannot transfer heat efficiently and wall temperature rises abruptly. This phenomenon is known as dry out, which is extremely detrimental to the wall material. Post dry-out section of the pipe consists of vapor flow consolidated with liquid drops, which is formally known as mist flow. In this section pipe due to low conductivity the fluid becomes unable to absorb the heat efficiently as a result wall temperature rises drastically. This may lead to meltdown of the boiler in the

powerplant applications. Specifically, in case of nuclear reactor heat flux is very high. Hence such dry-out in Boiling water reactor (BWR) type nuclear reactor may lead to leakage of nuclear substance and serious nuclear hazard.

Mainly two reasons are responsible for this dry out phenomena.

i. Liquid entrainment into vapour core
ii. Boiling in the liquid film

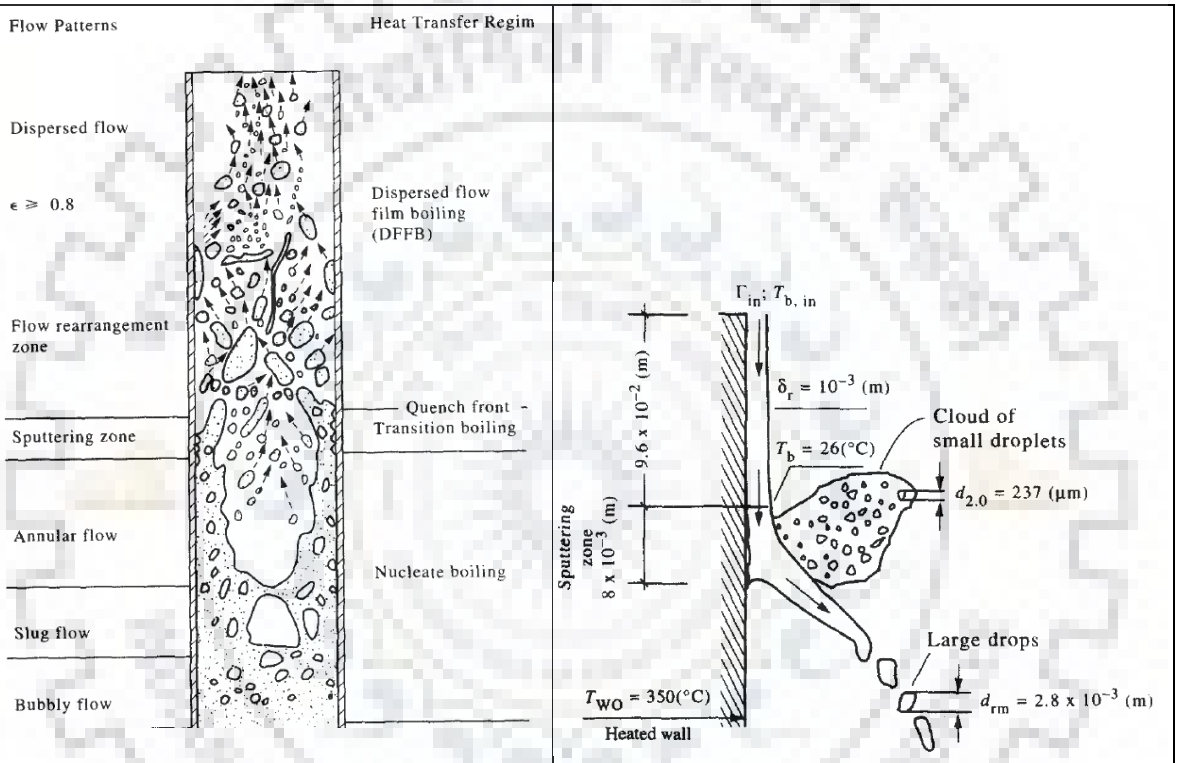

(a) Andreani et al. 1994 (b) Cumo et al. 1980

Figure 1.4: Schematic representation of sputtering process

Liquid entrainment itself is a multiphysics problem involving atomisation, droplet breakup, coalescence and deposition. Along with that addition of boiling makes the problem more complex and interesting. At the end of annular flow before the dry out a transition region is observed. At the end of this transition region, quench front is formed after which complete film dry out occurs. Dhir et al. (1979) showed that an oscillating foamy region existed about the quench front. Actually, here due to heating from the tube wall some small vapor bubbles are generated below the liquid film. These vapor bubbles flows with the liquid film and propagates along the length

of the tube. Some bubble merging is also observed, which allows the growth of the bubble further. Near the quench front the bubble becomes nearly comparable to film thickness and burst to be released. Due to this bubble bursting finer, liquid droplets are also generated. This is also known as sputtering. A schematic of the same is shown in Figure 1.4. In the next section, some literature related to bubble bubble interaction in boiling heat transfer is discussed before providing present status of knowledge of annular flow.

1.5 Literature Review

In this section, literatures related to annular flow boiling available in open domain has been categorised into two subsections. In first section some studies related to boiling heat transfer and bubble dynamics have been mentioned. Thereafter literature related to annular flow are discussed in next section.

1.5.2 Boiling

Boiling has also been studied by numerous researchers specially using experimental route both for pool and flow boiling. First major improvement in understanding in the field of boiling was made by the famous experiments of Shiro Nukiyama (1966). From his observation of boiling around the wire, he came up with a boiling curve representing the heat flux as a function of the degree of wall superheat. To elaborate different regimes of pool boiling around wires, he has pointed out bubble nucleation, its departure, and subsequent film formation. He identified the maximum heat flux of nucleate boiling while rising temperature and minimum temperature of film boiling while reducing the temperature as shown in figure 1.1. Later on, researchers tried performing boiling experiments on different types of wires and came up with specific boiling correlations (Rohsenow, 1951; Nishikawa and Yamagata, 1960; Zuber, 1963). Commensurate analytical models have also been proposed by different researchers (Tien, 1962; Haramura and Katto, 1983) for both nucleate and film boiling regime. Coexistence of nucleate and film boiling on a wire has been successfully investigated by Semeria and Martine (1965), Van Ouwerkerk (1972) and Lu and Lee (1989). Effect of microgravity on boiling modes around the heated wire is a major topic of research for years (Tokura et al., 1994; Shatto and Peterson, 1999; Di

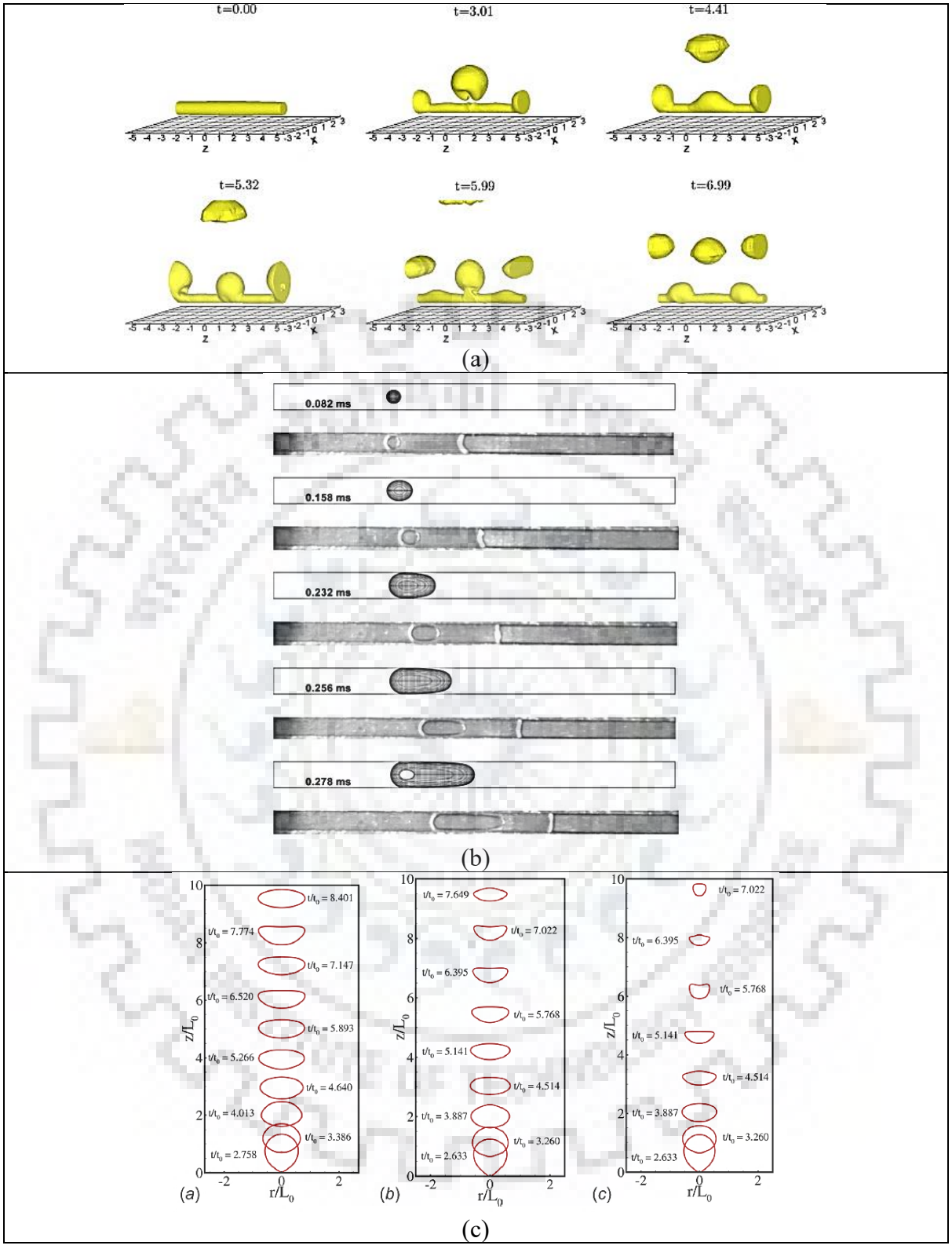

Figure 1.5: (a)Boiling around cylinder as presented by Son and Dhir, 2008 (b) Flow boiling in micro-channel (Mukherjee and Kandlikar, 2005) (c) Temporal evolution of bubble interface for different degree of subcooling as represented by Pandey et al. (2018)

Marco and Grassi, 2002). Pryazhnikov and Minakov (2017) even experimentally tried to understand the effect of nanofluid on boiling heat transfer around the wire.

Due to a sustainable increase in need of energy and process miniaturization, the primary focus of research nowadays hovers around the effort to increase the rate of energy transfer at a lower degree of superheat. Various augmentation techniques are hereby invented either through the imposition of the external force field (Das et al., 2007) or surface modifications (Das et al., 2009). Majority of these efforts are intuitive or only based on knowledge of bubble departure and liquid replenishment from an individual site. A thorough understanding of bubble dynamics around simple most boiling occurrence around a wire is still due which may throw some channelized guideline for augmentation of heat transfer coefficient. With advancement in nanotechnology in present days is to improve the heat transfer characteristics with nanostructured surface. Hendricks et al. (2010) has done pool boiling experiments with ZnO on copper and aluminium surface and reported 10 times better heat transfer characteristics with 4 times higher CHF.

The pioneering work in numerical simulation of boiling over a flat surface has been done by Son and Dhir (1997). They have shown bubble generation from the heated surface and merging of bubbles successfully in a two-dimensional domain (Figure 1.5a). They have also done three-dimensional simulations of film boiling on a horizontal cylinder (Son and Dhir, 2008). Flow boiling has also been tried numerically by various research. Mukherjee and Kandlikar (2005) has simulated the growth of a vapor bubble inside a micro channel during flow boiling numerically with level set method (Figure 1.5b). Recently Pandey et al. (2018) numerically simulated growth of a single bubble with a thin liquid microlayer evaporation model. They have also investigated the effect of liquid pool subcooling on growth of bubble before departure and also bubble dynamics after departure (Figure 1.5c). At higher subcooling, ceasing of bubble departure and oscillation of the bubbles has also been reported.

1.5.2 Annular Flow

Lots of research work have been done on annular flow on the numerical and experimental route. Amongst the preliminary works, Hewitt & Lacey, (1965) has conducted an experiment to find out the minimum liquid flow rate required for rewetting. In this experiment to observe film break down mechanism in vertical air-

water annular flow a compressed air jet is imparted in certain section of the film for some time duration and there after the jet is stopped and it is checked whether the film is able to rewet the dried section again or not. A schematic of their arrangement is shown in Figure 1.6 along with dry section. From this experiment they came up with a conclusion that minimum liquid flow rate required to re-establish the film decreases with higher gas velocity.

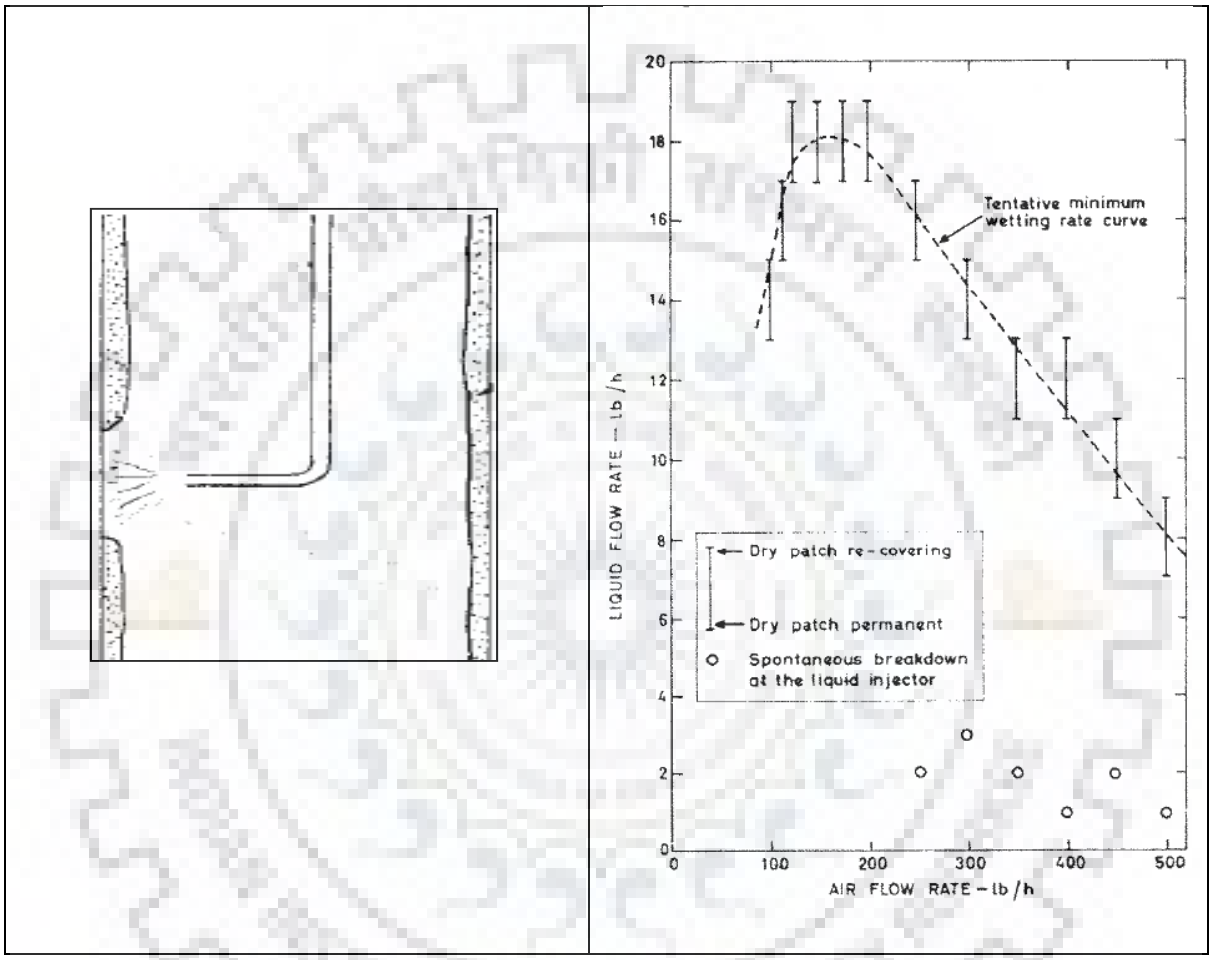

Figure 1.6: Dry out of liquid film by compressed air (Hewitt & Lacey, 1965)

Many researchers have tried flow boiling experimentally but in case of inside tube boiling visualising annular flow is not possible due to presence of heater section outside it. For this reason, Barbosa et al. (2003) has tried annular flow boiling outside tube where heater is placed inside tube. As one can see in Figure 1.7, Barbosa et al. (2003). has reported wave formation, liquid ligament formation and entrainment to gas similar to inside tube adiabatic annular flow. They have also pointed out bubbles to be nucleating beneath the disturbance wave. Similar type of nucleation beneath the disturbance wave has also been observed by Yang et al. (2017) numerically with the help of CFD tool TransAT.

Due to extreme complexities of boiling, in industries, to predict dry-out in flow boiling conditions empirical relations developed based on experiments, are being used (Tong, 2018). 1-D theoretical models FIDAS (Sugawara & Miyamoto, 1990, Sugawara et al. 1991), MONA-3 (Hoyer 1998), COBRA-TF (Glück M 2007), CATHARE-3 (Emonot et al. 2011, Valette et al. 2011), and VIPRE-W (Adamsson and Corre, 2011) are popular for dryout prediction, with incorporation of three fields, the vapor, the liquid film and the droplets separately. For annular flow, total energy theory has been explored previously (El-Genk and Saber, 2001) to predict the minimum stable film thickness, however, it is not valid in case of annular mist flow. But these empirical models do not take care of the hydrodynamics of the liquid gas flow directly, and do not explore heat transfer mechanism from the fundamental principle of phase change.

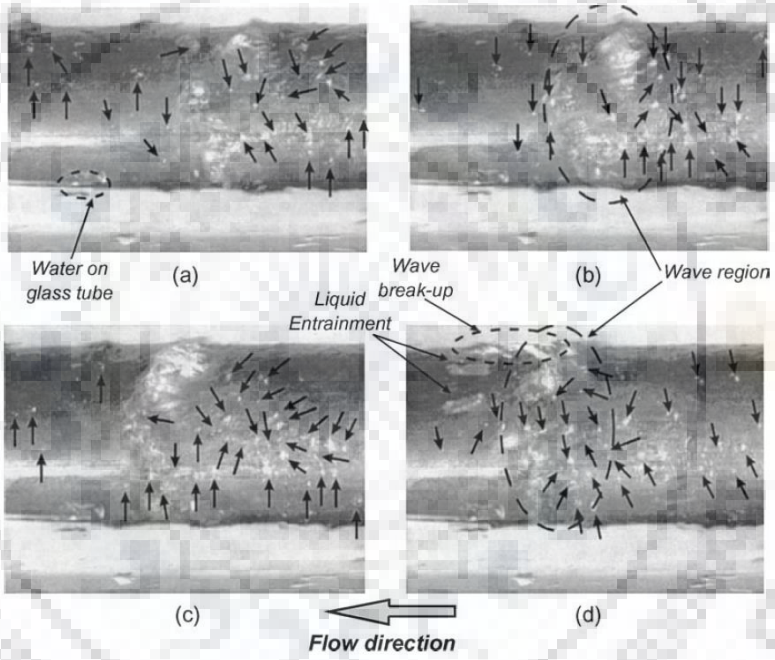

Figure 1.7: Experimental figure of outside tube annular flow boiling as reported by Barbosa et al. (2003)

Though lot of experimental work have been done on annular flow by different researchers but very few targeted for the numerical simulations in this domain. Kumar et al. (2016) have done numerical simulations to understand the physics behind the annular to droplet flow. For this reason, they have taken co-current, upward gas-liquid flow through a cylindrical tube and simulated using grid-based volume of fluid framework of Gerris. They have investigated all three droplet generation mechanisms namely, orificing, rolling and undercutting.

In case, where the gas and liquid velocities are nearly comparable, initially nearly symmetric type of waves are observed due to Kelvin Helmholtz instability. These waves grow radially to reduce the gas flow area, consequentially air velocity at that location rises. Due to this high air velocity, droplets shear off from the tip of the wave as shown in the Figure 1.8 (a). They have also reported that due to upward pull for gas velocity the waves become somewhat asymmetric and the tip of the wave shifts downward from the midpoint of the wave.

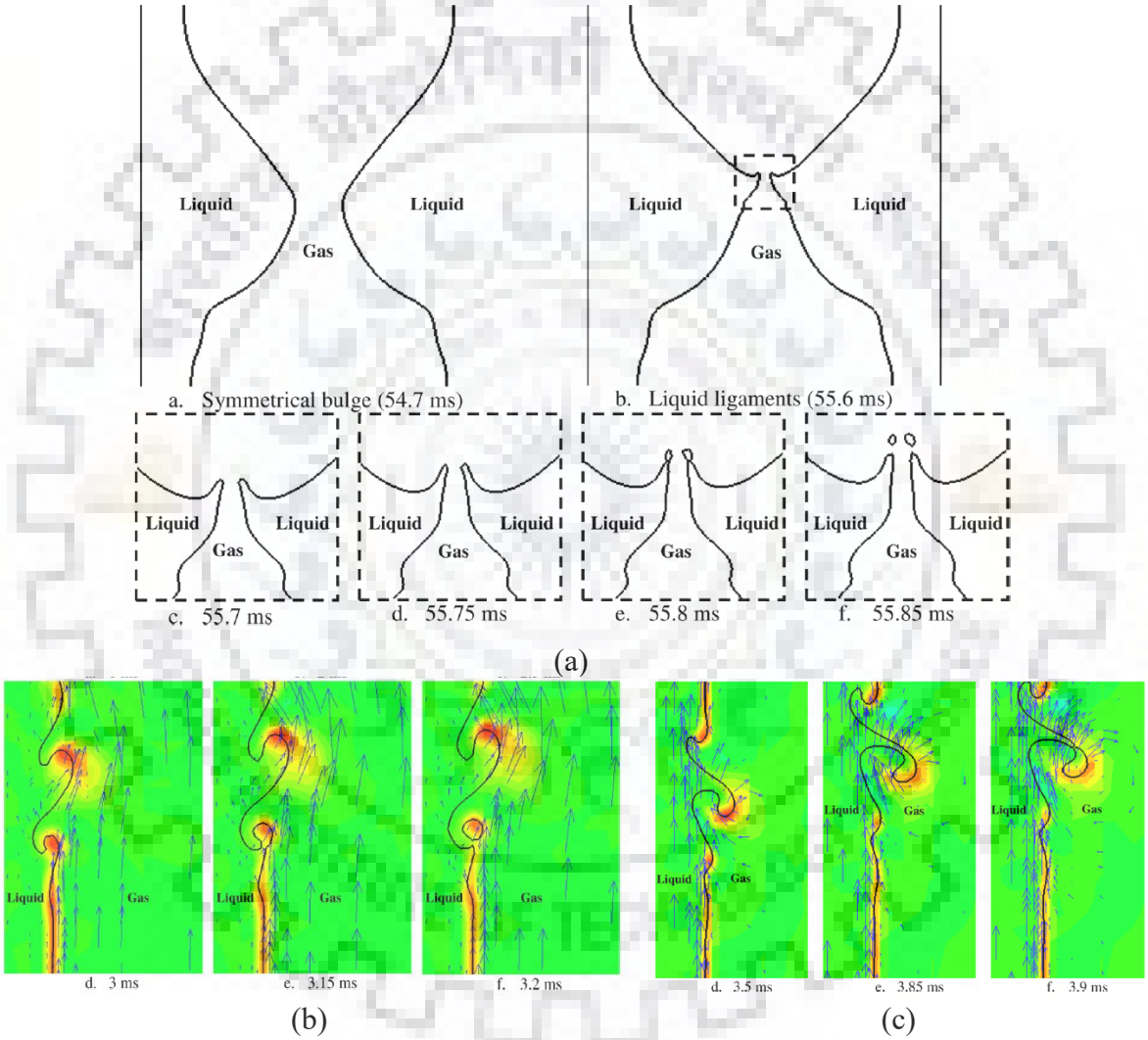

Figure 1.8: Entrainment from the annular film through (a) Orificing, (b) Rolling and (c) Undercutting (Kumar et al. 2016)

They have also observed rolling for higher gas velocity as compared to liquid. In this case as the wave tries to grow radially, due to higher air velocity, the waves bend toward direction of flow due to air drag. Subsequently, droplet shears off and gets carries out by the core air flow, as shown in the Figure 1.8 (b). In this case due

to radially outward circulation around the peak of the wave the probability of droplets deposition increases. On the other hand, in case of higher liquid velocity due to lower air inertia here, gravitational pull becomes dominant, which pulls the liquid bulge and as a result the wave bends opposite to flow direction. This leads to lamella formation from the liquid bulge. Air near to the liquid film attains high velocity due to drag of the liquid film. High velocity air near the liquid film creates strong circulation around the lamella causing elongation of lamella. Subsequently necking occur in the lamella and finally liquid drop dislodges from the liquid film. This whole phenomenon is called undercutting (Figure 1.8 (c)). Here, direction of the circulation is radially inward to the pipe. So, there is less chance for the dislodged lamella to be reattached to the liquid film.

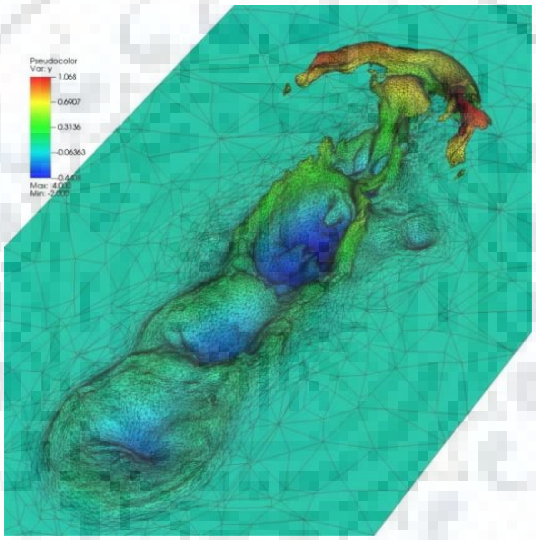

Figure 1.9: Interfacial deformation due to droplet impact on annular film as reported by Xie et al. (2017)

Recently Xie et al. (2017) numerically tried to investigate droplet deposition on annular two-phase flow. They have presented the complex interfacial deformation due to single droplet impact on the film as shown in the figure 1.9. Further liquid entrainment has been observed due to this deposition. Also, they concluded that the fluid properties are having significant contribution on the nature of interfacial structure.

1.6 Lacuna of the Literature:

From the literature reviews we can see that both annular flow and bubble-bubble interaction during boiling have been in the radar of the researchers for long

time but most of them are experimental. In last nine decades lots of works have been done on boiling. Still basic understanding of the boiling is pending due to its complexity and overlapping of different phenomena like bubble growth, merging, pinch off, rising. As boiling is a very fast and chaotic phenomena it's understanding from the experiments is quite difficult. Till date boiling has been handled numerically for very limited cases and that too for single nucleation site or single bubble. Son and Dhir (2008) has numerically simulated boiling around cylindrical surface with periodic boundary condition, but boiling from finite length wire is yet to be studied. Further effect of inclination of wire and interaction of neighbouring active or passive wire on the boiling are due from literature.

Actual mechanism of annular boiling is not well understood till date. Due to poor visualization of internal boiling, for better understanding of the interfacial features of annular boiling, it needs to be investigated numerically. Kumar et al. (2016) has studied adiabatic annular flow but annular flow boiling has not been targeted yet.

1.7 Objectives of the work:

Taking queue from the literature following objectives have been decided for the present study:

1.5.2 Wire Boiling

- Study of fundamental boiling heat transfer around wire geometry to observe nucleation, growth, sliding, merging and other complex interactions.
- To observe the effect of wire inclination on bubble generation and bubble population
- Study of effect of neighboring active and passive wires placed at different orientation on boiling and bubble dynamics

1.5.2 Internal Annular Boiling

- Numerical simulation of annular flow boiling targeting exploring reasons behind dryout and study the stages of annular to droplet flow transition.

- Understanding the effect of degree of superheat, liquid and vapor flow rate on the transition.

1.8 Organization of the thesis:

The whole thesis has been subdivided in 5 chapters. Brief content of each chapter has been given below:

Chapter 1: In the present chapter basics of boiling and literatures available in open domain about boiling and annular flow has been discussed. Also scope of the present study has been derived from the lacuna of the literature.

Chapter 2: Numerical methodology along with governing equations has been explained in this chapter.

Chapter 3: Results of horizontal and inclined wire boiling has been discussed next. Also wire boiling at presence of neighbouring active and passive wire has been studied.

Chapter 4: Results obtained from the study internal annular boiling has been discussed in chapter 4. Different stages of annular flow to dryout has been described. Effect of phase velocities and wall degree of superheat has been studied.

Chapter 5: In the last chapter significant findings from the study has been summarised and some future work has been proposed.

CHAPTER 2 NUMERICAL MODEL

To study boiling heat transfer around heated cylinder conservation of mass momentum and energy equations are modelled. For the prediction of the location of space and time-varying interface, the volume of fluid based methodology has been adopted. Here the two phases have been considered as incompressible and immiscible. For solution of the equations staggered grid structure has been utilised. But storage of all the field variable has been done with help of collocated grid structure to reduce storage complexity. For this reason, at the start of the iterations face values of the vector fields are calculated at the cell faces from the cell centred value. From there onward the face centred value of vector field and cell centred value of scalar fields are used for rest of the simulations. To simulate boiling numerically in the present study phaseChangeHeatFoam solver has been used with the help of OpenFOAM 2.2.0 libraries. This solver has been developed by Samkhaniani and Ansari (2017A&B).

2.1 Phase fraction continuity equation:

One set of conservation equation is used with a control over thermophysical properties by using information of phase fraction at a cell. Based on the formulation of one-fluid assumption global continuity equation can be written as:

$$\frac{\partial}{\partial t}(\rho) + \nabla.\left(\rho\vec{U}\right) = 0 \tag{2.1}$$

It is to be noted that phase change due to boiling will not include a source term in the global continuity equation. Mass transfer due to change of phase ($\dot{m}'''$) can be handled using transport equation of phase fraction, α_L. The phase fraction, bounded in between 0 and 1, can be defined in the domain as:

$$\alpha_L(\vec{x}, t) = \frac{V_{Liquid}}{V} \tag{2.2}$$

Generalized thermophysical properties (y) of two immiscible fluids such as viscosity (μ), density (ρ), thermal conductivity (k) and specific heats (C) are calculated using a phase fraction weighted average:

$$y = \alpha_L y_L + (1.0 - \alpha_L) y_G, \tag{2.3}$$

Now similarly replacing the density in the continuity equation 2.1 with the help of liquid and vapor phase density following form of phase fraction continuity equation can be obtained:

$$\frac{\partial \alpha_L}{\partial t} + \vec{U}.\nabla\alpha_L + \alpha_L \nabla.\vec{U} = -\frac{\rho_G \nabla.\vec{U}}{\rho_L - \rho_G} \tag{2.4}$$

For single phase incompressible system $\nabla.\vec{U} = 0$. But Considering phase change from the interface it can be shown that

$$\nabla.\vec{U} = \dot{m}'''\left(\frac{1}{\rho_L} - \frac{1}{\rho_G}\right) \tag{2.5}$$

Hence replacing $\nabla.\vec{U}$ in equation 2.4 α_L can be expressed as function of space and time its evolution, which can be linked up with mass transfer due to boiling as:

$$\frac{\partial \alpha_L}{\partial t} + \vec{U}.\nabla\alpha_L + \nabla.(\alpha_L(1-\alpha_L)\vec{U}_C) = -\dot{m}'''\left[\frac{1}{\rho_L} - \alpha_L\left(\frac{1}{\rho_L} - \frac{1}{\rho_G}\right)\right] \tag{2.6}$$

In the above equation one additional term can also be observed consisting of compressive velocity, $\vec{U}_C$. To avoid dispersion, in the normal direction to the interface, $\vec{U}_C$ can be written as:

$$\vec{U}_C = max|U|\,\frac{\nabla\alpha_L}{|\nabla\alpha_L|} \tag{2.7}$$

This compressive velocity being dependent on $\nabla\alpha_L$, it comes into account in the interface only, where α_L changes. In rest of the domain this term becomes zero and it doesn't influence the flow velocity.

To evaluate the thermodynamic value of $\dot{m}'''$, we took the phase change model as proposed by Tanasawa (1991). He proposed $\dot{m}'''$ at the liquid–vapour interface can be written as:

$$\dot{m}''' = 2\sqrt{\frac{1.0}{2\pi R}}\frac{\rho_G H_{LG}(T - T_{sat})}{T_{sat}^{3/2}}\nabla\alpha_L \tag{2.8}$$

where T_{Sat} is local saturation temperature at given pressure and H_{LG} is the latent heat necessary for boiling.

2.2 Momentum Equation

The balance of momentum in each cell accounting for the forces can be estimated as:

$$\frac{\partial(\rho\vec{U})}{\partial t} + \nabla.\left(\rho\vec{U}\vec{U}\right) - \nabla.\left(\mu\left(\nabla\vec{U}^T + \nabla\vec{U}\right)\right) = -\nabla p + \rho\vec{g} + \sigma\kappa\nabla\alpha_L \tag{2.9}$$

Incorporation of surface tension can be observed through the last term in the momentum equation which takes only non-zero value near the interface. Surface tension coefficient (σ) and interface curvature (κ) will dictate the magnitude of the surface force by following the continuum surface force model, proposed by Brackbill et al. (1992). The calculation of curvature at the interface is done from following equation:

$$\kappa = -\nabla.\left(\frac{\nabla\widetilde{\alpha_L}}{|\nabla\widetilde{\alpha_L}|}\right) \tag{2.10}$$

Where, $\widetilde{\alpha_L}$ is obtained by smoothing α_L locally to suppress spurious currents generated due to sharp change of α_L. This smoothening has been done as per Lafaurie et al. (1994)'s proposal, shown below

$$\widetilde{\alpha_{Lp}} = \frac{\sum_{f=1}^{n} \alpha_{Lf} S_f}{\sum_{f=1}^{n} S_f} \tag{2.11}$$

Here, n is the number of faces of the cell. f represents the face value and p represents the cell centred value. So, at first α_{Lf} is calculated at the face from linear interpolation of α_{Lp} of adjacent cells. After that smoothened $\widetilde{\alpha_{Lp}}$ is calculated as the average of all faces of the individual cells as shown in equation 2.7. This operation can be done multiple time to have a better smoothening. But if this smoothening is done more than twice changes becomes insignificant (Hoang et al. 2013). For this reason, in present study 2 iterations of smoothening has been applied.

By considering liquid and vapour as incompressible, the equation for pressure can be linked with mass conservation as:

$$\nabla.\left(\frac{1}{A_D}\nabla p\right) = \nabla.\dot{V}'' - \dot{m}'''\left(\frac{1}{\rho_G} - \frac{1}{\rho_L}\right) \tag{2.12}$$

A_D is the diagonal entries of the coefficient matrix of momentum equation (Weller et al. 1998) and $\dot{V}''$ is the volume fluxes through the cell faces.

2.3 Energy equation:

To extract the information of energy content in each cell, energy conservation equation is needed to be solved. The functional form of the equation can be written as:

$$\frac{\partial}{\partial t}(T) + \nabla.\left(\vec{U}\mathrm{T}\right) - \nabla.\left(\frac{k_L\alpha_L + k_G(1-\alpha_L)}{\rho_L C_L \alpha_L + \rho_G C_G (1-\alpha_L)}\nabla \mathrm{T}\right) = -\frac{1}{\rho_L C_L \alpha_L + \rho_G C_G (1-\alpha_L)}\dot{m}''' \times (\mathrm{H_{LG}} + (\mathrm{C_L} - \mathrm{C_G})\mathrm{T_{sat}}) \tag{2.13}$$

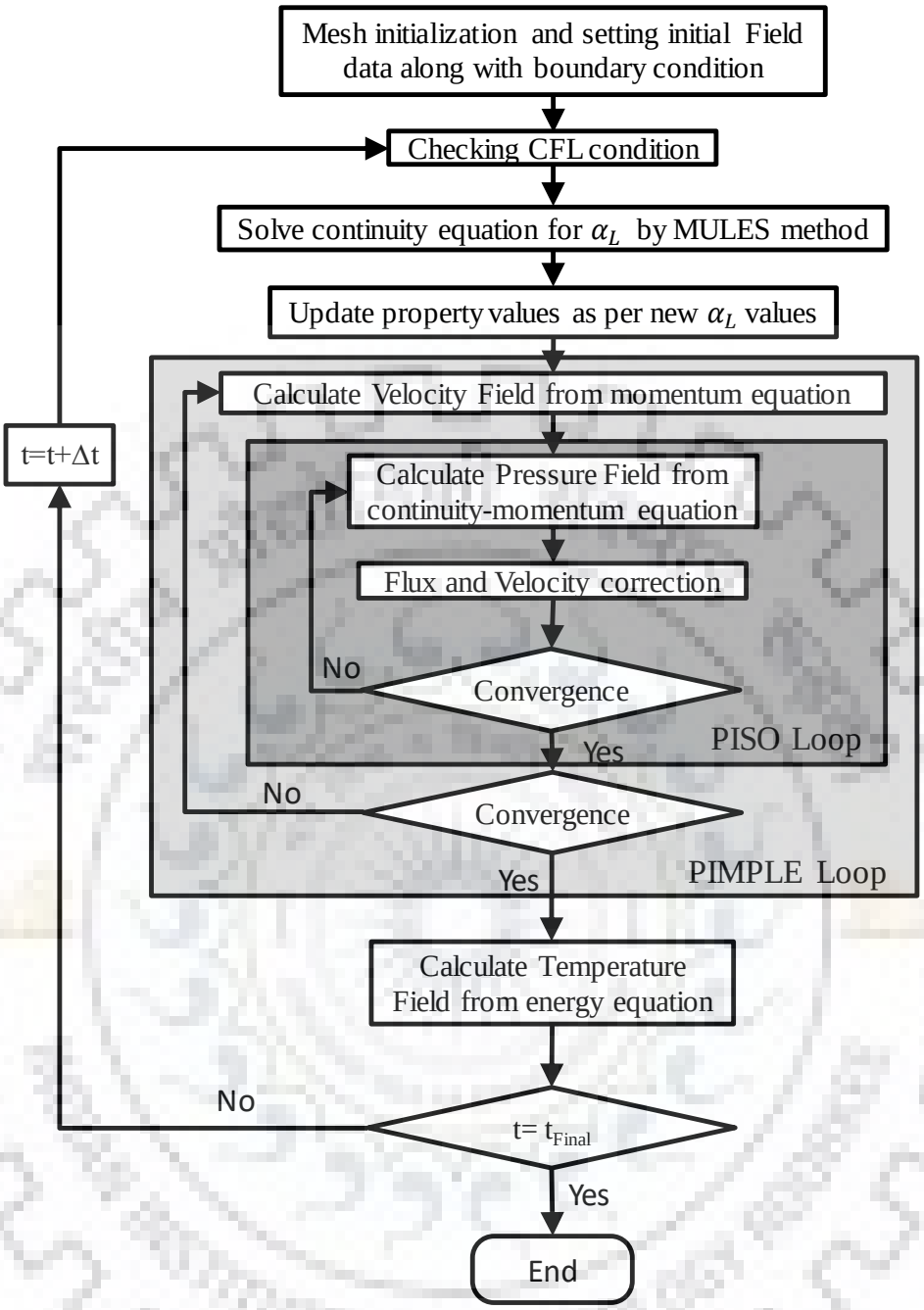

Figure 2.1: Flow chart of the mathematical model behind the solver

Here T_{sat} is the saturation temperature which is the function of the pressure. Though in the present study there is not much variation of pressure but locally there can be small pressure fluctuation. For this reason, correction of saturation temperature has been done with the help of following simplified version of Clausius–Clapeyron relation:

$$\ln\frac{p}{p_{sat}} = \frac{M \times H_{lg}}{R}\left(\frac{1}{T_{sat}} - \frac{1}{T_{sat^0}}\right) \tag{2.9}$$

Here T_{sat^0} represents global saturation temperature and T_{sat} is the local one, which is calculated from this equation. Also, p_{sat} is the global saturation pressure corresponding to T_{sat^0} and p is the local pressure.

2.4 Solver algorithm

The algorithm of the solver can be summarized as follows.

(a) Initialization of the mesh and loading the initial and boundary field data.

(b) Start of main solver loop with the check of CFL condition and modification of time step if required.

(c) The discretized volume fraction is solved from equation 2.3 using the MULES method (Multidimensional Universal Limiter with Explicit Solver) and accordingly, all the property values are updated as per equation 2.10.

(d) Then the solver enters the PIMPLE loop (Ong et al. 2011), which is actually merged PISO (Pressure Implicit with Splitting of Operators) and SIMPLE (Semi Implicit Method for Pressure Linked Equations) algorithm, to solve equation 6 and equation of state 2.8, where pressure and velocity fields are corrected in a number of iterations.

(e) Finally, energy conservation equation 2.8 is solved to obtain the temperature field.

In the figure 2.1 working of the solver has been described with a sequential flowchart for ease of understanding.

CHAPTER 3 WIRE BOILING

3.1 Domain description:

Present effort studies boiling around a heated wire in a domain 110 (L) mm × 20 mm (W) × 50 mm (H) space as shown in Figure 3.1. A wire of diameter 2 mm and length of 100 mm is placed in the domain at a height of 10 mm from the bottom surface. Initially, the whole domain except wire is considered to be filled with water having a 373 K temperature (Saturated liquid at 1 bar) and the wire surface temperature is kept constant at 10 K superheat. A thin vapour film of 0.5 mm thickness around the wire is initiated to avoid singularity during phase change. Pressure and temperature of the vapour film are kept the same as it has been described for liquid water.

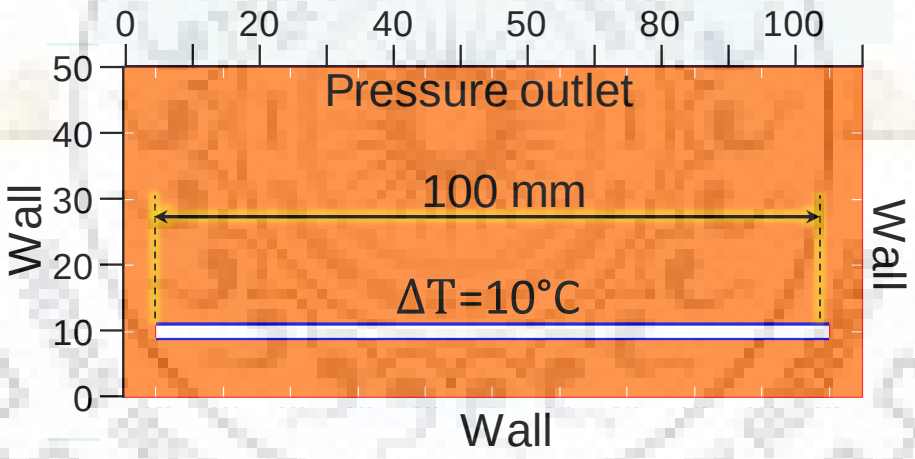

Figure 3.1 Domain description and boundary conditions

For the simulation, a rectangular domain has been selected around wire(s), as per requirement of the situations studied. Care has been given to avoid boundary influence by choosing proper domain size. No-slip boundary condition has been applied at the periphery of wire and external boundaries of the domain are set to pressure outflow type, for easy removal of produced vapour. To evaluate the fields and study vapor dynamics, the domain has been discretised in hexagonal cells. No restriction has been put on the maximum temperature of vapour bubble. During up rise

after departure, bubble will equilibrate its thermal energy by interacting with saturated liquid pool.

3.2 Grid independence and Validation:

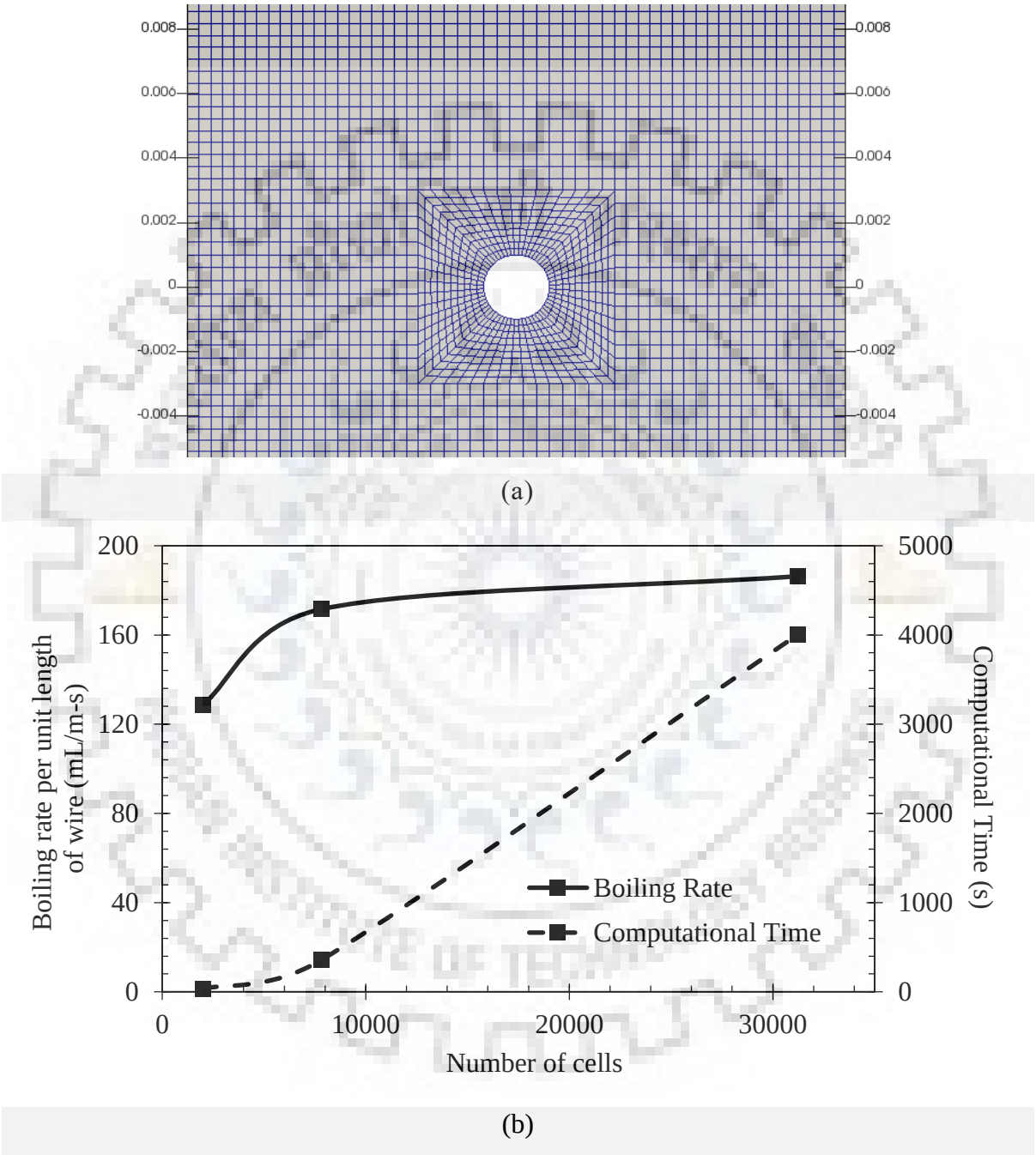

Figure 3.2 (a) Mesh structure around the wire, (b) Grid Independence Study; Optimum mesh size has been chosen as 0.1 mm.

Grid independence study has been performed before choosing suitable mesh size for the simulations. Encrypts of the study is reported in Figure 3.2 (b). Optimum

cell size has been chosen as 0.1 mm (~8000 cells in the domain) after thorough analysis of mesh independence, checked in terms of extent of vapour generation or boiling rate. Above the reported optimum size, reduction in mesh size results in marginal improvement in accuracy at the cost of ~8 times computational effort. In Figure 3.2 (a) mesh structure around the wire has been shown for the selected optimum mesh size.

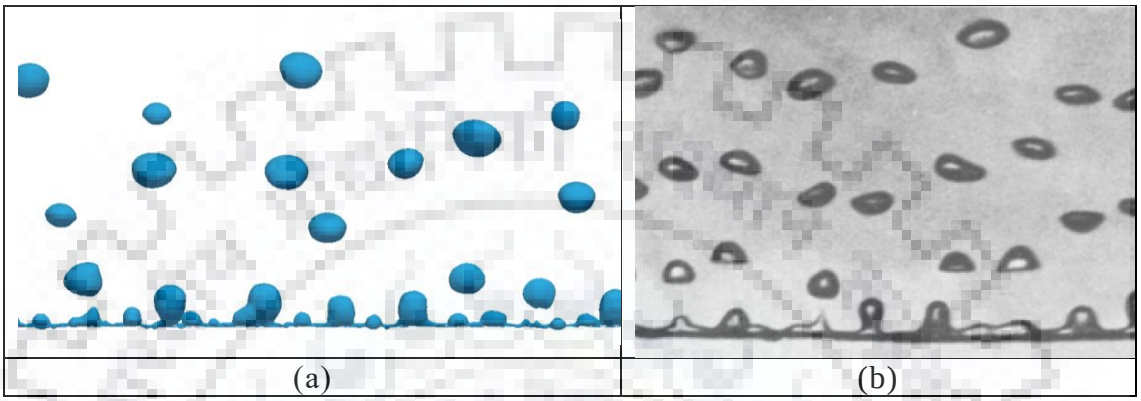

Figure 3.3 Qualitative validation of (a) present numerical simulation with (b) photographic observation of Reimann and Grigull (1975)

Numerical set up and considered grid structure has been validated with similar experimental observations. In Figure 3.3 bubble formation and its population from numerical simulation has been compared with experimental observations of Reimann and Grigull (1975). A good match in number of nucleation size and bubble release pattern between experimental observations and present numerical simulations shows consistency of developed model. Next section, describes the domain of the simulations performed.

3.3 Results and discussion:

3.3.1 Horizontal Wire Boiling:

Overall phase change phenomenon around the heated wire has been demonstrated as obtained from the numerical simulation using a phase contour of α_L = 0.5 in Figure 3.4. It has been observed that at the beginning film grows radially due to boiling around the wire (0.025 s) and it tries to contract longitudinally by virtue of surface tension to form a bulge at both the ends (0.035 s), as shown in Figure 3.4. This growth subsequently leads towards the nucleation of the first bubble from the corners

(0.055 s). Subsequently, the film gets destabilized and shows a wave-like pattern in the periphery as a result of Rayleigh-Taylor instability generated due to density difference between vapor and heavier liquid, present above it. At the peak of the wave, the growth of the film continues to produce nucleation sites for the bubble departure. Around 10-12 nucleation sites are observed along the length (100 mm) of the wire (0.15 s). Nucleation and pinch off of the bubbles from different parts of the film around heated wire continue randomly which creates a bubble population over the wire. These bubbles show their own dynamics, interface reorientation and wobbling up climb motion due to buoyancies.

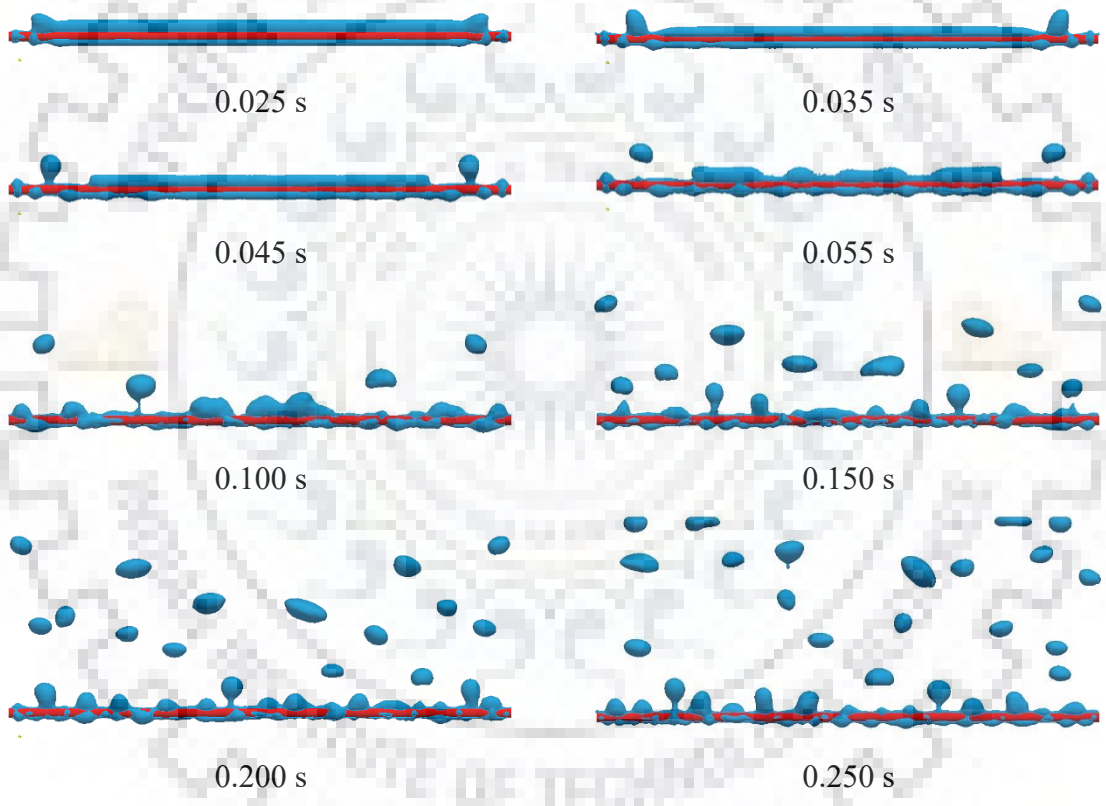

Figure 3.4: Temporal progress of boiling phenomenon around heated wire; film growth, nucleation, pinch off and the free rise of the bubble

To understand the transformation of film around the wire to nucleation in the form of a bubble, in Figure 3.5, phase contour of $\alpha_L < 0.5$ have been plotted on a sectional plane. It can be observed from Figure 3.5 that initially the film is not azimuthally symmetric. Starting from the very thin film at the bottom, film thickness gradually increases as one move azimuthally toward the top of the wire and it is

thickest at the topmost point (0.04 s). Initially, film cross-section remains nearly circular due to azimuthally homogeneous boiling rate, but as film thickens, buoyancy dominates, further interface becomes oval (0.05 s). Once film grows beyond certain thickness it starts collecting vapour mass above the wire and grow faster (0.06-0.07 s) to produce a bubble-like shape. During this time the vapour bubble mostly grows in height. Afterwards, vapour mass supply from azimuthally asymmetric interconnected film diminishes but due to inertia effect bubble top keeps moving at same speed. After growing up to a critical diameter, formation of neck starts, immediately over the wire (0.07 s). It continues for a while and creates a nucleation like bubble over the heated wire (0.09 s). In this process, the necking plane gradually moves up. Also, one can observe a vapour stem at the bottom of the nucleation like vapour mass. Apart from

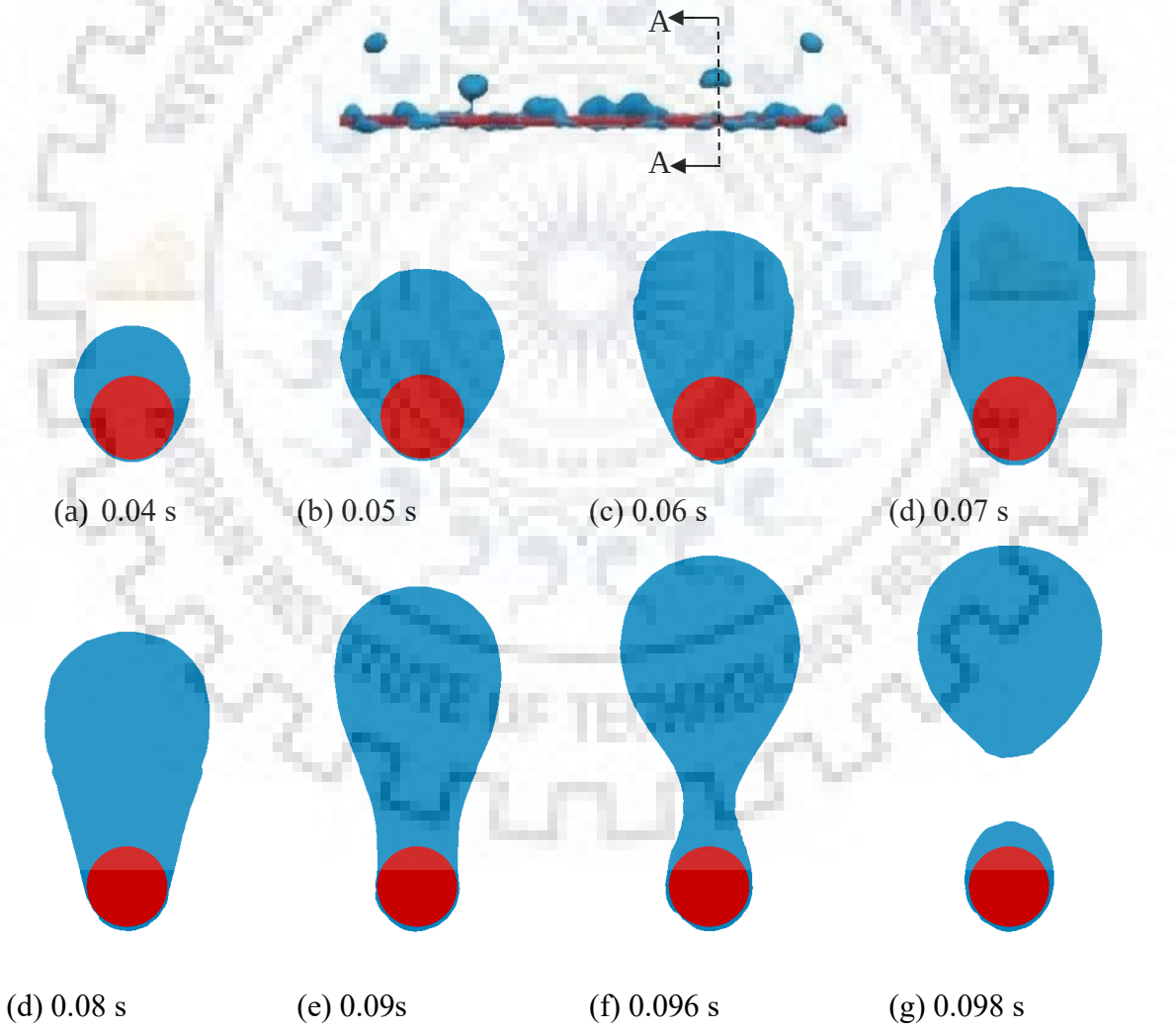

Figure 3.5: Sectional view of Bubble Cycle at section plane A-A

the vapour column, connecting bubble on top, the film around the wire gets more or less azimuthally symmetric at this stage (0.096 s). The vapour column elongates and due to interfacial instability pinches off a bubble above the wire (0.098 s). This leaves a residue of vapour as a potential site for next pinch off. The process continues at different sites to produce a population of vapour bubble at the top of the wire.

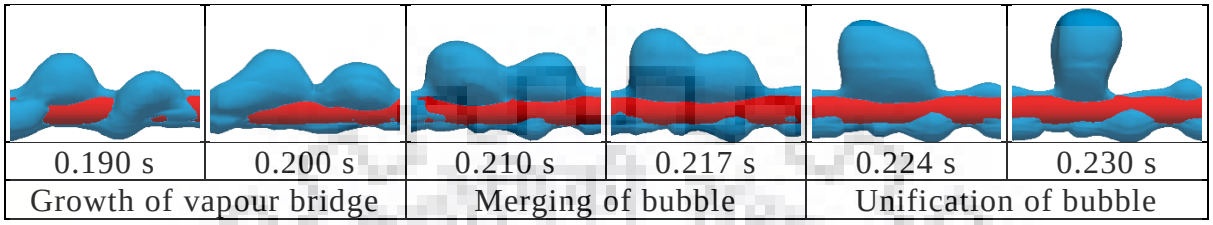

Figure 3.6: Merging of bubbles on the wire

At the time of nucleation and pinch off of bubbles, merging between several bubbles along a horizontal plane has been observed around the wire. A temporal history of such merging process is shown in Figure 3.6. A close look at the merging process shows that merging is not instantaneous. As two bubbles come closer to each other a thin bridge is formed and some mass transfer in the form of vapour occurs from smaller to bigger bubble, which helps in the growth of vapour bridge (0.2 s). After that interfaces of the bubbles merge (0.217 s) and gets unified to form a single bigger bubble (0.23 s). As buoyancy force on bigger bubbles is dominant compared to surface tension, they are more unstable resulting in faster vapour removal from the film around the wire.

An effort has been also made to observe the effect of the degree of superheat on the density of bubble population using numerical simulation. It has been observed from Figure 3.7 that pinch off time of first bubbles at the corners is independent of the degree of superheat (0.05 s). But one can observe larger release diameter in case of wire having more superheat (30° C). Both the wires having 10° and 30° superheat, continuously releases vapour bubbles at different sites but one can clearly visualize from the comparison between same time stamps that larger size bubbles are being produced at a higher degree of superheat. Bubble population density increases with time for both the wires having 10° and 30° superheat. A marginally higher population density is observed for a wire having 30° superheat in comparison to 10° one.

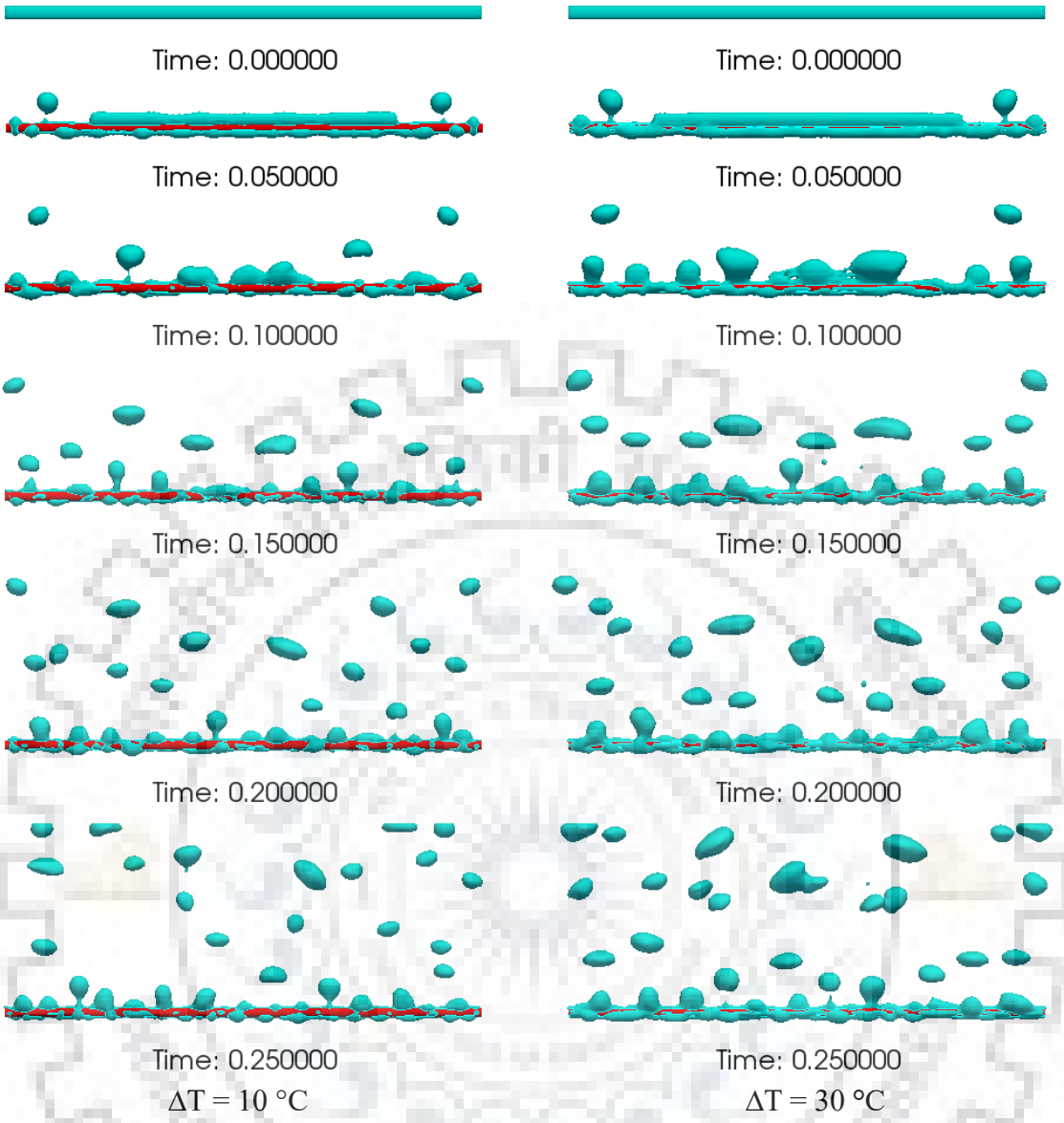

Figure 3.7: Comparative view of the temporal progress of boiling phenomenon at different

Simulations are also performed to observe the comparison between the different degree of superheats of wire. Figure 3.8 reports the bubble cluster at 0.25 s for 10°, 20° and 30° superheat side by side after the simulation. Along with the marginal increase in the concentration of bubbles, increase in average bubble size can be clearly observed from Figure 3.8. But a number of nucleation sites along the length of the wire do not vary with the degree of superheat. It can be also observed that with an increase in temperature, the vapour film thickness is increasing gradually, which will affect the heat transfer coefficient. Figure 3.9 (a) clearly depicts the same through plot between vapour volume and time for three different degrees of superheat. Here, the increase in vapour generation rate from ΔT =20°C to ΔT =30°C is much smaller as

compared to that from ΔT =10°C to ΔT =20°C. Not only the rate of boiling but the bubble diameter is also increasing with increase in the degree of superheat, which can

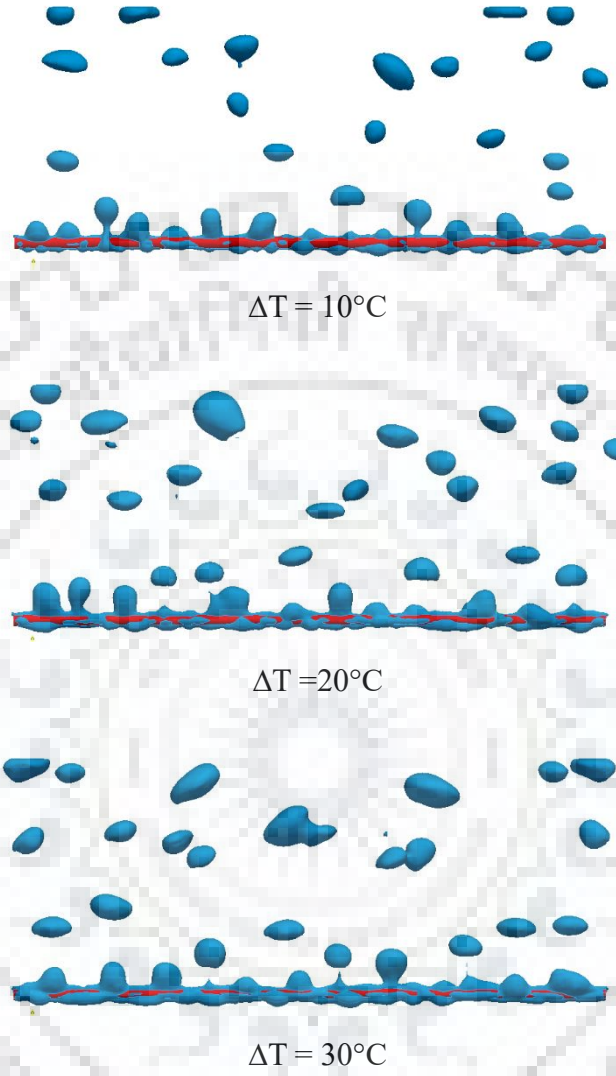

Figure 3.8: Comparison of bubble population for different degree of superheat at time 0.25 s

be clearly understood from Figure 3.9 (b). Here, the distribution of bubble diameter in the population after 0.25 s has been plotted by breaking the whole range of possible diameters in smaller intervals. The abscissa of the graphs shows the mean of the diameter intervals. It shows that the peak of the distribution is shifting toward the higher diameter side with an increase in the degree of wall superheat. Also, the height of the peak and minimum pinch off diameter of the bubble are observed to be increased at ΔT =30°C than ΔT =10°C.

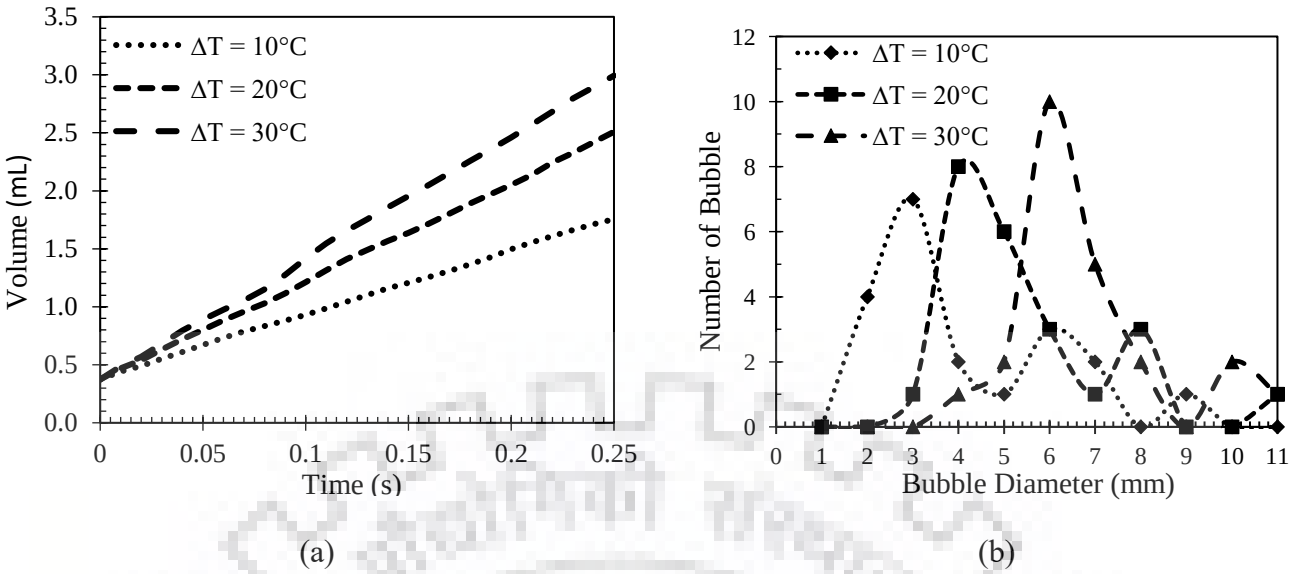

Figure 3.9: (a) Increase in vapour volume with time and (b) Distribution of bubble diameter at different degrees of superheat for boiling around the horizontal wire

3.3.2 Inclined and Vertical Wire Boiling

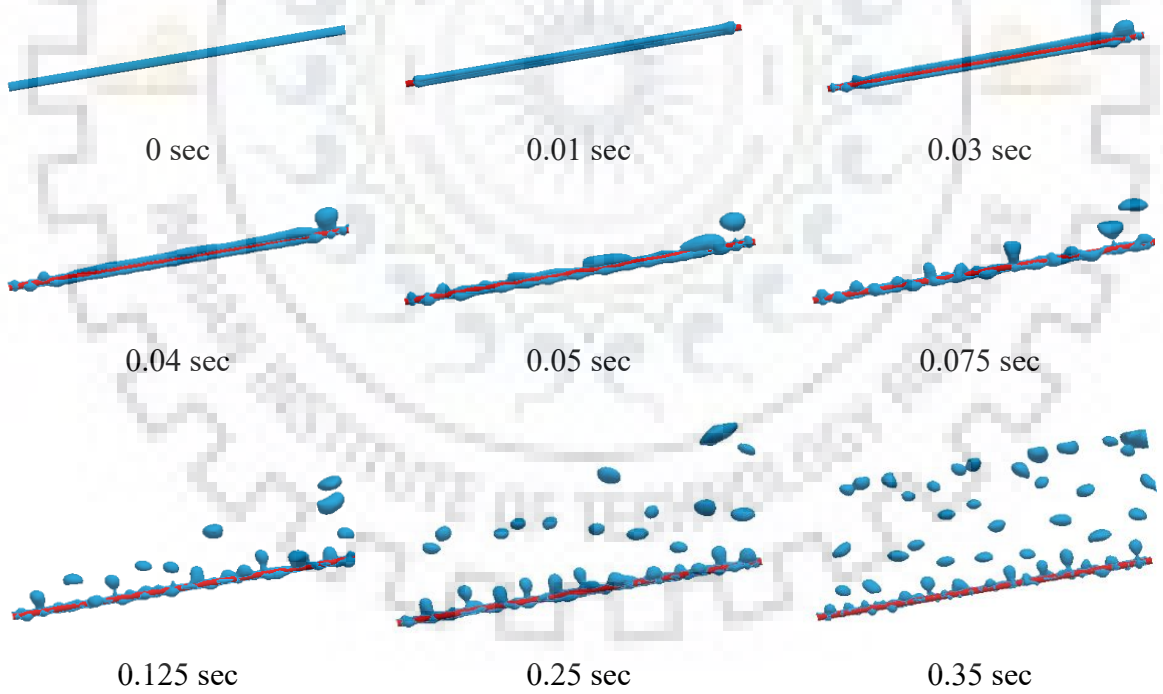

Figure 3.10: Temporal snaps of boiling phenomenon around the heated wire, inclined at an angle of 10°. Superheat is maintained at 10° C and wire diameter is considered as 2 mm.

From the numerical simulations, described above it is prudent that departure of bubbles around the wire is definitely dependent on buoyancy force. To observe the

effect of inclination in wire boiling similar simulations have been tried at 10° and 45° inclination keeping superheat fixed at 10°C. From the temporal history of boiling around inclined wires (Figure 3.10 and Figure 3.11) one can see that initially, film thickens near the upper tip of the wire and a bubble first forms from there. Afterwards, the film gets destabilized to activate other nucleation sites for both the inclinations. Also, from these temporal views, it can be observed that bubble concentration is higher above the upper portion of the wire as compared to that of the lower portion. Bubble sizes are also bigger toward the upper portion of the wire than bottom one. This variation is more prominent in case of 45° inclination as compared to that of 10° inclination.

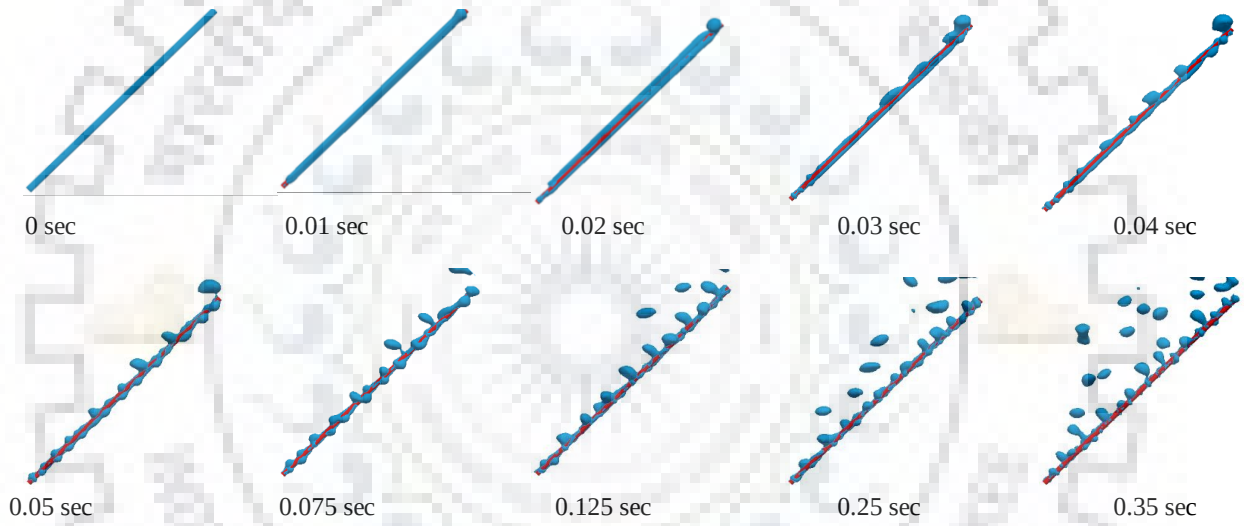

Figure 3.11: Temporal snaps of boiling phenomenon around the heated wire, inclined at an angle of 45°. Superheat is maintained at 10° C and wire diameter is considered as 2 mm.

Further, simulations have been also done with 60° inclined and vertical wire in 110 mm (L) × 20 mm (W) × 50 mm (H) and 110 mm (L) × 30 mm (W) × 30 mm (H) domain, respectively. In Figure 12, as representative, interface distribution of vapour is shown at different time steps from a simulation with vertical wire. Here, one can see that at the start of the simulation the vapour film tries to thicken toward the top of the wire and eventually breaks in small bubbles. These bubbles also start moving toward the top. During this sliding motion, bubbles grow in size due to continuous feed due to boiling. In case of vertical boiling as the effect of gravity is azimuthally symmetric. Initially, the bubbles remain azimuthally symmetric and cover the wire in

all azimuthal directions (0.035s, 0.05s). But gradually when the bubble starts sliding, it faces higher viscous drag due to higher wire surface contact. For this reason, whenever there is slightest azimuthal imbalance the bubble shifts itself in that direction and the azimuthal symmetry is lost (0.1s, 0.15s). After the vapour bubbles get mobilized along the wire, frequent merging has also been observed. As a result, a gradual increase in bubble diameter has been observed (0.2s, 0.25s) along the wire from bottom to top. As the bubble diameter gets increased, the shape of the bubble also departs from its spherical shape. This shows inertia force to be dominated over the surface tension force.

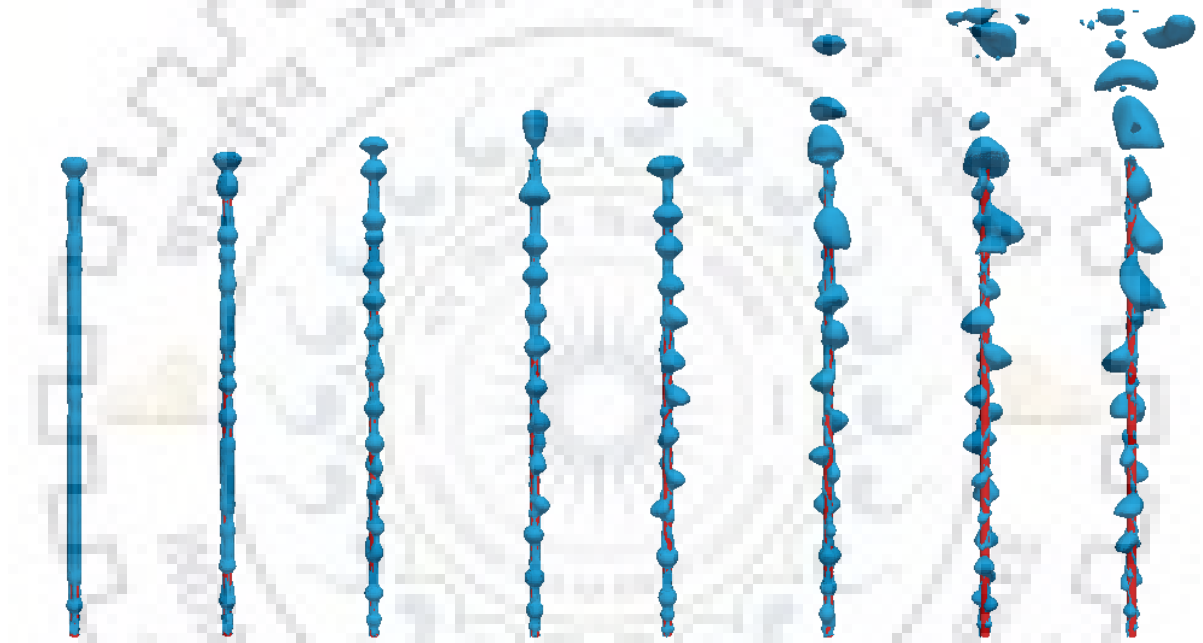

0.025 s 0.035 0.05 s 0.075 s 0.100 s 0.150 s 0.200 s 0.250 s

Figure 3.12: Temporal snaps of boiling phenomenon around the vertical heated wire. Superheat is maintained at 10° C and wire diameter is considered as 2 mm.

To circumvent variation of these different boiling cases in details, in Figure 3.13 (a) volume of vapour is compared against time for different degrees of inclination. Here, it has been observed that with an increase in angle of inclination, the rate of vapour generation increases for horizontal to 60° inclination. But for vertical wire boiling the nature of the curve changes to nonlinear one. Initially, the slope of vertical wire boiling remains lower than a horizontal one. For horizontal and inclined boiling case, the vapour film and bubbles shift azimuthally to allow liquid to

come in contact with the heated wire. But in the case of vertical wire, initially, the azimuthal shift does not happen.

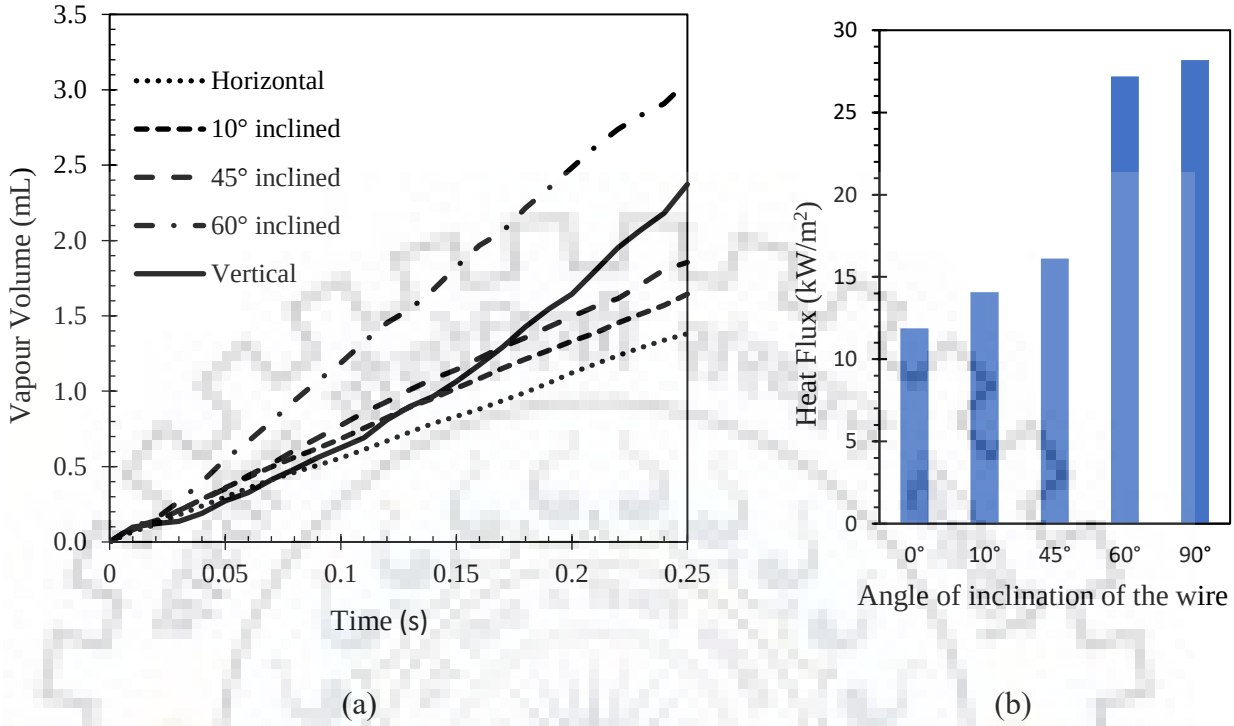

Figure 3.13: (a) Change in vapour volume with time and (b) Final stabilized heat flux at different wire inclinations with 10° C superheat

For this reason, the initial heat flux of the wire is very low. But gradually when the bubbles get mobilized and shift axially (as shown in Figure 3.12), the boiling rate shoots up and shows a non-linear nature and finally stabilizes to a much higher slope in Figure 3.13 (a). Axial mobility of bubbles causes premature departure of nucleation ahead of it, causing increase in vapour volume generation rate. On the other hand, in inclined and horizontal orientation, sliding bubble takes a serpentine path which will have lesser potential in promotion of premature departure. The heat flux for different inclinations have been shown as a bar diagram in Figure 3.13 (b), after calculating it from the final stabilized rate of vapour generation. An increase in heat flux is observed due to a change in inclination from 10° to 45°. But when one moves beyond 45° inclination, the buoyancy force plays the key role and faster removal of vapour has been observed. As a result, in the case of 60° inclination, the rate of boiling is much higher compared to 45°. On the other hand, in the case of vertical boiling though better mobilization of the vapour bubble happens, but there is no chance of bubble

detachment from the middle of the wire. So, the bubbles continue to grow larger and move along the wire length to be released from the upper end of the wire. As a result, the heat transfer from the wire is hindered and results in a very small increase in boiling rate compared to 60° inclination.

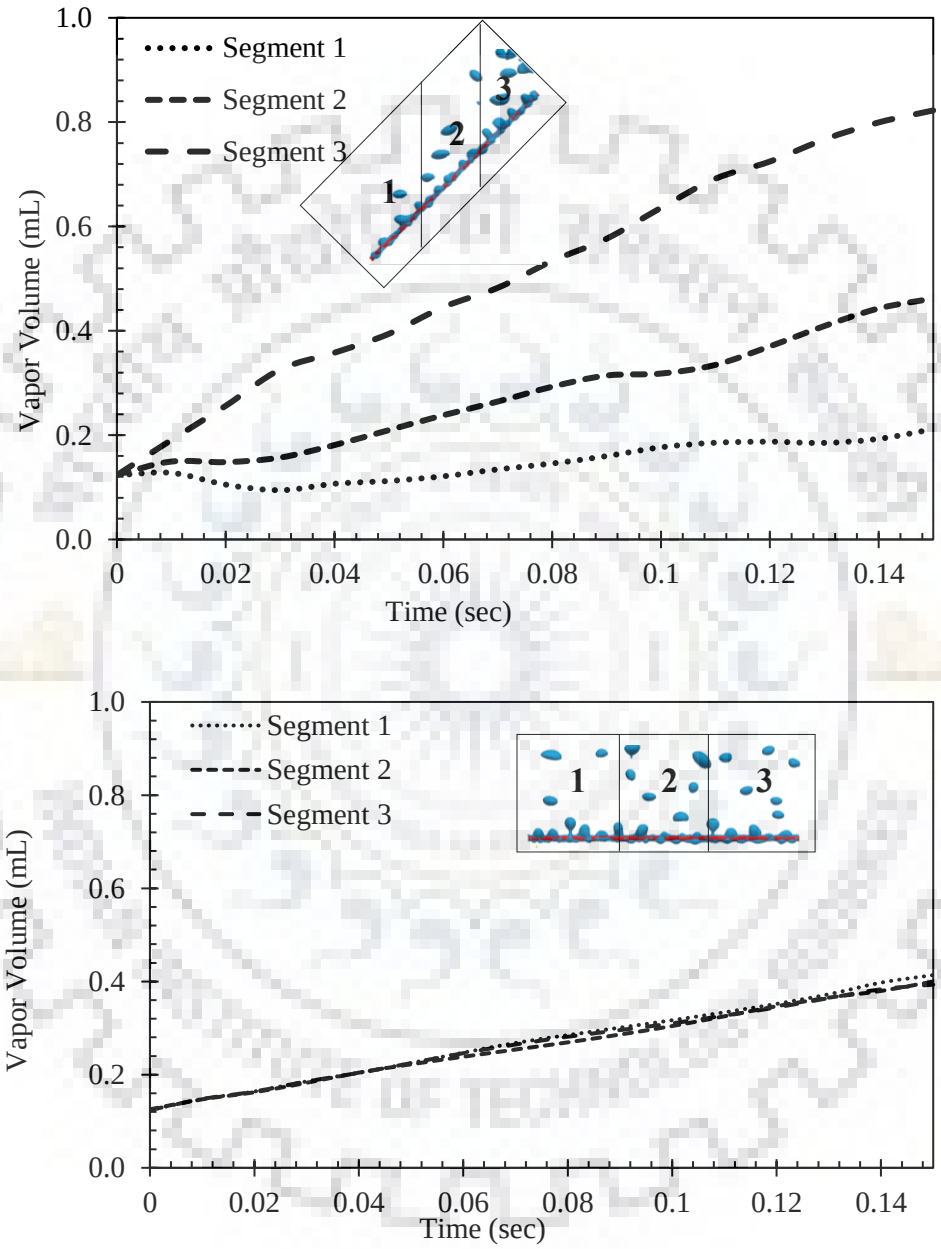

Figure 3.14: Segmental vapour volume variation with time for 45° inclined and horizontal wire

To have a better understanding of the boiling phenomena across the inclined wire the total domain of 45° inclined wire and horizontal wire are subdivided into 3

zones containing the equal length of wire as shown in the inset of Figure 3.14. Variation of vapour volumes of each has been plotted against time. Here, it can be clearly seen that for horizontal wire vapour volume is almost same for all the three zones at any instant of time, but for 45° inclined wire vapour volume differs a lot for the three zones. The slope of the curve for the zone containing lowermost part of the wire is least and that for the zone containing uppermost part of the wire is the highest. The slope of the curve for the central segment (Segment 2) of 45° inclined wire is approximately same as that of the segments of the horizontal wire, but the slope of segment 3 is more than double of the segment 2.

To understand the fundamental reason behind the differential vapour volume growth at different segments of inclined wire bubble sliding along the 45° inclined wire has been identified in Figure 3.15. Here one can observe four types of phenomena, which explains the unequal axial variation of vapour growth.

i. Axial bubble sliding can be observed in the figures a-b-c-d-e-f-g-h. Encircled bubble slides along the top surface of the inclined surface and engulfs smaller bubbles in the path to grow in size.

ii. In the figures c-d-e-f-g-h, the squared bubble, starting from the bottom surface of the wire, glided peripherally along the wire and come on the top surface showing sliding. When any bubble on the bottom surface of wire grows beyond a limiting size, such peripheral bubble sliding has been observed. Peripheral bubble sliding is much faster as compared to axial sliding.

iii. In figures h-i-j-k-l-m, merging has been observed in between the encircled and squared bubble. This merging process is quite similar to merging observed in the horizontal wire (Figure 3.3), but unlike horizontal boiling here both bubbles move in the same direction. As a result, after merging the velocity of the merged bubble becomes higher than the individual bubble velocity and part of the surface energy is also converted to kinetic energy.

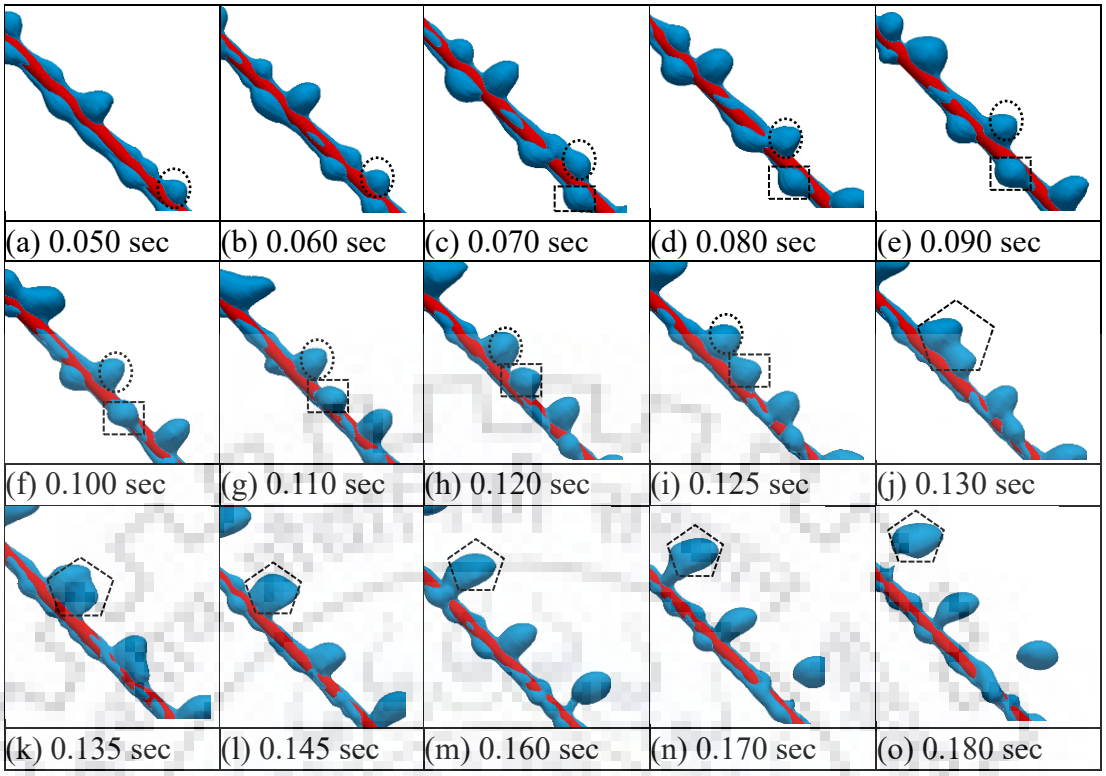

Figure 3.15: Axial and peripheral bubble sliding along with bubble merging in 45° inclined wire

iv. Pinch off: In figures m-n-o bubble pinch off has been pointed out. Here bubble pinch off does not prefer vertical direction but released in the normal direction to the wire. Soon buoyancy control picks up and bubble changes its direction of motion to move vertically up.

This axial sliding explains the reason behind higher bubble concentration near the upper section of the inclined wire and merging explains higher bubble size. Axial sliding takes away the vapour, forms at the lower segment of the inclined wire and merging results into more effective and faster bubble pinch off from the upper section. Finally, these two reasons together help more water to come in contact with the wire, leading to a higher rate of boiling.

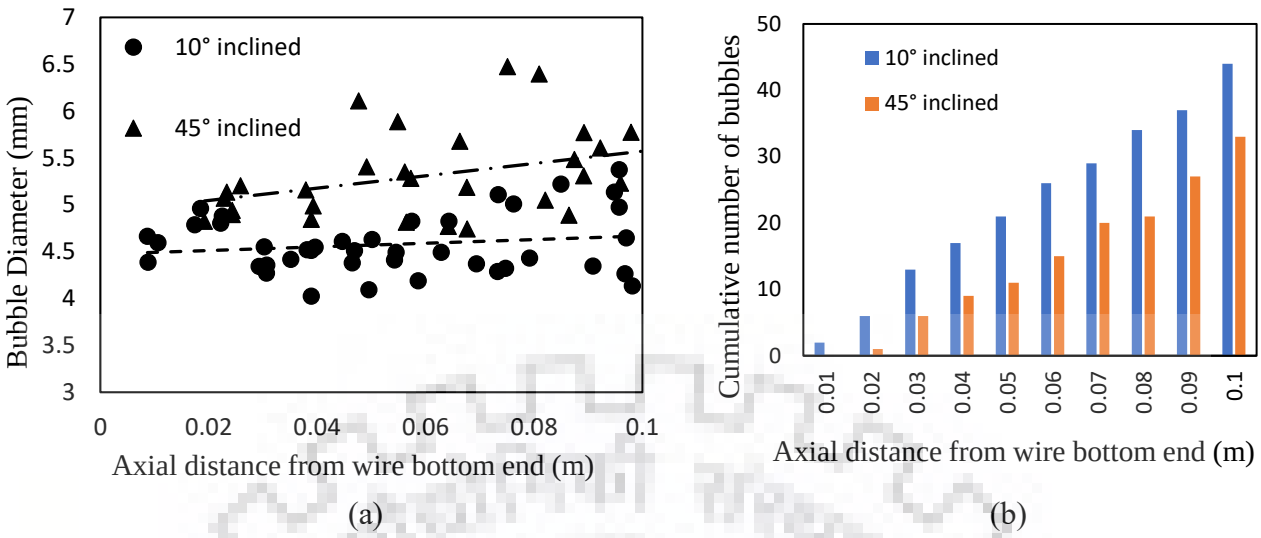

Figure 3.16: (a) Distribution of bubble diameter and (b) cumulative number of vapour bubbles along the length of the wire

To have a better idea about variation of bubble size along the axial direction with different angle of inclination, in Figure 3.16 (a), diameters of all the bubbles pinched off at 0.4 s have been plotted against the axial distance of the bubble pinch off location from the bottom end of the wire for both 10° and 45° inclinations. Here, it can be clearly observed that at the lower end, the bubble diameter varies in comparatively narrower range but as we move toward the upper-end variation of bubble diameter increases. This is due to the combination of merged and unmerged bubbles. Merged bubbles are having quite higher diameter compared to the unmerged one. Comparison between the data points for these two inclinations shows that at 45° inclination, wire boiling results into bigger diameter bubbles. Also, to have an idea of average diameter at the different axial location of the wire, a linear trend line has been added. This average line shows an increase in diameter along the axial length. Also, these two lines show the difference between the average diameter for these cases. Further, a close look at these two lines reveals a higher slope for higher inclination. This is the result of the fact that with an increase in inclination, the bubbles slide for longer length and chance of merging also increases. This causes the average bubble diameter to grow at a faster rate. Another reason of the same is the better sliding tendency of the bubbles, which allows it to flow along the wire faster and due to inertia, it keeps sliding even after accumulating enough vapour to pinch off from lower

inclination wire. In Figure 3.16 (b), a cumulative number of bubbles, pinched off in 0.4 s, has been plotted against the axial distance of the bubble pinch off location from the bottom end of the wire. One can see that the number of bubbles pinched off decreases with an increase in inclination. This happens as a result of better bubble sliding and merging. Due to better sliding, no bubble pinches off has been observed from the first 1cm of the 45° inclined wire. Bubbles get removed from the lower section before accumulating enough mass for pinch off. From this graph, one can see bubble pinch off reduces nearly 20%, for 45° inclination as compared to 10° inclination.

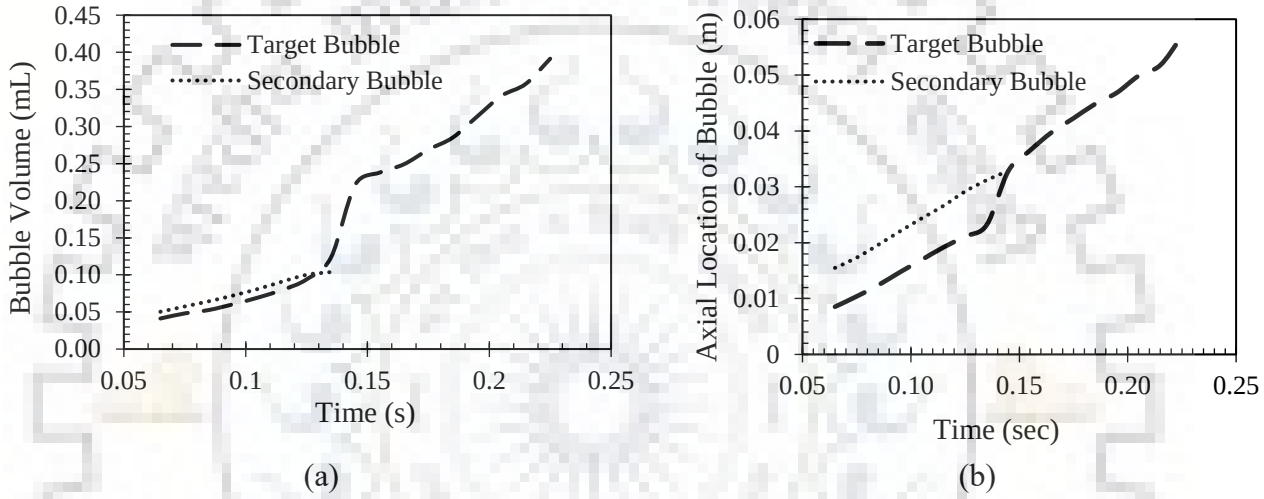

Figure 3.17: (a) Variation of bubble volume with time (b) Movement of bubble along the axial direction before and after merging in vertical wire boiling

To have a better understanding of the bubble lifecycle while sliding over the vertical wire, a bubble has been tracked in Figure 3.17. To understand the bubble growth, in Figure 3.17 (a), bubble volume has been plotted against time. In this graph, two lines are plotted for two separate bubbles. One is our targeted bubble another is one which has been merged with the target bubble while sliding on the wire. In Figure 3.17 (b), the axial distance of the center of the same two bubbles from the center of the wire has been described with time. Initially, in Figure 3.14 (a), we can see that the volumes of the bubbles are nearly the same and their rate of increase of the volume is also the same. Figure 3.17 (b) shows the distance between their centers. The same slope of the two curve signifies nearly the same velocity of the bubbles. Though the center to center distance of the two bubbles remains more or less constant with time,

an end to end distance i.e. the distance between the upper end of the lower target bubble and the lower end of the upper secondary bubble reduces gradually with the growth of bubble volume and diameter. Eventually, near 0.14 sec, a vapour bridge is formed between two bubbles and they get merged. Due to this merging, the sudden rise of target bubble volume can be observed in Figure 3.17 (a). The similar sudden rise has also been observed in Figure 3.17 (b) at the time of merging. After the formation of vapour bridge, movement of the bubble becomes easier and very fast flow of the target bubble into the secondary bubble happens. After merging slope of the axial location curve increases. There are mainly two reasons behind this increase in slope. First one is the surface energy which has been converted to kinetic one and another is the increase in buoyancy force due increase in bubble volume. But the later one is more dominant in the present case. Further close look in Figure 3.17 (a) reveals that the slope of the curve increases after merging. Not only that some non-linearity has been observed in both the segment (before and after merging). Non-linearity is more prominent after merging. So, it can be said that slope increases with the increase in bubble volume. As the bubble volume increases the bubble diameter also increases. So, more surface of the wire is covered by the bubble that means catchment area of the bubble increases. As a result, bubbles accumulate and increase in the bubble volume is observed.

3.3.3 Horizontal Boiling in Two Neighbouring Wires:

To observe the mutual interaction between vapour masses formed around neighbouring wires, numerical simulations are made, first, for the vertical placement of wires. A domain of 110 mm (L) × 20 mm (W) × 30 mm (H) has been considered to be filled with saturated liquid water at 373 K. The wires of 2 mm diameter are placed, keeping axis horizontal in same vertical plane having a central distance of 6 mm, i.e. with a spacing of 4 mm. In Figure 3.15 boiling phenomena has been represented with the help of the phase contour of $\alpha_L = 0.5$ around two vertically stacked wires. From the figure, it can be observed that at the initial stage of boiling the vapour film thickens and waviness is observed along the length of the film for both the wires. The peak of these waves gradually results in nucleation point for the bubbles. Nearly after 0.1 sec, we can see the bubbles of lower wire start touching the upper wire vapour film.

Subsequently, the vapour pinches off occurs from the upper wire and these process repeats to generate more and more bubbles.

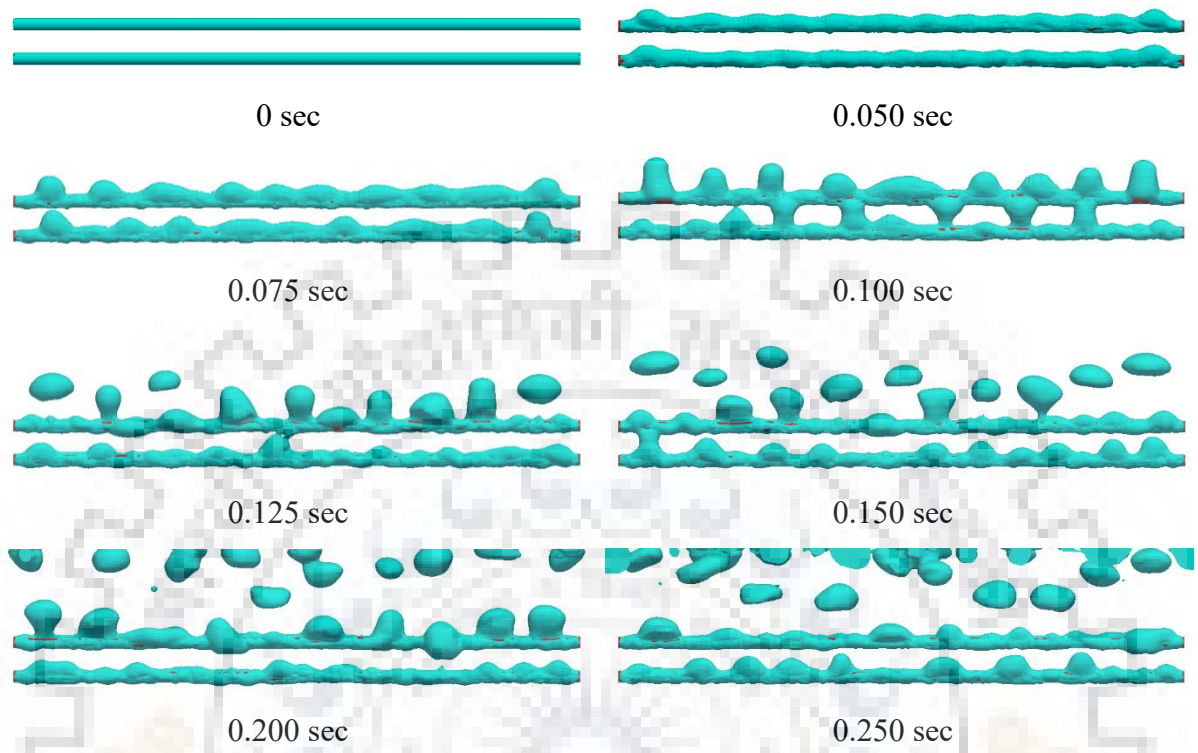

Figure 3.18: Temporal progress of boiling phenomenon around two horizontal heated wire arranged in a same vertical plane

To have a better understanding of boiling around neighbouring wires, certain sections across length are minutely monitored. In Figure 3.19 a-b vapour at lower wire grows and touches the thin vapour film at the bottom of the upper wire and a narrow vapour bridge is generated. After that in Figure 3.19 c, we can see that due to the effect of buoyancy vapour gets transferred to the upper wire and the bridge widens at the top. But, simultaneously vapour bridge becomes narrower at the lower portion and after a certain time when most part of the vapour bubble is transferred at the upper wire the bridge is torn and a bubble is formed at the bottom of the upper wire. In upper wire transferred bubble behaves like a vapour bubble produced around the single wire, even it merges with another protruded bubble from the upper wire. In Figure 3.19 e, transferred lower bubble is being swallowed by another one. While flowing into the upper bubble vapours inside the lower bubble gains some kinetic energy which helps the merged bubble to move upward and detach (Figure 3.19 h).

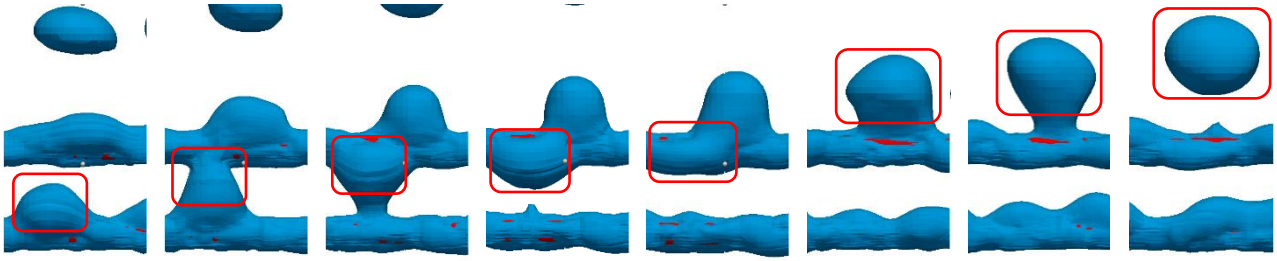

(a) 0.165 s (b) 0.180 s (c) 0.188 s (d) 0.193 s (e) 0.198 s (f) 0.215 s (g) 0.227 s (h) 0.238 s

Figure 3.19: Formation of bubble bridge, vapour transfer and bubble merging in between two horizontal wires placed in a same vertical plane

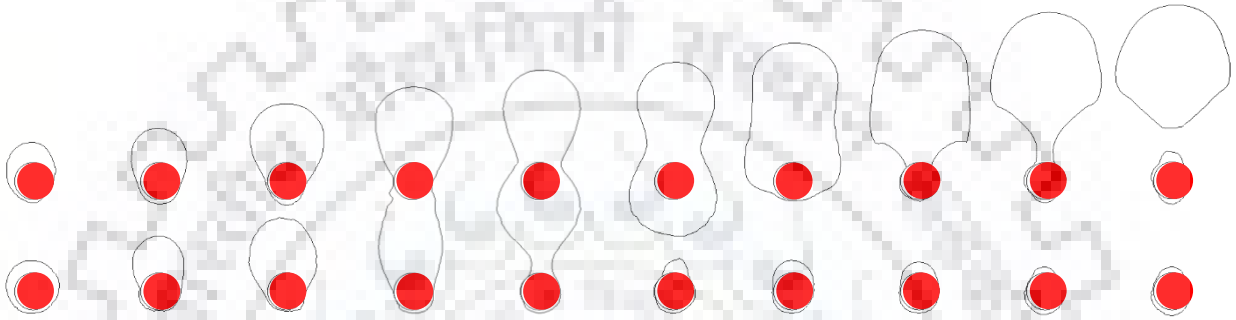

(a) 0.050 s (b) 0.075 s (c) 0.090 s (d) 0.098 s (e) 0.106 s (f) 0.110 s (g) 0.118 s (h) 0.123 s (i) 0.130 s (j) 0.133 s

Figure 3.20: Growth of vapour bubbles, merging and pinch off from neighbouring horizontal wires arranged in a same vertical plane; Sectional view

In order to study cross-sectional features, in Figure 3.20 phase contour of $\alpha_L = 0.5$ has been plotted against time on a particular section where two bubbles have been observed to be growing simultaneously from the wires. In Figure 3.20 a-b-c, the growth of vapour bubbles has been observed with nearly the same rate, but significant difference in shape has been noticed. The shape of the bubble on the upper wire nearly resembles the shape of the bubble shown in Figure 3.5 for a single wire. But, the vapour bubble in the lower wire shows suppressed flat top. Observation confirms that due to the presence of the upper wire effect of gravity gets weakened. In Figure 3.20 d-e-f bubble merging occurs. It is observed clearly that the mass transfer occurs from both the wires and a thick vapour film covers the wire during this time. In Figure 3.20 g-h the inertia effect scavenges all the vapour masses at the side of the upper wire and leaves a thin vapour film around it. After that vapour bubble starts rising, thinning the bubble near the upper wire (Figure 3.20 i) and finally, it gets detached from the wire in Figure 3.20 j.

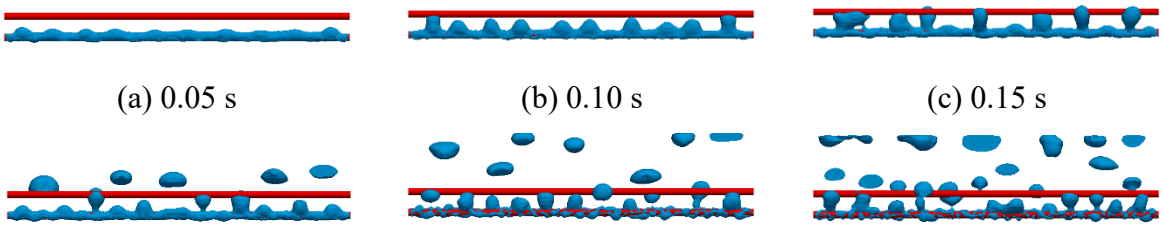

(a) 0.05 s (b) 0.10 s (c) 0.15 s

(d) 0.20 s (e) 0.25 s (f) 0.30 s

Figure 3.21 Temporal snaps from a simulation of boiling phenomenon from a horizontal wire with one passive wire above it at the same vertical plane

Next, to observe the effect of passive wire above an active heated wire on vapour dynamics, a similar domain has been used. Here, the upper wire is kept at saturation temperature and the lower wire is kept at 10° superheat. Different time snaps of the simulation have been shown in Figure 3.21. One can see that the vapour bubbles are forming from the initial film on the lower wire and eventually they touch the upper wire and gets stuck up in the space between the wires. After some time, these bubbles cross the upper wire and gets pinched off from the upper wire. Though the upper wire is not at all contributing in the boiling, still bigger size bubbles have been observed to pinch off from the upper wire due to delayed departure. The departure of these bubbles delay in comparison to bubble release from a single wire.

To investigate the reason behind the higher bubble size, cross-sectional view of a bubble growth has been studied in Figure 3.22. Once the initial (0.05s, 0.075s) bubble shapes of this case are compared to the same in single wire (Figure 3.8) case, a significant difference can be observed in bubble shape. In this case, the bubble shape is much wider than that of a single wire bubble having similar height. This shows that due to obstruction of the passive wire, the bubble is not able to grow in the vertical direction as it has grown in single wire case. Once the bubble touches the upper wire, it draws the bubble mass upward very fast. Though in this stage the bubble tries to cover the passive wire symmetrically from both the directions (0.125s), but after covering a certain sectoral area of the upper wire, the movement slows down. Further growth in sectorial wrap requires much higher surface energy. At this position, the bubble gets stuck up between the wires and grows in volume. Once due to some disturbance if the bubble of one side of the wire becomes bigger compared to another side (0.14s), then due to the difference on curvature, the whole bubble mass is pushed toward the bigger side. As the result, the bubble is shifted to one side of the passive wire (0.16s). Due to this shift a circulation is

generated around the passive wire, which pushes the interface further. As a result of this push and buoyancy force, necking happens (0.166 s) and eventually the bubble is pinched off from the lower wire (0.167 s). After that surface tension smoothens the sharp edges of the bubble and the residual vapor very fast (0.168). And there after bubble rolls at the surface of upper wire to reach the top of the wire and then gets pinched off from passive upper wire without changing its volume.

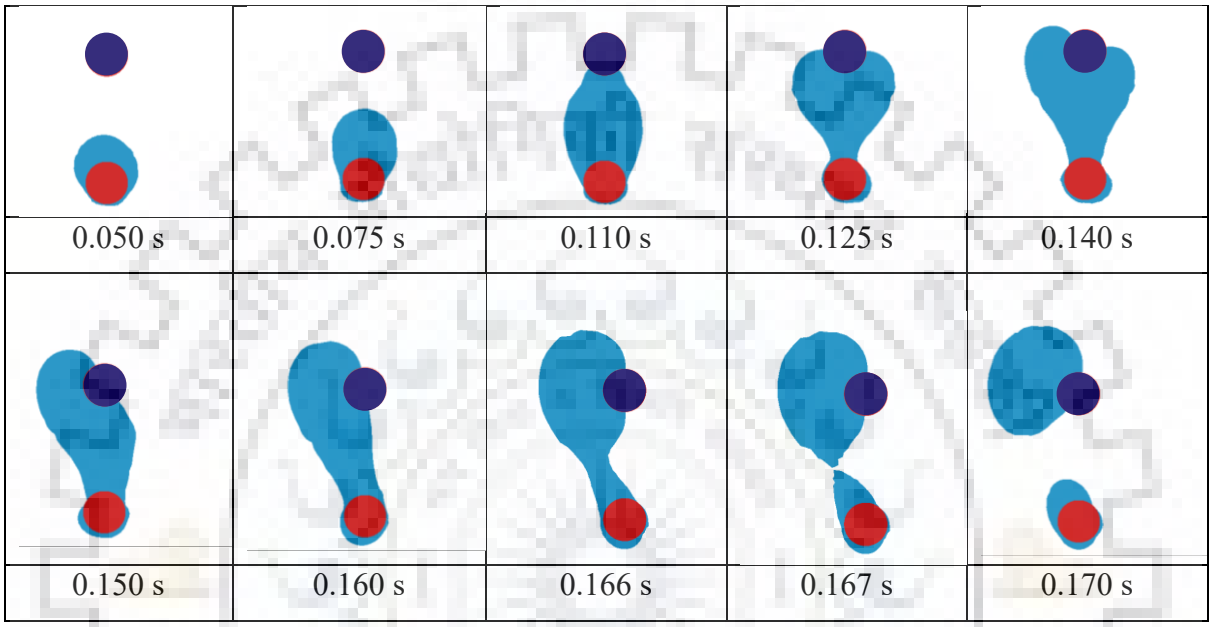

Figure 3.22: Cross-sectional views of bubble growth from active wire and its interaction with passive wire, placed on top of the vertical plane

An effort has been also made to study the interaction between evaporating wires when placed horizontally. For simulation, two parallel wire placed at a same horizontal level has been considered with different spacings. Wire dimension has been kept similar to previous two wire boiling cases. The domain size has been kept as 110 mm (L) × 20 mm (W) × 20 mm (H). Here, both the wires have been maintained at 10° superheat. Three different wire spacings as 2 mm, 3 mm and 4 mm have been tried. In Figure 3.23, bubble growth and merging for wire spacing of 3 mm have been depicted. In the figure, one can see that initially the bubble growth nearly resembles that in the case of a single wire (Figure 3.8). But gradually as they grow larger in diameter, they touch each other and vapour bridge is created (0.112 s). Then, this bridge expands and unifies the bubbles to a single bubble (0.12 s). Once bubbles are merged then it tries to take nearly spherical shape (0.127 s) and as after merging the bubble size becomes quite larger, buoyancy force becomes dominant. As a result, the bubble starts rising very fast (0.133

s) and eventually gets detached from both the wires (0.14 s). In the present case, bubble sizes observed to be quite larger as compared to single wire and even larger that vertically stacked two wire boiling case.

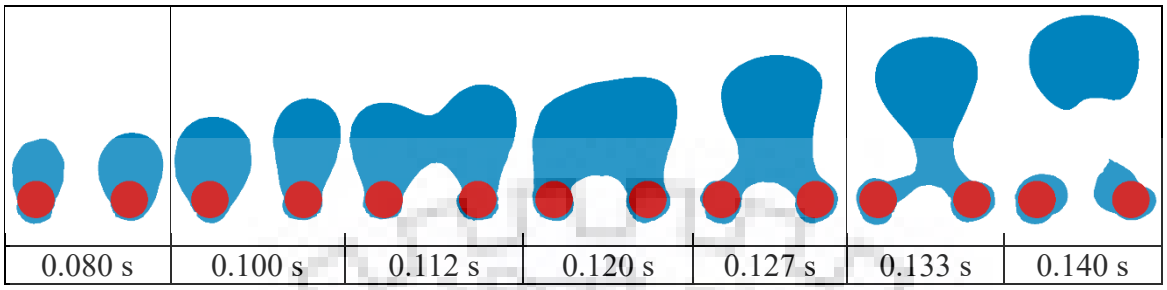

Figure 3.23: Bubble merging and pinch off from two heated wire kept parallel in the same horizontal plane.

Merging has not been observed in numerical simulation when the spacing between the wires is kept to be 4 mm. Their bubble dynamics seems to be similar to the single wire case. On the other hand, in the case of 2 mm spacing, faster merging has been observed. More significantly, in case of 2 mm spacing, continuous vapour bridge has been observed at certain sections of the wires. This continuous bubble bridge restricts liquid replenishment between the wires and as a result boiling is hampered.

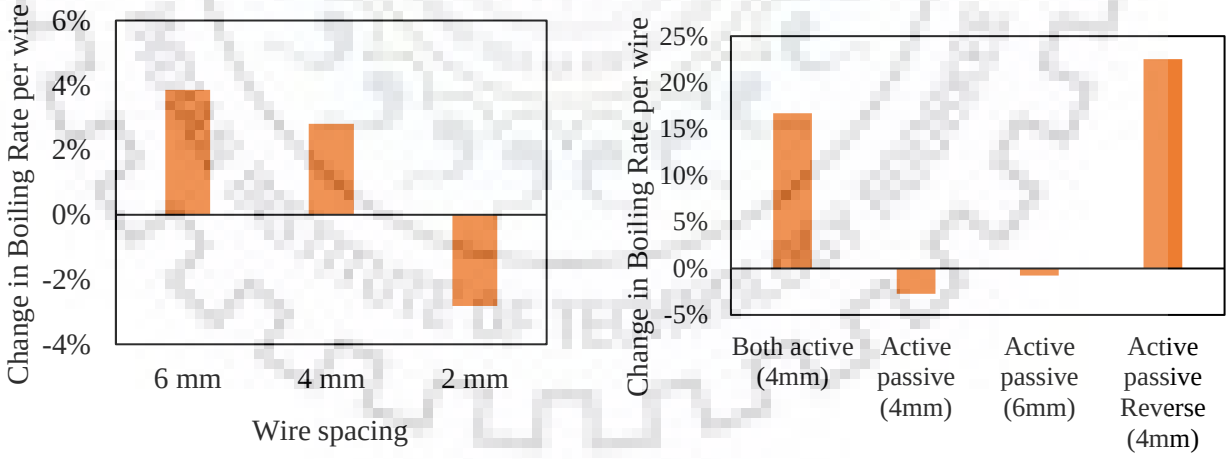

(a) (b)

Figure 3.24: Percentage increase in boiling rate per wire for two wires cases when wires are stacked (a) Horizontally (b) Vertically

A careful comparison of numerical simulations may establish the influence of active and passive neighbours on vapour dynamics. The overall effect of adding a neighbouring wire

in different directions is depicted in terms of rate of mass transfer during phase change by comparing combined wire simulation with single horizontal wire. For both the cases degree of superheat is kept at 10°C. In Figure 3.24 (a), increase in boiling rate for two wires placed in the same horizontal plane has been plotted against decreasing wire spacing. In case of 6 mm wire spacing, where no bubble merging has been observed between wires, enhancement in boiling rate than the single wire is maximum. In this case (6 mm horizontal spacing), interacting circulations at the stage of bubble pinch off get strengthened and dislodges bubble faster than a single wire. It also promotes better liquid replenishment due to circulatory flow than its single wire version for promoting enhancement in mass transfer. But in the case of 4 mm spacing due to bubble merging liquid contact to the wire gets reduced, and boiling rate decreases marginally. For 2 mm spacing as continuous vapour, the bridge is created between the wires, liquid contact to the wires reduces heavily. As a result, boiling rate per wire becomes even lower than single wire case.

In Figure 3.24 (b), similarly, increase in boiling rate per heated wire has been plotted for different two-wire boiling cases, placed in a same vertical plane. When both the wires are heated, we can see that the boiling rate per wire increases compared to single wire case. The main reason behind this increase is the scavenging effect, which occurs when the bubble from the bottom wire flow over the upper wire. Though there will be some reduction in boiling rate at the upper wire as the bubble from the lower covers the upper wire for some interval of time, but soon scavenging effect becomes dominant. Moreover, the bubbles on the lower wire touch the upper wire even before fully developing to the bubble size, as observed in the single wire case. As soon as it touches the upper wire it is dragged up very fast. Hence, the boiling rate of lower wire is also increased due to lower bubble residence time on the wire. But in case of active-passive association (where only the lower wire is heated), as the upper wire remains wetted with the water the vapour bubble is unable to pass around the upper wire smoothly but gets stuck up in the space between the wires. So, boiling is hampered in that zone and boiling rates reduces compared to single wire case. But this effect reduces as the spacing between the wires is increased. As we increase the spacing from 4 mm to 6 mm, the vapour bubble gets enough space to grow and pinch off from the lower wire. So, in the latter case, the bubble is released from the lower wire as soon as the bubble gets stuck up to the upper wire and liquid can come in contact to the lower wire. So, the reduction in boiling rate is lower in the case of 6 mm spacing. Also, it can be observed in Figure 3.24 (b) that the boiling rate of the active-

passive reverse case (where only the upper wire is heated) is surprisingly high. Though here no direct vapour bubble interaction is happening with the passive wire, the liquid flow structure and the circulation pattern is changed due to the presence of the lower passive wire and works in favour of bubble departure. The passive wire is acting as the enhancer from the bottom which restricts film growth in a downward direction freely and results in faster bubble release due to the buoyancy of the upward direction in the top wire.

CHAPTER 4 INTERNAL ANNULAR BOILING

4.1 Domain Description:

For the simulation of annular flow boiling of water inside a tube, a representative cylindrical fluid domain of 11 mm diameter (D) and 50 mm length (L) has been chosen in the present study. A schematic of the domain along with necessary initial and boundary conditions are shown in Figure 4.1 (a). As in the majority of the industrial applications, boiling is performed at elevated pressure than the atmosphere, present simulations have been performed at representative 40 bar pressure (p_b). To mimic annular like situation, initially a thin 0.5 mm thermally saturated liquid film (t) has been positioned at the outer periphery of the cylindrical domain and the rest is considered to be filled with saturated vapor at the corresponding pressure. No slip and no penetration condition have been applied to the cylindrical boundary of the domain. Thermally the wall is considered to be maintaining ΔT_{wall} superheat as compared to saturation temperature at p_b (T_{sat}), given in fluid domain. Other parameters like pressure and volume fraction are not supposed to have any gradient across the tube wall. Conditions at the wall can be summarized as:

$$\vec{U} = (0,0,0), \qquad T = T_{sat} + \Delta T_{wall}\,, \qquad \frac{\partial p}{\partial r} = \frac{\partial \alpha_L}{\partial r} = 0 \tag{4.1}$$

From the bottom of the domain, uniform and constant velocity inflow conditions have been applied which has split the inlet plane into two parts, consisting of one outer annular region, matching thickness liquid film inside (t), from where liquid enters and through rest of the inlet section vapor enters. Provisions have been kept for varying the average magnitude of inflow velocities for liquid and gas (u_g , u_l), independently.

Inflow boundary condition can be mathematically described as:

$$\vec{U} = \begin{pmatrix} & u_g \ for\, r < \left(\frac{D}{2} - t\right) = 5\ mm \\ 0,0, & \\ & u_l \, for\, r \geq \left(\frac{D}{2} - t\right) = 5\ mm \end{pmatrix}, \qquad T = T_{sat}\,,$$

$$\alpha_L = \begin{matrix} 0 \ for\ r < \left(\frac{D}{2} - t\right) = 5\ mm \\ 1\ for\ r \geq \left(\frac{D}{2} - t\right) = 5\ mm \end{matrix} \tag{4.2}$$

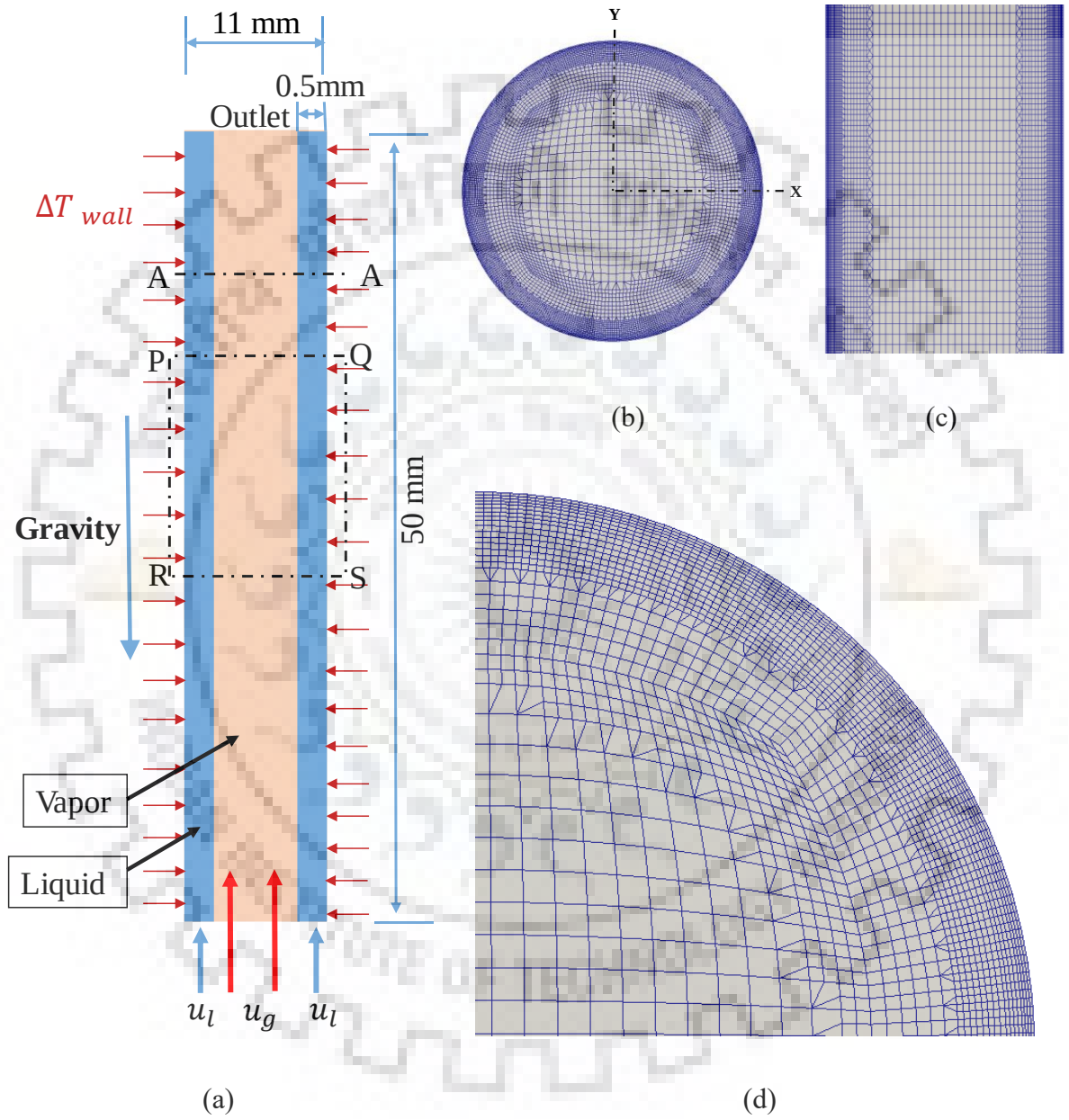

Figure 4.1: Domain description and mesh configuration (a) Fluid domain description along with boundary conditions (b) A-A cross-sectional view of the mesh (c) P-Q-R-S cross-sectional view of the mesh (d) One-fourth X-Y cut-section view of the mesh

The top boundary has been set as pressure outlet with a constant value of P_b, signifying no axial flux of temperature, volume fraction and velocity. The same can be mathematically expressed as:

$$p_{@z=L} = p_b, \quad \frac{\partial T}{\partial z} = \frac{\partial \alpha_L}{\partial z} = \frac{\partial \vec{U}}{\partial z} = 0 \tag{4.3}$$

All the steam and liquid water properties are taken at (P_b, T_{sat}). Representative values for the present simulation are shown in Table 4.1.

Table 4.1: Account of gas and liquid properties, fed in the code at $(p_b = 40\ bar, T_{sat})$

Property	Liquid	Vapour
Density (kg/m^3)	798.7	20
Thermal Conductivity (W/mK)	0.62	0.0513
Viscosity (m/s^2)	1.3521×10^{-7}	9×10^{-7}
Specific Heat (J/kgK)	4865	3795
Latent Heat (kJ/kg)	1714	
Surface Tension(N/m)	0.02301	
Gravity (m/s^2)	9.81	

4.2 Mesh details:

The mesh structure of the domain in cross-sectional and longitudinal view can be observed in Figure 4.1 (b) and (c), respectively. As boiling will occur near the wall only, the highly refined hexagonal mesh has been generated near the wall to have a better understanding of bubble nucleation due to boiling. Enough care has also been taken to refine mesh near the interface. This can be clearly seen from the enlarged cross-sectional view, as shown in Figure 4.1 (d). The grid-independent study has been carried out for 3 different cases of grid sizes as shown in table 4.2 and Figure 4.2. From the plot of vapor volume generated in the annular region over the time shows that there is a very small change in the trend between medium and fine mesh as compared to coarse mesh. The medium mesh was selected to carry out further simulations for different cases.

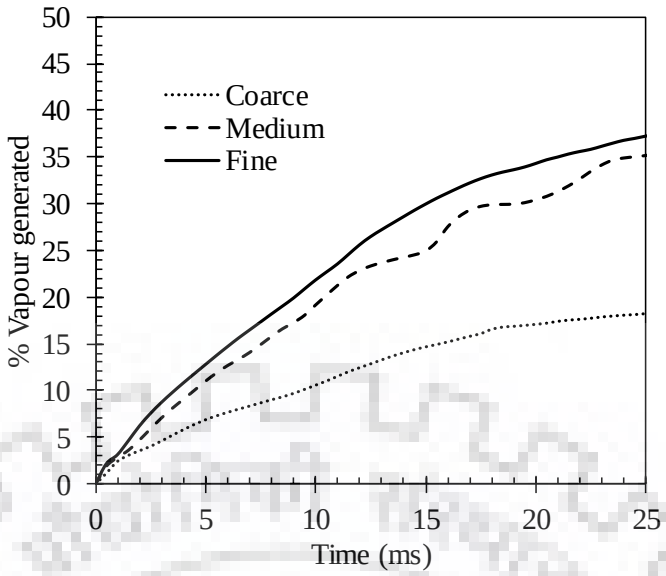

Figure 4.2: Grid Independent study

Table 4.2: Grid independence test mesh statistics

	Coarse	Medium	Fine
Number of cells	1799864	3764926	6631248
Min. cell size (mm)	0.045	0.03	0.02
Run time for 2 ms (hr)	1.629	8.51	29.25

Table 4.3: Description of simulation parameters for annular flow with phase change

Case	p_b in bar	(u_g, u_l) in m/s	ΔT_{wall} (℃)
A	40	(2.5,1)	20
B		(3.4,1)	10
C			20
D			50
E		(4.5,1)	20
F		(10,1)	20
G		(15,1)	50
H		(3.4,1.5)	20

The simulations were performed for various liquid and vapor velocities as well as with different degrees of superheats. The present discussion will be only describing a few of these

mentioned in table 4.3, which will help in understanding the parametric effect on interfacial dynamics.

4.3 Validation:

As interfacial dynamics is not reported in the literature for annular flow boiling, for validation, boiling on a rectangular parallelepiped geometry, having similar mesh configuration as a cylinder, has been studied. The growth history of a bubble in terms of equivalent diameter is plotted in Figure 4.3 over time before it gets detached from the surface. The same has been compared with the simple but most fundamental and popular correlation of Plesset-Zwick (1954). Our simulation predicts the trend of growth rate quite well once the bubble takes nearly spherical shape and a maximum error of less than 2.7% has been noticed, before departure. Encouraging accuracy and observation ability of interfacial dynamics of present model prompt confidence in modeling interface dynamics during flow boiling cases. Results of the same are described in the next section.

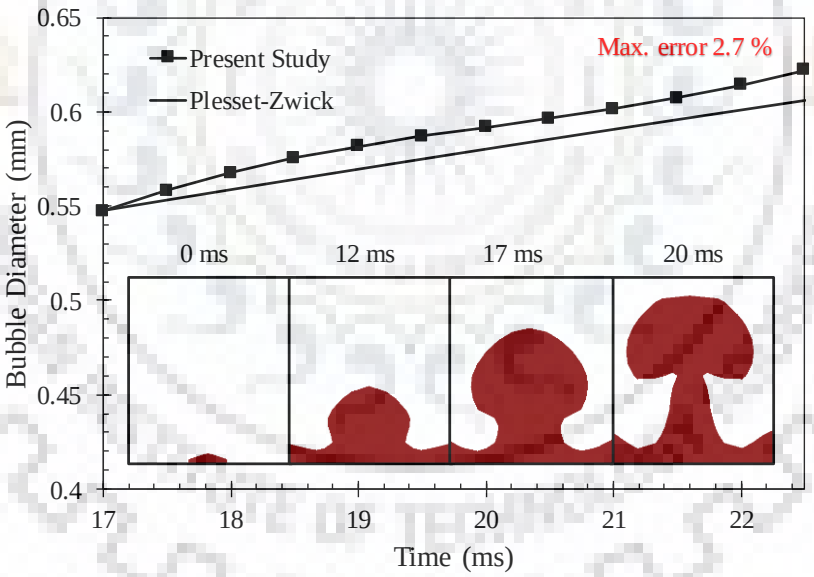

Figure 4.3: Comparison of bubble diameter calculated with Plesset-Zwick equation and the present study

4.4 Results and discussion:

4.4.1 Stages of annular flow evolution

Observations of numerical simulation till initial 5 ms is analyzed in the form of phase (VOF) contour for understanding the breaking and making the process of the interface. Simulation parameters for the degree of superheat of wall and account of velocity inlet are given in table 4.3. As a representation, case E is described over here. The initial undisturbed film, at around 1 ms starts the growth and propagation of a disturbance wave. At the same time due to change of phase throughout the superheated wall, a thin vapor film generates which soon (~2 ms) transforms into discrete nucleations throughout the axial length. Along with the growth of these bubbles, the disturbance wave continues to transform into a roll like a lamella. Upon reaching at specific overhung, due to surface tension and nearby gaseous shear lamellas shed droplets (Kumar et al., 2016). These droplets inside the tube create a swarm and convert the flow pattern to droplet annular one. For adiabatic situation, the same has been already described by Kumar et al. 2016. In the presence of phase change, at the foothill of disturbance wave, nucleating bubble bursts to form a local vapor patch which creates dry out like situation, commonly happening in annular flow with the heated wall. A close look at the interfacial nature of the bubble, generated due to phase change, shows several stages in its life cycle. Distinctly, these stages can be identified as (i) nucleation (ii) growth (iii) merging with neighbors and (iv) bursting at the film-free surface. On the other hand, in the film, droplet pinches off, as a result of excessive amplitude in the wave, can be observed. The cumulative effect of generated bubble dynamics and the aftermath of pinch-off lead towards local dry-out. Description of individual stages is given below.

i. **Nucleation:** At the beginning, a thin vapor film (<50μm) is formed at the wall by evaporating the saturated liquid adjacent to the superheated wall. Soon the film becomes asymmetric axially due to buoyancy and one can see several nucleation sites based on mutual interaction of buoyancy-driven flow and surface tension instability. These nucleating bubbles are in the size range of 0.5 mm which decreases in radius of curvature as time progresses. Nucleation due to strong surface tension effect converts into bubble shape and climbs up before entering into growth stage. Nucleation stage is shown as phase contour in-between 9 ms and 11 ms in Figure 4.5.

ii. **Bubble Growth:** In this stage, liquid inertia drives the nucleated bubbles to advance in upward direction and since constant wall temperature is applied over the wall, heat

transfer will take place resulting further growth of bubbles in size. This process continues until two neighboring bubbles (preceding and succeeding), as shown in Figure 4.5, come closer to each other and indulges in the mutual merging process.

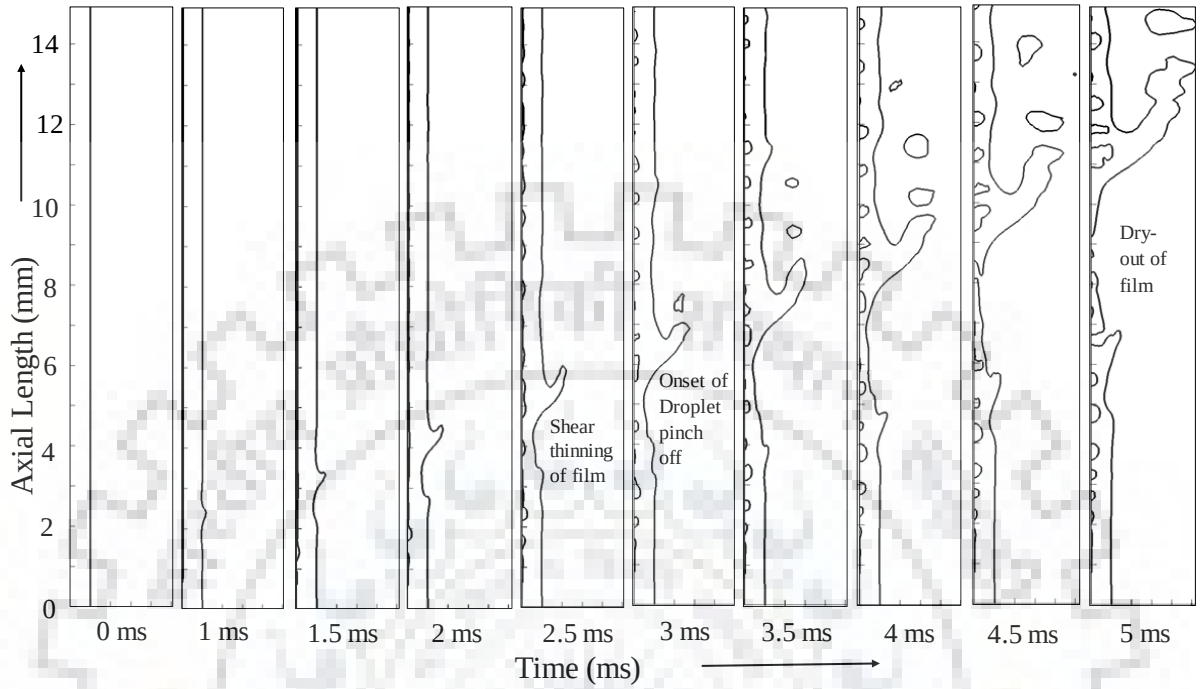

Figure 4.4: Liquid vapor interfacial dynamics for water inside a tube; VOF contour is shown in one half of the axial plane. Simultaneous initiation of vapor bubble and liquid drop can be observed as an aftermath of inertial disturbance wave and phase change. Mechanism of dry out is also highlighted. (for case G in table 3)

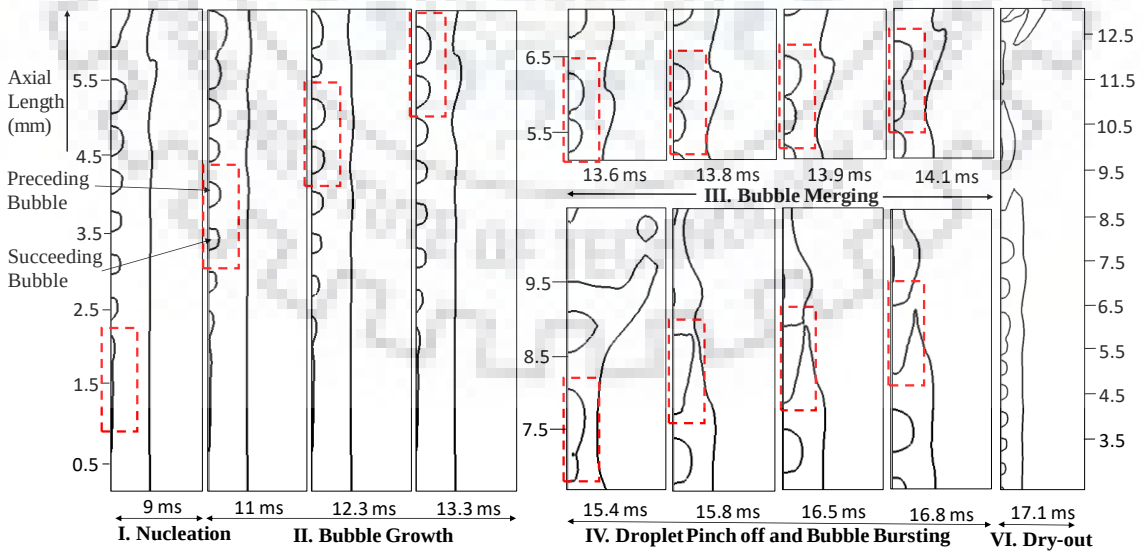

Figure 4.5: On-route to dry-out through stages of bubble evolution (case G in table 4.3)

iii. **Bubble Merging:** Due to the favorable difference of velocities in neighboring bubbles and their individual growth, lagging front of preceding bubble and leading front of succeeding bubble come close to each other by draining the liquid in-between. After overcoming thin film repulsive forces, these bubbles unify and reorientes its interface into a combined single bubble. This coalescence of bubbles results in a sudden increase in the vapor volume and size of the bubble.

iv. **Bubble Bursting:** As an aftermath of the sudden increase in bubble size due to merging, innermost point of the combined bubble may come closer to the wavy liquid film. In the case of lamella formation and pinch-off of the droplet due to the excessive amplitude of the wave, local ripping of film thickness can be observed at the foothill of the lamella. Incidentally, if the bubble merging happens at the foothill of the drop ejecting lamella then unified bubble may burst at the liquid-vapor interface. At around 15.8 ms of the present simulation, a similar situation can be observed where merged bubble opens up in the central vapor core through bubble bursting. Such procedure generates a local dry-out patch, which further elongates in length due to the circulation of air inside the burst vapor cavity.

v. **Droplet Pinch-off:** Simultaneously, one can also observe droplet pinch-off from the inner wavy interface, which plays a major role in the transformation of annular flow to dryout situation through droplet annular regime. Figure 4.5 also shows pinch-off of droplet around the merging of bubbles inside the liquid film. Similar pinch-offs happens many in number throughout the cylindrical wavy interface and generate droplet swarm in the core. The pinch-off process is well known as entrainment and its rate governs the mechanism of the dry-out.

In annular flow boiling, one can visualize complicated interfacial phenomenon which is difficult to understand from planner sectional view. For this reason, in Figure 4.6, a three-dimensional view of simulation has been portrayed, as representation, where the pipe is heated at 20° of superheat and liquid-vapor velocity is set at 1 and 3.4 m/s respectively (case C in table 3). Here a 90° sector of the pipe has been selected and visualized from the outer direction of the pipe (view AA). As discussed earlier in planar demonstration, initially due to heat transfer from the pipe wall a very thin vapor film is generated beneath the annular liquid film. But due to the film flow waves are generated as a result of Kelvin-Helmholtz instability and eventually, the vapor film breaks up. In Figure 4.6, the dark patches show the vapor nucleation sites,

covered by the liquid film. The darkness of the patches on the liquid film signifies the distance of the liquid interface from the wall surface. Near the entrance, the film breaks into azimuthally symmetric vapor rims and in rest of the pipe length, it breaks into tiny vapor bubbles (at 5-10 ms). The vapor rims also further break up into asymmetric parts which due to the effect of surface tension finally contracts itself and leads to nucleation of bubbles. These vapor bubbles further flow with the liquid film and grow in size. The growth of the bubble is earlier described in two-dimensional implementation in Figure 4.5. Subsequently as described earlier, when these bubbles grow beyond a certain size the liquid film above it bursts and the vapor inside it is released to the core. In the figure the white spots indicate the absence of liquid film above the vapor bubbles, which demarcates the event of the bubble bursting in Figure 4.6. After the bubble bursting the adjacent liquid film tries to rewet the space occupied by the bubble. As a result, at a distance of 10-15 mm from the inlet, the dimension of the vapor patches seems to be reduced compared to the dimensions of the upstream vapor patches. But as the liquid film propagates along the length its thickness reduces and the rewetting capability of the film also reduces. As a result, the dry patches, generated by the bubbles bursting start growing along the length beyond 15 mm from the entry section. After 25 mm the liquid films seems to be distorted due to the enormous growth of the dry patches and some liquid lamellas are only observed at the wall surface. This phenomenon can be represented as dry out. At further downstream, these lamellas become disjoint to each other and gradually reduces in size due to continuous boiling.

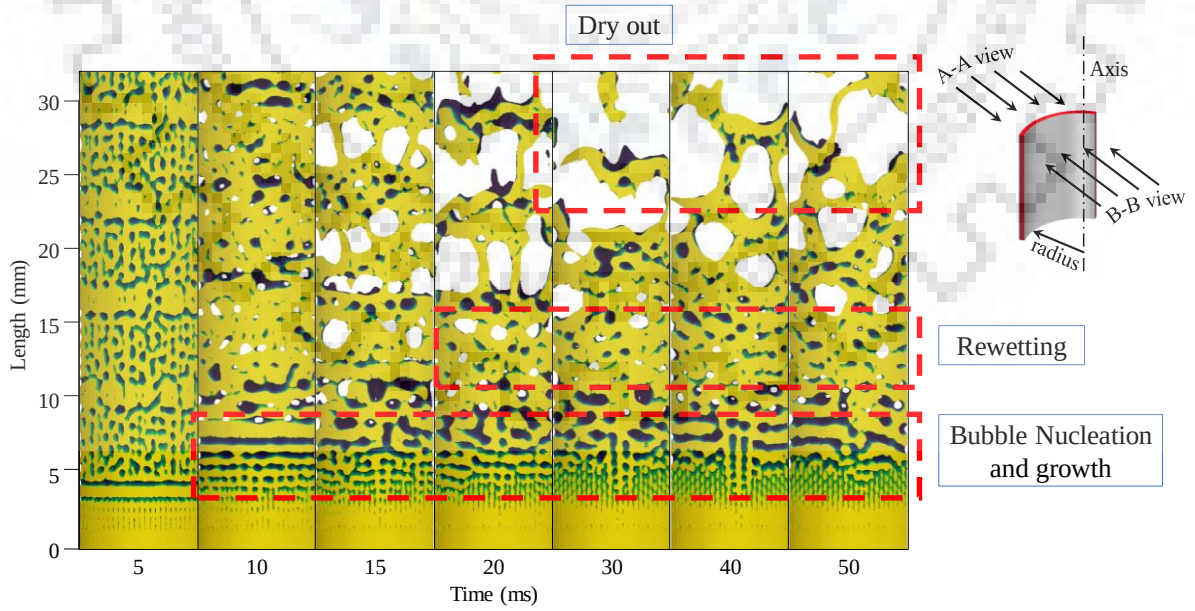

Figure 4.6: Three-dimensional view (from AA direction) of the temporal evolution of liquid film across the pipe length

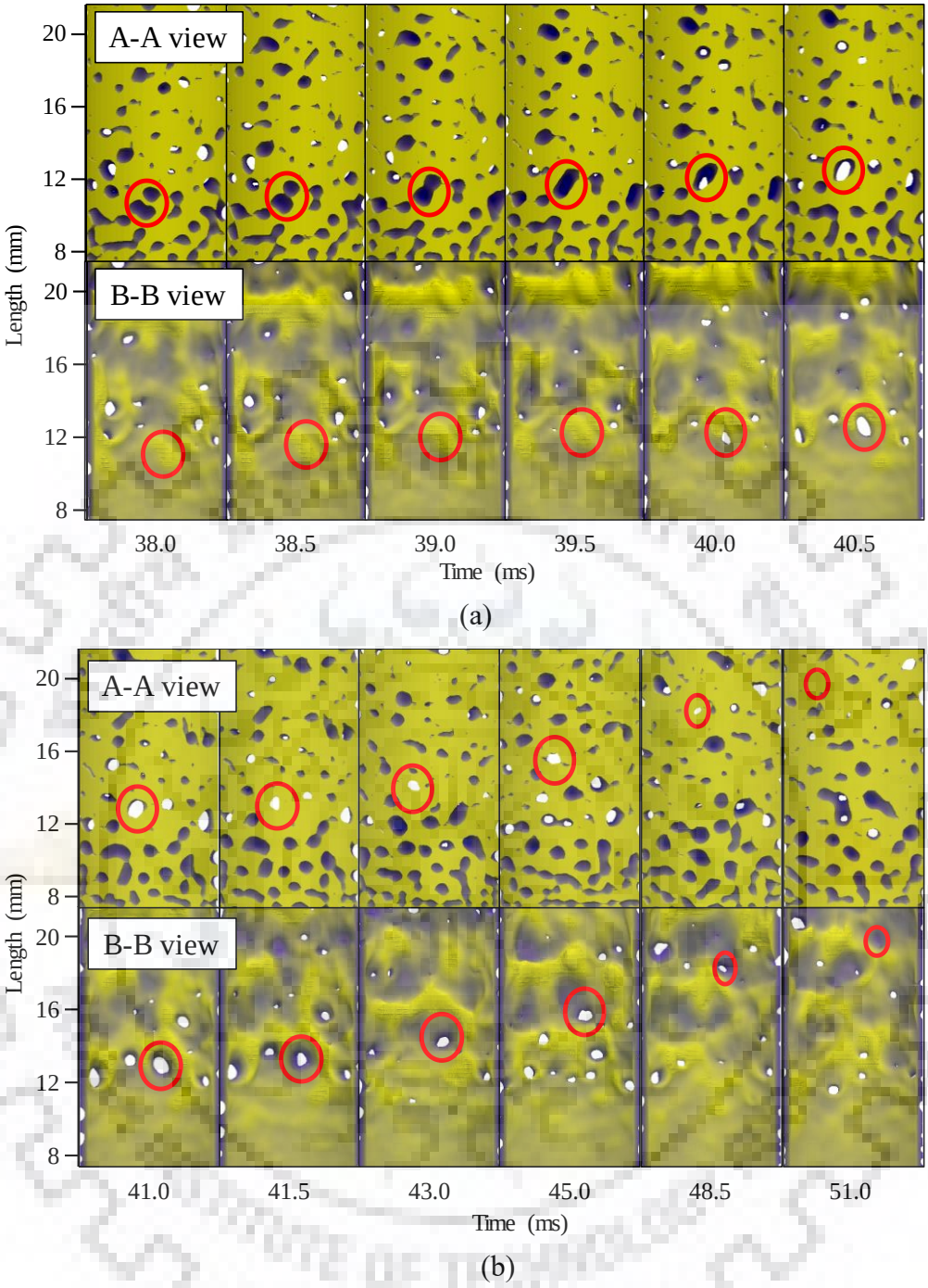

Figure 4.7: Interfacial evolution during two important features responsible for dry out (a) bubble merging and bursting (b) rewetting

One can clearly understand that the bulk behavior of dryout starts from local interfacial dynamics like bubble bursting and rewetting. Same has been demonstrated for representative two cases in the planner and in isometric interfacial profile (Figure 4.5 and 4.6, respectively). The effort has been made to understand some of these interfacial dynamics in detail. For that purpose, a case having slower interfacial evolution is targeted to get adequate temporal

resolution. In Figure 4.7, some bubbles have been tracked for case B and they have been visualized from both direction of the liquid film (view AA and BB; Figure 4.4) as shown in Figure 4.6. In the Figure 4.7 (a), A-A part represents temporal snaps of bubble interaction with film from the outer side of the tube (i.e. AA view) and corresponding inner side view (i.e. BB).

In the AA view, at 38 ms, two encircled bubbles can be observed at very close vicinity. While flowing with the liquid film these bubbles propagate and the distance between the bubbles reduces. As soon as these bubbles touch each other a vapor bridge is formed (38.5 ms) and gradually the bridge expands (39 ms). Finally, the bubbles get unified. But as all these stages occur beneath the liquid film these cannot be observed in BB view, but due to the presence of the bubble, the film seems to be thicker at that zone. Due to the merging process, bubble size increases and becomes unable to accommodate itself beneath the liquid film. As a result, the liquid film above the bubble becomes thinner and finally, bubble pierces the film above it (40 ms), which can be observed from both the views. Afterward, the perforation expands and the vapor inside the bubble gets released to the central vapor core. Once this vapor inside the bubble gets released the small dry patch left by the bubble gradually shrinks as one can see in Figure 4.7 (b). The phenomenon can be termed as rewetting which happens at a faster rate at the beginning (40.5-41.5 ms) and later on slows down. On the other hand, due to boiling liquid film adjacent to the dry patch loses mass, which works against the rewetting phenomenon. At 45-48.5 ms, a wave can be seen approaching to the dry patch from the upstream direction. The wave helps in rewetting and shrinkage of the dry patch. As a result, at 51 ms the dry patch gets totally rewetted but post rewetted film thickness is much thinner as compared to the initial film thickness. It can be observed that stability of rewetting phenomena mostly depends on mutual competition between the boiling rate and interfacial waves, where the first one drags the small dry patches toward dryout and the second one tries to rewet it again. As one move from the inlet to the exit side due to boiling film thickness reduces and the waves also become weaker. Consequently, the chance of rewetting of the dry patches reduces.

To explore the cross-sectional features in terms of interfacial evolutions, case C has been selected as representation. In Figure 4.8 (a) temporal evolution of annular flow has been depicted for two cross sections at 1.09 D and 2.73 D distance from the inlet. An initially similar type of bubbles is generated azimuthally at the heated wall of both the sections. But later on (8 ms onward) lower liquid area can clearly be observed for 2.73 D compared 1.09 D. At 2.73 D the film gets disintegrated into smaller parts and these liquid patches reduce in size. On the other hand, in 1.09 D, the film remains more or less continuous other than some smaller dry

patches. In 2.73 D cross section, entrainment can also be observed (10, 50 ms), but there exists a periodicity in the passage of droplet swarm. This has created occasional dry patches at the core (entrainment absent at 35 ms), whenever a cross section is in between regions of two traveling droplet swarms.

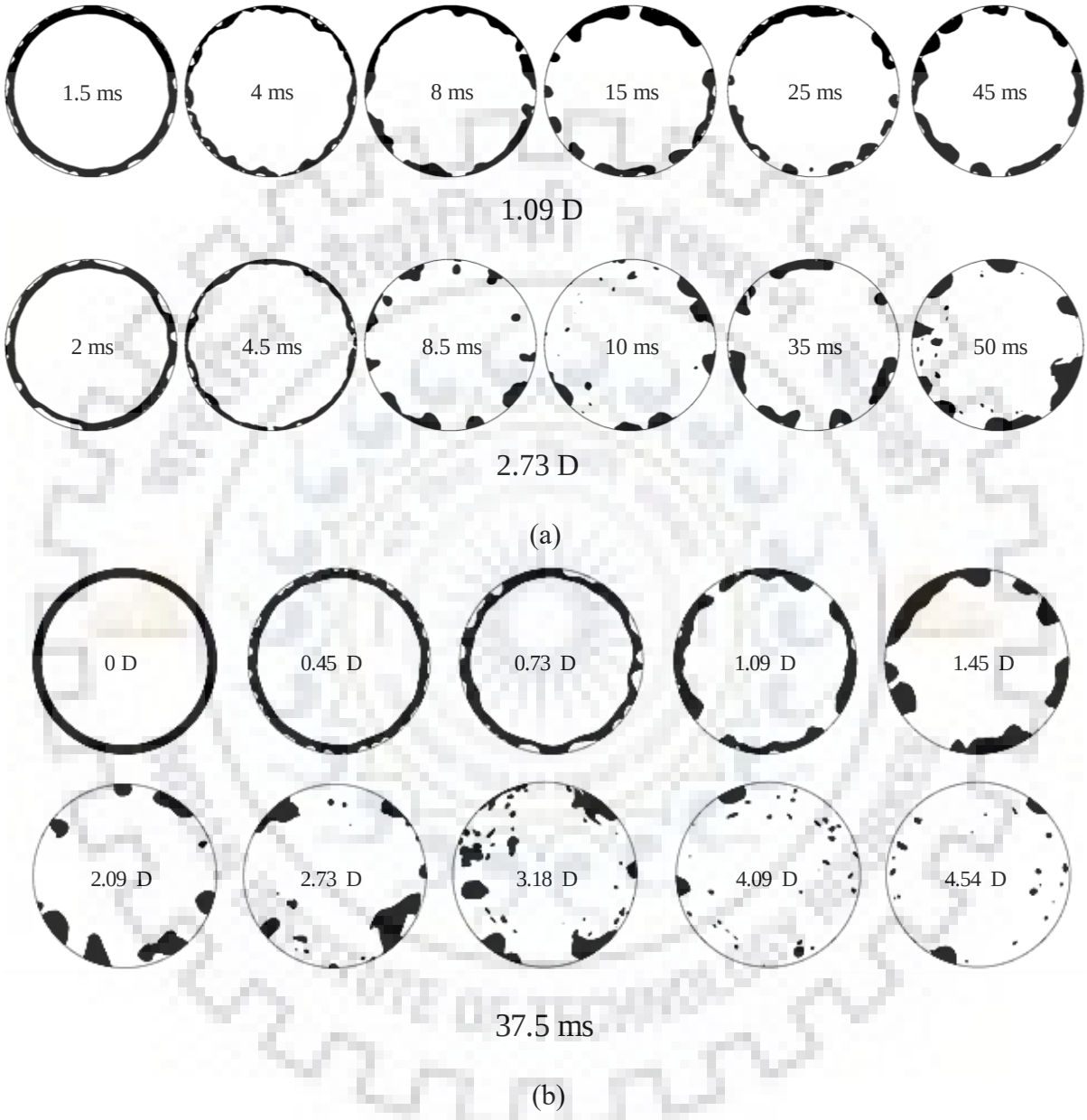

Figure 4.8: Cross-sectional view of annular to droplet flow (a) at different time instant (b) at different axial distance; wall flooding, dry out and droplet population can be clearly observed.

To have a more comprehensive view over the cross sections, in Figure 4.8 (b) liquid phase has been plotted at a particular time (37.5 ms) but for different cross-sectional planes. The non dimensionalized distance of the cross-sectional planes from the inlet plane has been

inscribed inside the Figures 4.8 (b) in terms of pipe diameter. As one can see, starting from uniform thickness annular entry at 0.45D, a huge number of tiny bubbles are formed near the wall. With further advancement in the axial direction (0.73 D) the number of bubbles in the cross-section reduces but bubble size increases due to growth and mutual merging. In the subsequent higher sectional views (1.09 D – 1.45 D), due to the bubble bursting the film becomes azimuthally discontinuous. Gradually, these discontinuities grow in number and length, as a result, the liquid film shrinks into thinner patches (2.09 D). At further downstream, liquid entrainment has been observed at the core of the cross-sectional views. These entrained liquid drops are randomly distributed over the whole space. Initially, this droplet population seems to be increasing with axial distance (2.73 D – 3.18 D) but once the liquid patches on the wall reduce droplet population also reduces gradually (4.09 D – 4.54 D) due to evaporation of mist flow.

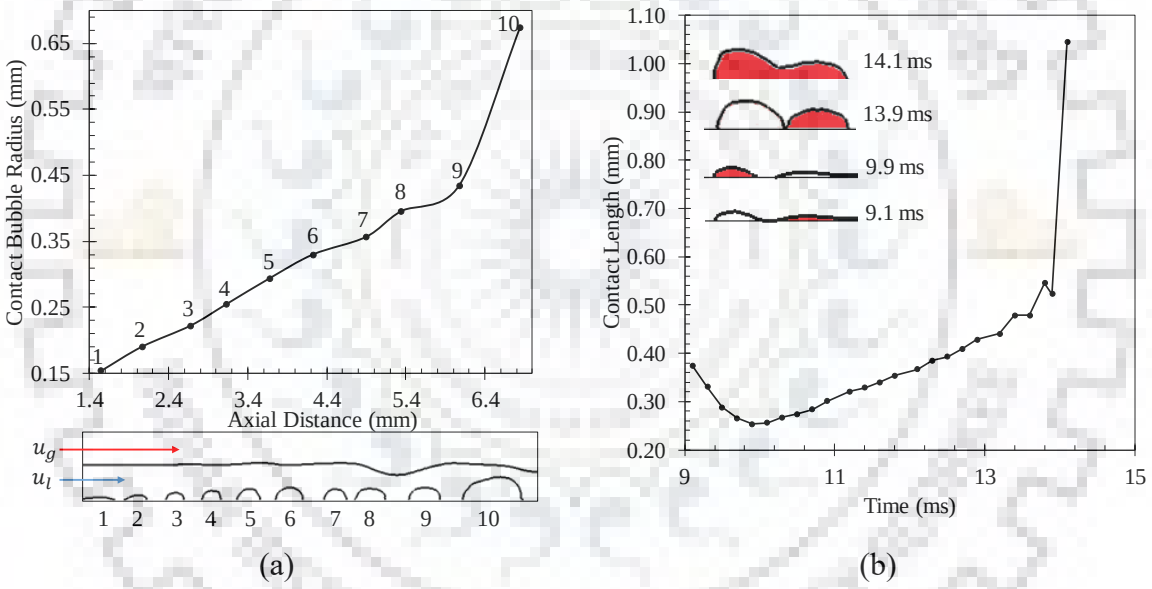

Figure 4.9: Characteristics of bubble growth (a) gradual increase of contact radius along with axial length (b) temporal history of growth at a site

From the results of interfacial behavior, efforts have been made to evaluate specific bubble dynamics in terms of growth rate and merging tendency. The spatial distribution of size for vapor bubbles across the length of the tube is as shown in Figure 4.9 (a). The Figure 4.9 (a) shows continuously increasing bubble size attached with the wall, as one moves up axially. Along with growth bubble are translating in the axial direction which results in a progressive increase in contact radius along the tube wall. Only a small swelling in the thin vapor film can be observed at point 1. Due to change of phase, the vapor is fed to the nucleation causing

growth and liquid inertia shifts the nucleation at point 2. As a result, at location 2, comparatively larger bubble size than point 1 is observed. This procedure continues until two axially neighboring bubbles get closer. The continuous increase in trend of bubble radius, in Figure 4.9 (a), along with axial location demonstrates the same. At point 9 along the axial direction, one can notice a sudden jump in contact radius of the bubble which may be resultant of merging between neighbors. This can be clearly understood from the temporal growth history of a bubble which has been plotted in Figure 4.9 (b). After point 10, the bursting of the bubble occurs from which point measurement of the bubble radius is not feasible. As a result, axial growth distribution of bubble has been only shown till point 10. Dry-out sets in after this axial location. Temporal history of bubble growth has been expressed in terms of contact length with along axial direction of solid at different phases of bubble lifecycle. As the bubble is starting to grow from the asymptotic film, at the beginning contact length seems to be reduced from an infinitely large value. Soon due to the growth of the truncated spherical sized bubble, one can see almost linear increase history of contact length. The pattern of growth in contact length continues until the departure of the bubble or merging with the neighbor happens. In that case, a sharp increase in contact length has been reported in Figure 4.9 (a). At a few time instances, the shape and size of bubbles are reported in Figure 4.9 (b).

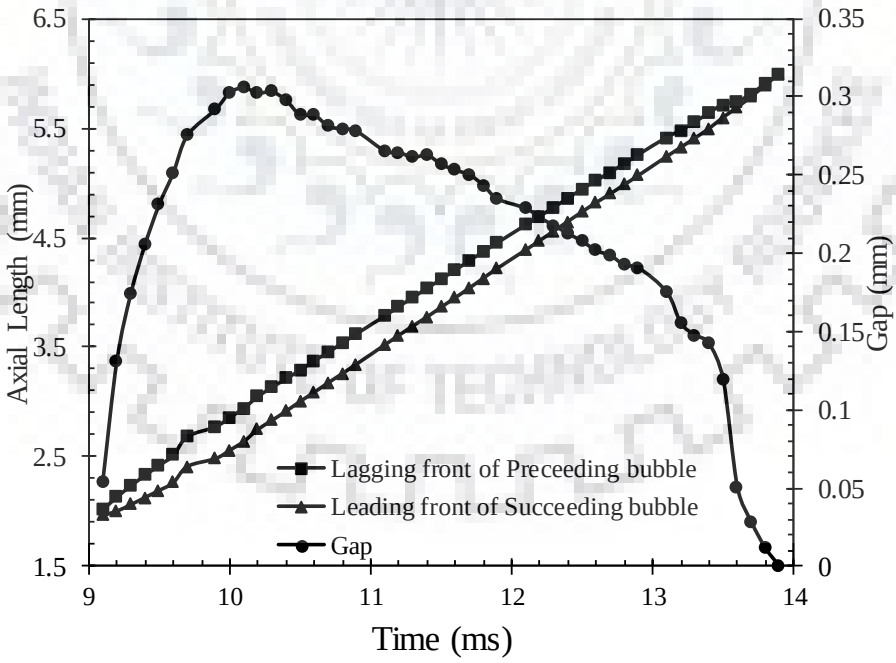

Figure 4.10: Temporal history of growth and drainage of liquid bridge between neighboring bubbles leading towards merging; advancing and receding fronts of succeeding and preceding bubbles are tracked to determine the gap at a particular time.

To observe the fluid dynamics around two bubbles indulging in the merging process, efforts have been made to identify and track advancing and receding fronts. As during nucleation (9.1 ms) both the bubbles start from a film, these are supposed to have almost no liquid bridge between them at a very high radius of curvature. With growth, these bubbles first go away from each other signifying reduction in radius of curvature and an increase in the mutual gap. Once these bubbles attain hemispherical shape due to a continuous supply of vapor, the radius of curvature starts to increase and bubbles come closer to each other. This will reduce the gap between bubbles by driving away the film. In this phase, advancing in front of succeeding bubble and receding front of the preceding bubble will come closer to each other. At the time instance of merging (14 ms), these two ends of bubbles coincide to initiate the unification process. Due to the flow of liquid both the bubbles are seen to move up even during the merging process which causes an increase in axial location of advancing and receding fronts of succeeding and preceding bubbles. Figure 4.10 describes the overall merging process along with an account of the gap between the bubbles.

4.5.2 Effect of degree of superheat and phase velocities:

To observe the effect of parametric variation on liquid film evolution across the pipe length in Figure 4.11 comparison of the same has been studied for the same time instant (62.5 ms) from A-A direction. In Figure 4.11 (a) comparison of three degrees of superheats has (10, 20 & 50˚C) been portrayed. One can clearly observe from the Figure 4.11 (a) that dry out length is continuously decreasing from ~3D (35 mm for 10˚C) to ~1.5D (15 mm for 50˚C) with an increase in wall degree of superheat. At a higher degree of superheat, due to a higher rate of boiling, increase in bubble diameter has also been observed beneath the liquid film. Close look on the post dry out region also shows that the size of the lamellas generated from the liquid film decreases at a higher degree of superheat. Effect of flow conditions on interfacial evolution has been also studied and some representative liquid distribution along axial lengths are shown in Figure 4.11 (b). Comparison of case C and H shows that at the higher liquid velocity the film dry out is delayed. Moreover, at higher liquid flow bubble bursting and rewetting zone is also shifted downstream. Variation of vapor flow rate can also be observed by comparing interfacial contours for the cases A, C, E, and F. Among cases A, C and E significant change in dry out length has not been observed, but with an increase in flow rate, nature of post dry out lamellas has changed to thinner one. But for case F due to very high gas velocity liquid film got disrupted

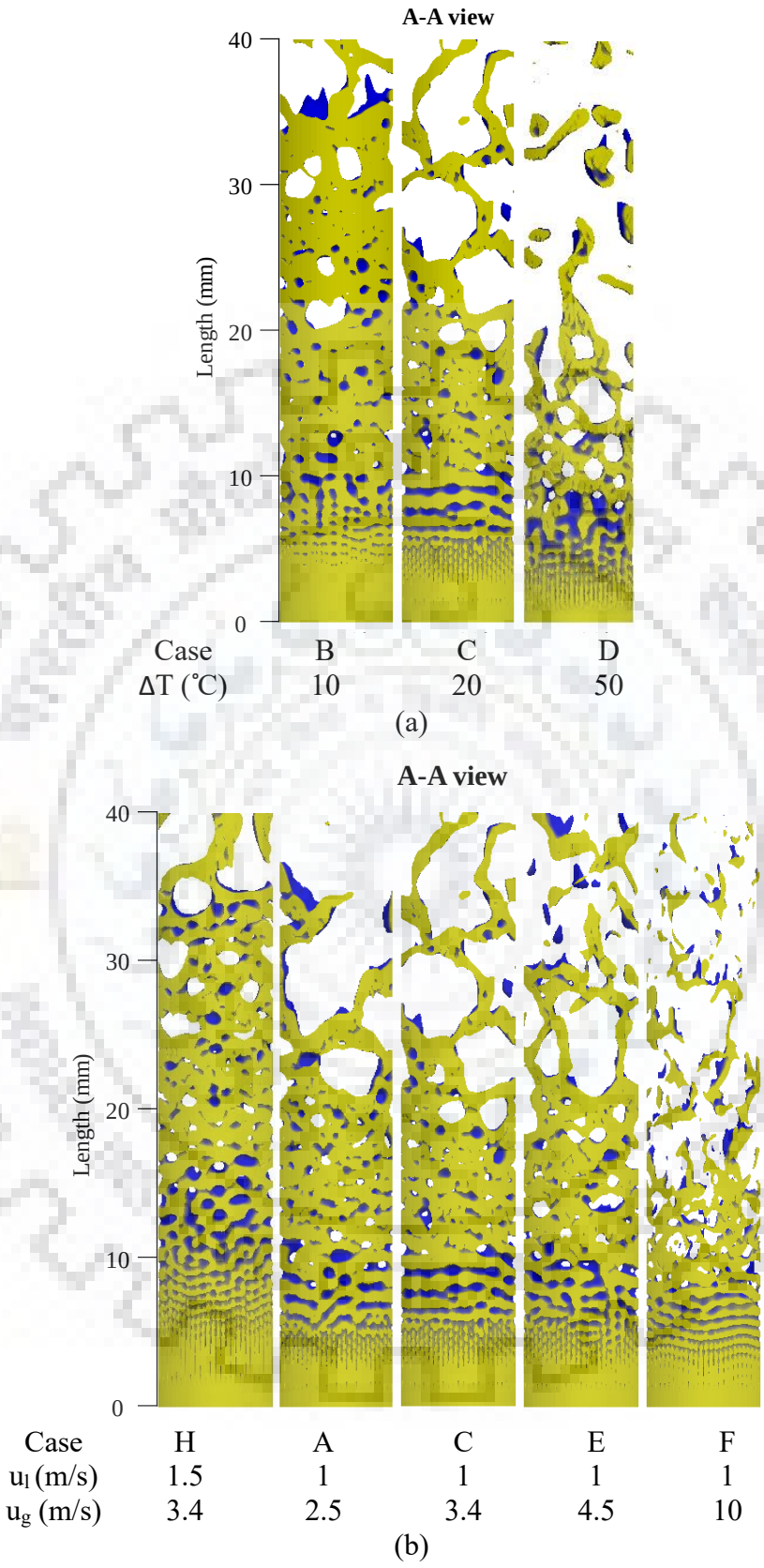

Figure 4.11: Comparison of liquid film evolution and dry out length (a) for different degree of superheats and (b) for different flow conditions

and dry out occurred well before compared to A, C, and D. This dry out is not due to boiling, but entrainment due to high gas velocity leads the liquid film toward dry out. Here, high gas velocity tears liquid film into smaller parts, as a result, elongated lamellas are not found at post dry out region.

Effect of bubble nucleation and its bursting at the annular film surface can be clearly understood from the percentage of vapor present in the annular liquid domain, given as initial condition. Nucleation and its growth will generate vapor inside annular film from the side of the wall due to heat transfer. On the other hand, the formation of a wave due to the relative velocity of liquid and vapor will allow gaseous vapor to penetrate from the core side of the annular film. Bursting of a growing bubble in the inner film adds on the situation and drastically increases vapor presence through the phase of dry-out. These three processes are a major reason for an increment of a percent in vapor present in the annular film. On the other hand, hot tube wall rewetting by liquid lowers the presence of vapor in the liquid region. Initially, due to heat transfer, the conducive situation for vapor formation increases the percentage presence as time progresses. Once the rewetting starts from local dry-out sites presence of local annular film becomes more or less stable. Similar pattern has been shown in Figure 4.12 (a), where at the beginning increasing trend of vapor presence has been observed for different degrees of superheat and then the presence of vapor in liquid film region gets stable. Comparison between three different degrees of superheats (10, 20, 50 °C; Case B, C, D) clearly depicts faster vapor intrusion in the liquid region with an increase in superheat. Bubbles are nucleated and burst at a faster rate at a high degree of superheat and reached to a higher percentage of steady state vapor presence in the liquid region, given at the beginning of the simulation. At steady state, the percentage of vapor present in the liquid region increases with increase in superheat.

Similar efforts to study the present presence of vapor volume in the annular region have been reported for varying liquid and vapor inflows (Figure 4.12 (b)) with an increase of vapor velocity (case C to case F) faster decrease in liquid occupancy is observed in the annular region. This symbolizes more frequent dry out spots at higher vapor velocities. It can be also noted that even at steady state percent of vapor volume in terms of initial annular liquid volume, is higher for higher values off vapor velocities. On the other hand, when liquid velocity increased there is the lesser provision of disturbance wave and formation of vapor in the annular liquid region will be mainly governed by nucleating bubble. Due to the reduction of amplitude in a wave from core side lesser vapor penetration will be there in the annular liquid when liquid velocity is increased (case C to case H). As a result, case H will stabilize at a further lower

percent of vapor presence than case C. More rewetting can be observed at higher liquid velocities along with lesser bubble bursting stages.

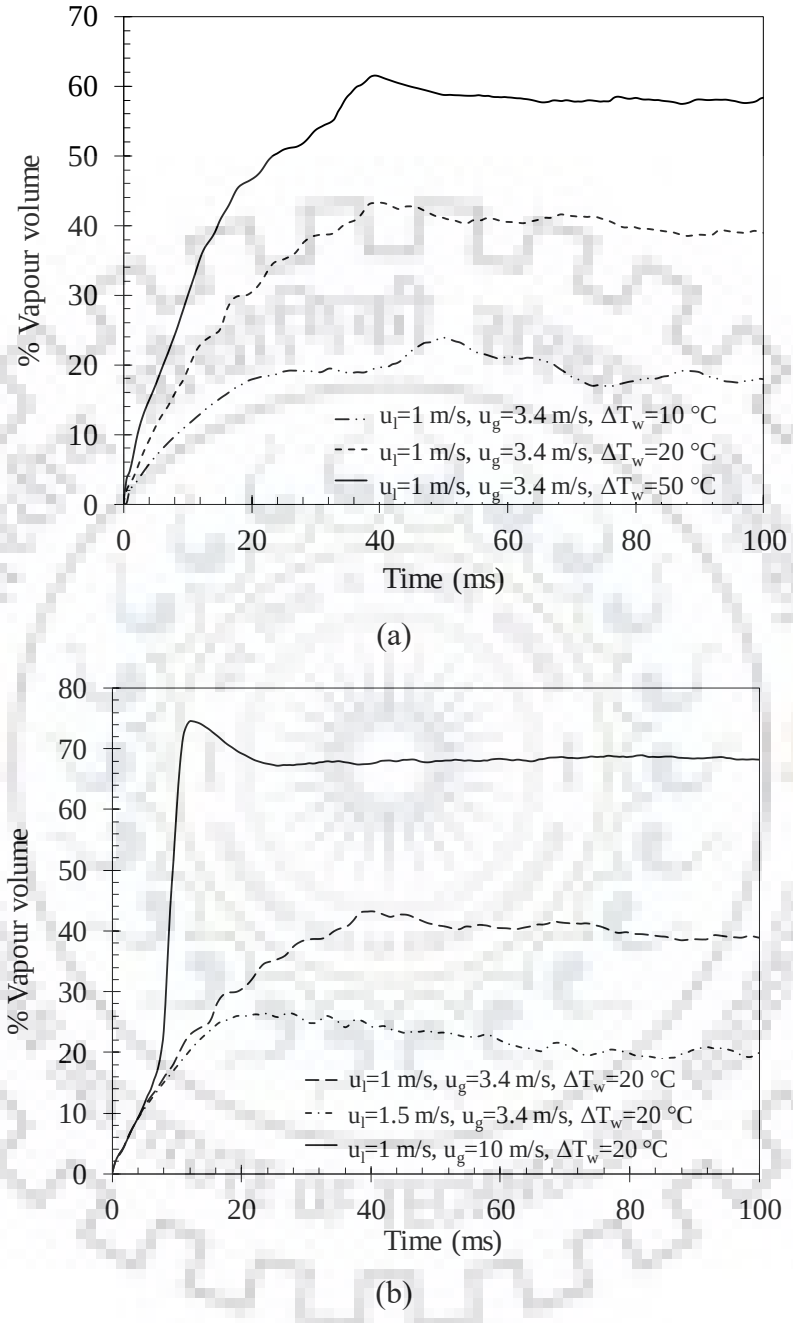

Figure 4.12: Plot of generated % vapor volume generated vs time (a) for different degrees of wall superheat (b) for different vapor velocities

Inventory of liquid and vapor has been also monitored at the different cross-sectional plane of the simulation, which may have randomly changing values due to transient interfacial dynamics. Figure 4.13 (a)-(b) depicts the presence of liquid in a few cross-sectional planes in terms of phase fraction for case C, as representative. At the inlet, due to the boundary condition,

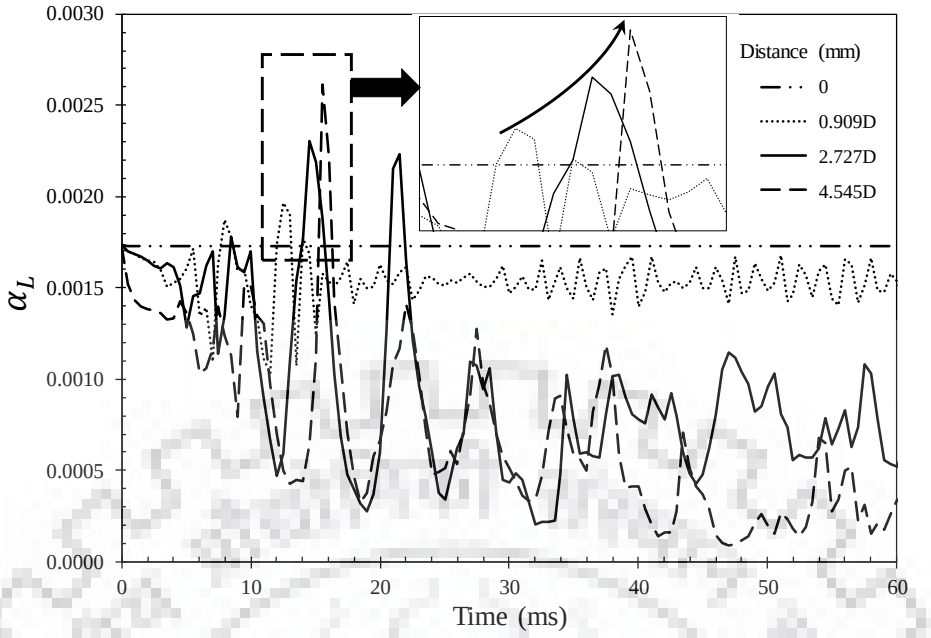

(a)

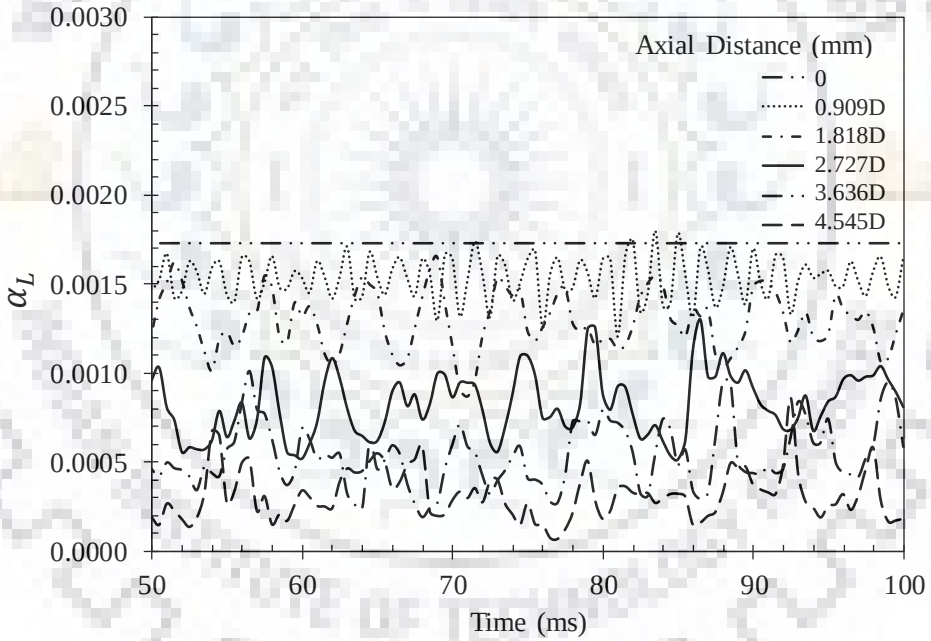

(b)

Figure 4.13: Fluctuation of liquid phase fraction with time at different cross-sections
(a) Passage of disturbance wave in the axial direction and its effect on liquid volume fraction in cross-sectional planes. (b) Account of steady-state fluctuations in liquid phase fraction due to life-cycle of a bubble generated in phase change.

liquid phase fraction remained constant. Afterward, lines for different cross-section starts reducing due to boiling. In parallel, some fluctuating component can also be observed in the

plots at a different plane, which is mainly due to wave and bubble passage through the cross-sections. At very initial stage passage of these waves can be clearly seen from the zoomed comparison of volume fraction history at different volume fraction planes. A peak in wave signifies the passage of disturbance wave in a cross-section and increase of the peak magnitude of liquid phase fraction shows continuous development of amplitude of disturbance wave. Disturbance wave reaches a later time in higher axial locations than 0.91D. In the later stages, these disturbance waves go away and interfacial phenomena mainly become dominated by vapor dynamics generated from the hot wall. Continuous breaking and making of these interfaces as described above will give rise lots of fluctuations in the account of liquid presence. The same can be seen in Figure 4.13 (a). These disturbances in liquid phase fraction will fluctuate around a steady value due to a similar rate of making of the interface during nucleation and breaking of the same during bursting. For case C, shown as representation, abrupt fluctuations due to disturbance wave goes away from the computational domain and volume fraction attains pseudo-steady value around 40 ms. At this steady state condition, a distinct range of phase fraction value for each cross-section can be identified from Figure 4.13 (b). In the signals, shown in Figure 4.13 (b), it can be clearly identified that with an increase in distance from the inlet section range of liquid phase fraction value shifts toward a lower value.

Efforts have been made to understand the details of these fluctuations by mathematical analysis of the same. To begin with, in Figure 4.14 (a), the average value of the temporal variation of the liquid phase fraction has been reported against the axial distance from the inlet. Account of average liquid volume fraction variation across axial distance is reported for three different degrees of wall superheat (Case B, C, and D). Average value of liquid fraction decreases continuously as the flow moves up, which is evident from the effect of heat transfer and subsequent phase change. In all three cases, one can observe instantaneous dry-out at some azimuthal locations followed by rewetting by liquid packets. A careful comparison between average values at different degrees of superheat reveals that dry-out occurs more frequently and azimuthally at a greater number of places while higher (50 °C) superheat is applied, causing temporal average of liquid phase fraction value to reach very near to zero. It is also observed that at a higher degree of superheat the liquid fraction reduces faster along the length. A close look on the trend of these plots reveals a lower slope region near to the entrance, after that the slope of increases and post dry out slope reduces again. One can refer Figure 4.6, where dry out happens near 30 mm distance from the entrance and in Figure 4.14 (a) also slope of the 20°C (Case C) superheat line reduces at almost same axial position (~30 mm). To understand

the reason behind fluctuating values of liquid phase fraction, the standard deviation of the same has also been plotted in Figure 4.14 (a). Due to uniform and constant inlet velocity boundary condition near the entrance standard deviation is very small. Afterward, as the flow propagate

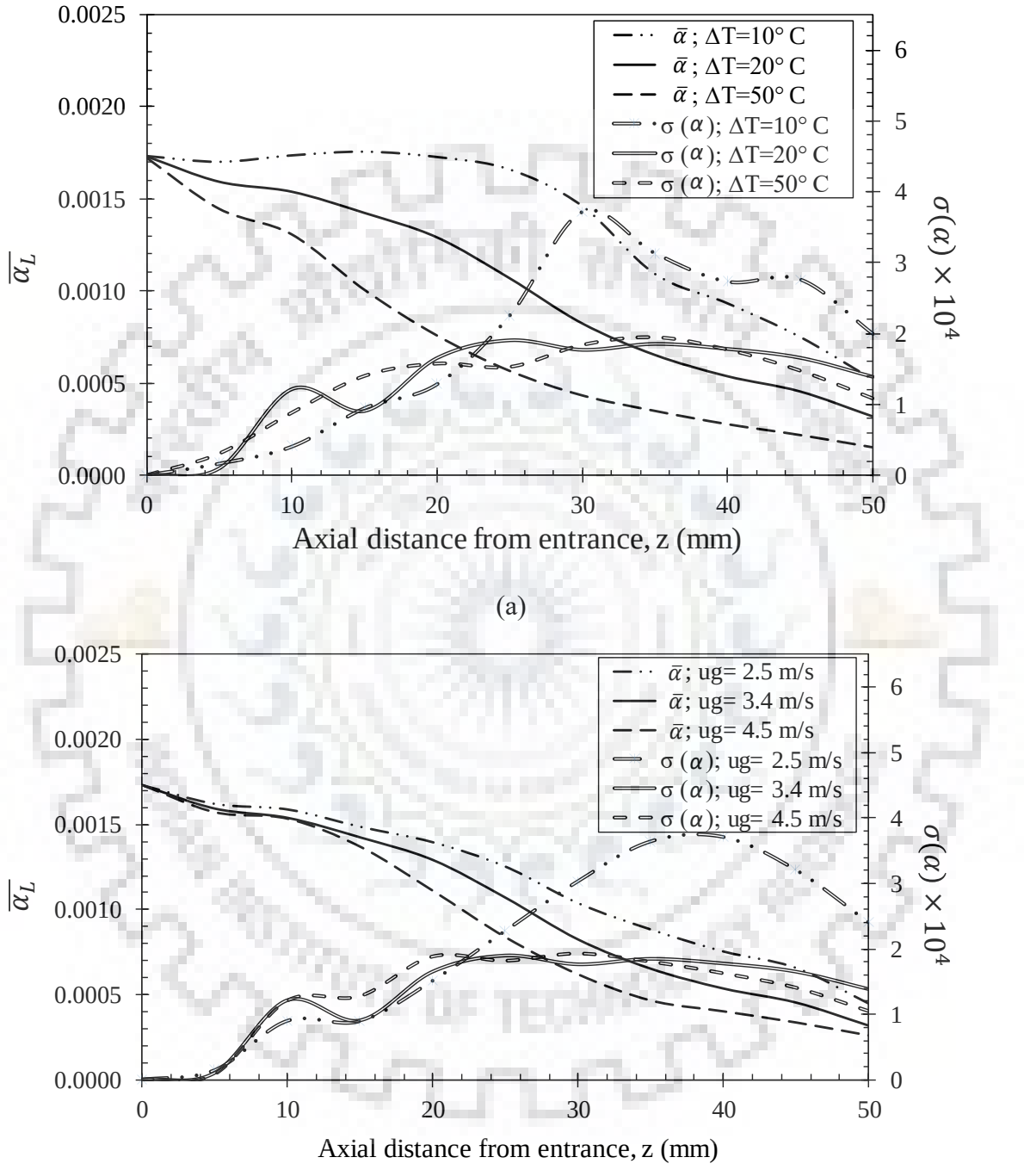

Figure 4.14: Variation of mean and standard deviation of liquid phase fraction over the length of the pipe (a) for different degrees of superheat (b) for different vapor flow rates

away from the entrance, due to wave and vapor bubble generation, the standard deviation of the liquid fraction rises up to a certain value. But soon dry out triggers in and liquid quantity left in the domain becomes very small. As a result, fluctuation in liquid fraction reduces and standard deviation becomes lower. From Figure 4.14(a) one can observe that standard deviation for 20°C and 50°C superheat does not show much difference in value but for 10°C superheat one sharp peak is obtained. This peak is due to the formation of bigger lumps of liquid from the liquid film under the presence of a lower evaporation rate. But in case of the higher degree of superheat liquid film dries up faster and only smaller lamellas can form instead of bigger lumps. As a result, such a peak of standard deviation is not observed in higher degrees of superheat (Case C & D).

A similar effort has been made to observe the effect of vapor flow on average liquid phase fraction. In Figure 4.14 (b), mean and standard deviation of liquid phase fraction for three different vapor velocities (2.5 m/s, 3.4 m/s and 4.5 m/s) have been shown against axial distance. Though the difference in this case is not that distinct as compared to the variation of the degree of wall superheat, still at higher vapor flow rate faster drop in cross-sectional average liquid phase fraction can be clearly noticed. At higher vapor flow rate liquid film will also be accelerated, which finally helps in enhancing convective heat transfer and subsequently results into a higher rate of boiling. On the other hand, the standard deviation curves for 3.4 and 4.5 m/s vapor velocities nearly shows a similar pattern but as the vapor velocity is reduced to 2.5 m/s, vapor becomes unable to drag the liquid film effectively. As a result, the film transforms into larger liquid lumps leading to a higher value to standard deviation.

To have a comprehensive view of the variation in liquid phase fraction, attractor, a plot of ($\beta_{L,x.t+\Delta t}$, $\beta_{L,x,t}$), has been carefully studied, where liquid phase fraction has been mapped to itself after non-dimensionalisation as $\beta_{L,x,t} = {}^{\alpha_{L,x,t}}/_{\alpha_{L,x=0,t}}$.In Figure 4.15 (a) attractor plot for different cross sections of 20°C superheat has been demonstrated. Near the inlet (10 mm) all the mapped data points of the attractor plot are concentrated over small region. Afterward, as flow moves at 20 mm from the inlet, data points spread towards origin. Thereafter, at 30 mm the range of liquid phase fraction sharply drops and a similar trend has been followed for further axial locations from inlet keeping nature of scattering intact. At 50 mm, attractor plot data points again accumulate over a smaller area near the origin, because due to complete dry out fluctuations also have died down significantly. Comparison of attractors at different planes

shows the tendency of liquid phase fraction towards dry-out and fluctuations are reported through scatter in the intermediate axial lengths, away from inlet and dry-out locations.

In Figure 4.15 (b), a mutual comparison of the attractor plots for different degrees of superheat has been presented. It can be observed that for 10°C many data points cross the inlet liquid fraction value marked by red dotted line. Even some data points for axial distance 30 mm are crossing the inlet phase fraction and some others are also extended till 0.5 value, which shows the extent of dispersion of the data points. This also shows randomness in the interfacial evolution through breaking and making, in the whole span of bubble life-cycle. On the contrary, in case of 50°C superheat all the data points of the attractor plot are much below the red dotted line (phase fraction at inlet) and they are accumulated within smaller area showing lesser randomness and quick reach towards dry-out.

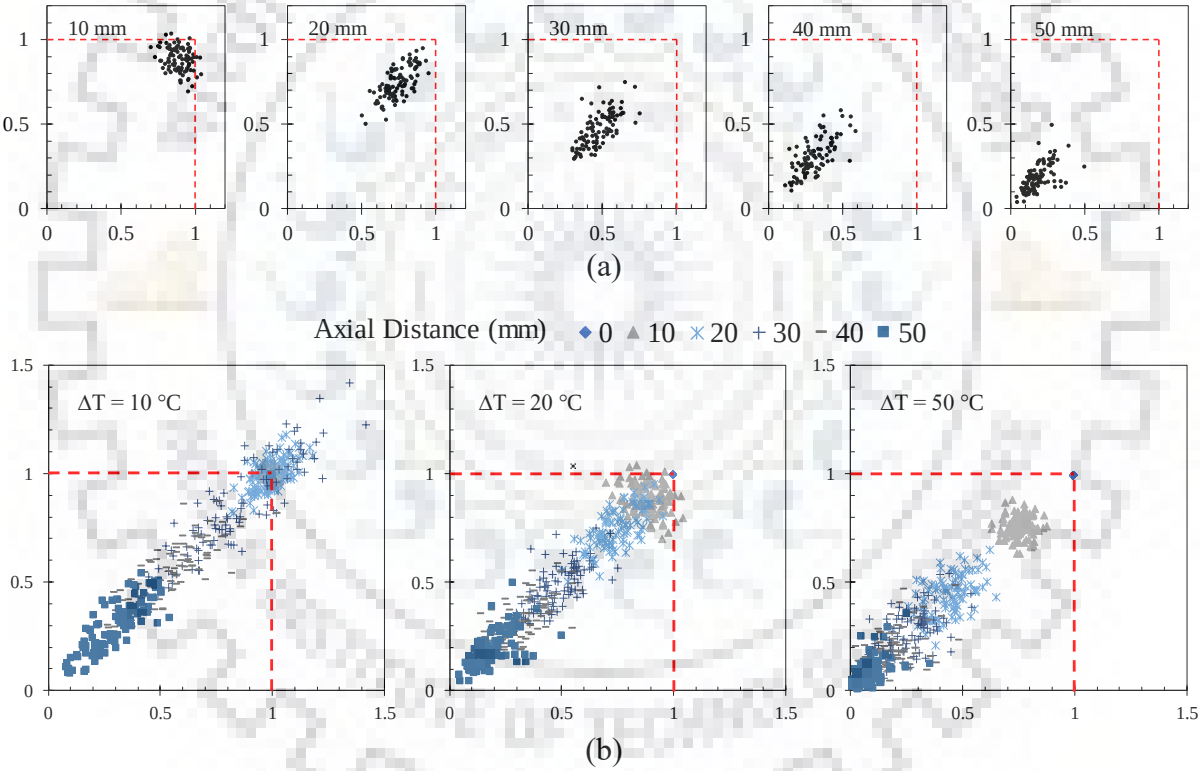

Figure 4.15: Attractor plot of non-dimensionalised liquid phase fraction (a) at different cross sections for 20°C superheat; Case C (b) at different degrees of superheats; Case B, C & D

An effort has been also made to understand the thermal analysis of interfacial making and breaking process. To characterize the same, average heat transfer coefficient at different axial planes have been evaluated from simulations. An axial variation of the same has been plotted in Figure 4.16 (a) & (b). For mutual comparison of heat transfer characteristics between different applied degrees of superheat at the wall, in Figure 4.16 (a), plots are shown for 10, 20

& 50 °C (Case B, C & D). Careful analysis of each curve shows an initial drop of heat transfer coefficient for a very prompt period. This has resulted from the formation of thin vapor cover

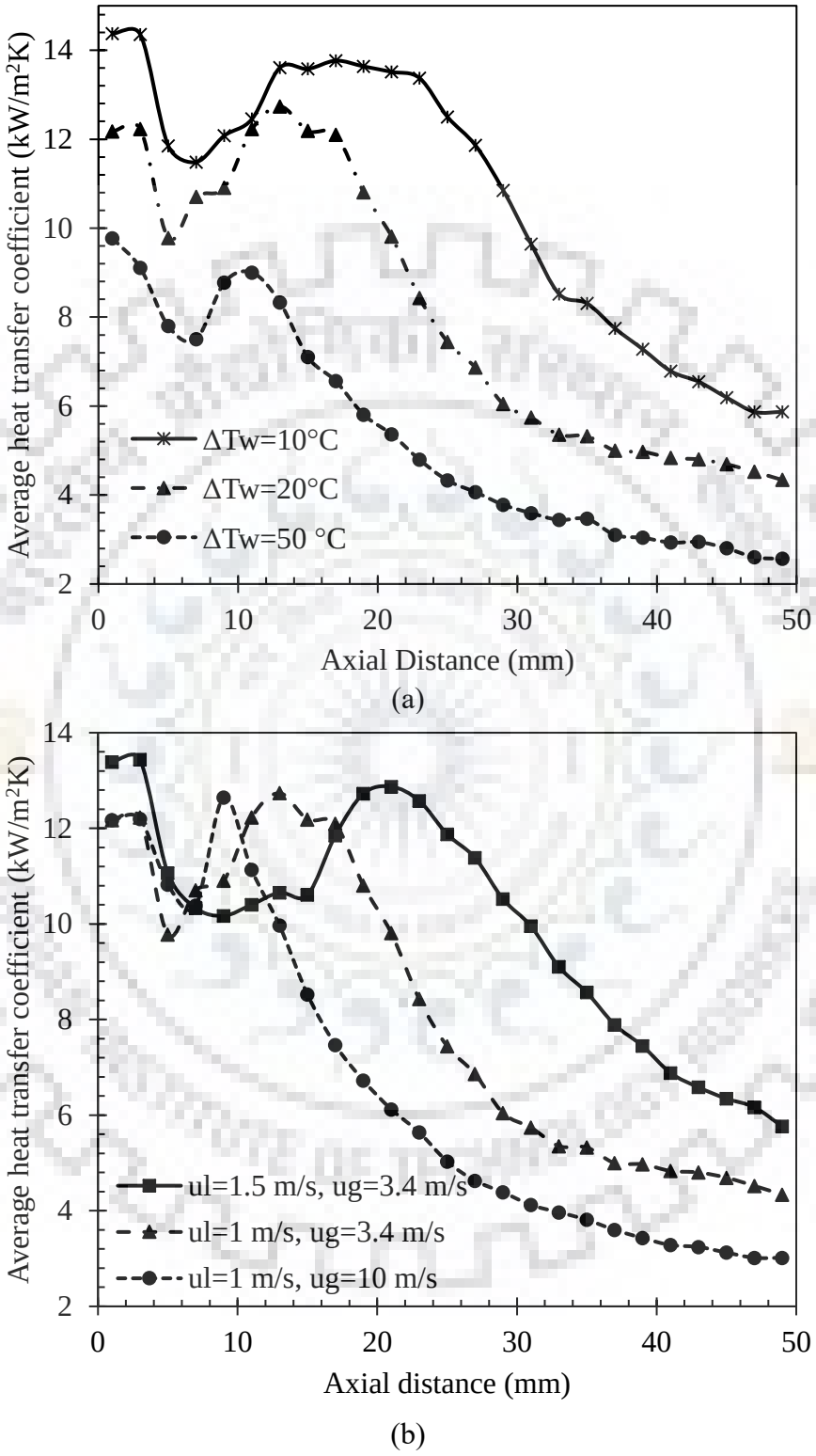

Figure 4.16: Variation of heat transfer coefficient against axial distance (a) for different degree of superheat (b) for different liquid and vapour velocity

throughout the domain at a lower axial length. As flow progresses in a higher axial domain, vapor film becomes thicker due to buoyancy and instability triggers in nucleation. In this region of axial location, due to the release of vapor and replenishment of liquid from the film, the heat transfer coefficient has been seen to be increased. Such nucleation and growth process continues up to certain length before bubble bursts at annular interfacial surface. This results in a small drop in the heat transfer coefficient for all the applied degrees of superheat in the wall. As a next consequence, rewetting happens which increases the heat transfer coefficient from dryout in a very prompt zone. But this rewetting will diminish its effect due to more and more dryout spots created in different azimuthal locations. Hence, in heat transfer pattern a continuous decrease is noticed signifying more and more dryout spots as flow moves up axially.

A careful comparison between different curves in Figure 4.16 (a), for variable degrees of superheats, establishes lesser span of the axial zone for nucleation for higher degree of superheat. Heat transfer coefficient throughout the tube reduces drastically for an increase in the applied degree of superheat due to an increased rate of change of phase. It can be also noticed that at higher degree of superheat heat transfer coefficient is nearing towards a very small value, owing to arriving at faster dry-out. similar trend is seen for average heat transfer coefficient for different liquid and vapor velocities.

At higher liquid velocity nucleation and bursting of bubbles at higher axial heights causing delay in reaching the highest heat flux. As the superheat is same in both liquid velocities, maximum average heat transfer coefficient has been also noticed as same. But in the dry out zone higher liquid velocity shows better heat transfer coefficient due to transportiveness of heat. On the other hand, at higher vapor velocity (case F) film becomes thinner causing bursting and dry out faster than the same in low liquid velocity (case C). Figure 4.16 (b) also shows that the average heat transfer coefficient may fall to a very low value in case of high vapor velocity.

CHAPTER 5

CONCLUSION AND FUTURE WORK

In present study boiling has been investigated numerically. The detailed study of wire boiling has been performed with both single and two wires at different orientations and arrangements. Also route to dry out has been investigated in case of annular flow inside cylinder with external heat supply and salient features of annular flow boiling has been identified. Significant findings of this study are summarised in this chapter. At the end of the chapter future work has also been mentioned.

5.1 Key findings

5.1.2 Wire Boiling:

i. Even in the case of wire boiling with perfectly smooth horizontal wire (i.e. in absence of any physical nucleation site), due to buoyancy and film instability nucleation of bubble happens.

ii. In case of horizontal boiling around the horizontal wire, with an increase in the degree of superheat boiling rate increases and simultaneously the bubble size and population also grows. Due to bubble merging, away from corners of the wire bigger size bubbles are released.

iii. With increase is wire inclination, the bubble sliding tendency along the wire increases and the frequency of successful merging enhances. In boiling around the inclined wire, increase in average bubble size has also been noticed along the axial length of the wire toward upward direction. At higher inclination average bubble size and boiling rate increases but bubble population reduces.

iv. In boiling around the vertical wire, non-linear type of boiling curve has been reported, which later on stabilizes to a nearly constant rate.

v. When an active or a passive wire is placed above an active wire, bubble suppression has been observed at the bottom wire. For active upper wire due to merging with the bubbles of upper wire, size increases during departure. For

passive upper wire, delayed bubble departure is observed, leading to bigger bubble size at departure. In the former case, enhancement in boiling heat transfer has been reported but in the latter one boiling heat transfer reduces. Also, boiling rate is increased when the passive wire is placed below the active wire.

vi. In case of boiling around two active wires placed in a same horizontal plane, with a decrease in wire spacing, the boiling rate reduces due to trapping of vapour bubbles in between two wires. At 2 mm wire spacing, continuous vapour film is generated in between wires.

5.1.2 Internal Annular Boiling:

i. In the annular flow boiling small bubbles are generated beneath the liquid film and they grow due to boiling and merge among themselves.

ii. When the bubbles grow comparable to the film thickness, they burst and small dry patches are generated. Waves on liquid film tries to rewet the dry patches but boiling tries to expand them. Relative strength of them finally decides the fate of the dry patch, whether it will be rewetted or be expanded to dry out condition.

iii. Rewetting enhances heat transfer but its length reduces with higher degree of superheat, leading the flow toward early dry out.

iv. Entrainment of liquid drops and lamellas observed from the waves of liquid film. Maximum entrainment of liquid has been observed near the dry out region. Post dry out droplet population gradually reduces in axial direction.

v. Stronger waves and higher temporal fluctuation of phase fraction has been observed for lower degree of superheat. On the other hand, at higher degree of superheat liquid phase fraction shows faster decrement with less fluctuation.

vi. Heat transfer coefficient shows axial variation before dropping down to a very low value as observed in dry out. Higher degrees of superheat, lesser liquid flow rate and higher vapour flow rate may lead towards very small value of heat transfer coefficient signifying dry out.

5.2 Future work

While going through the present study few new research areas has been identified, which can push our understanding about boiling one step forward.

5.2.1 Wire Boiling:

i. Saturated pool wire boiling has been studied in present work. It will be interesting to see numerical simulation of subcooled wire boiling, which may lead us to better explanation of bubble oscillation around boiling wire.
ii. Effect of wire dimension on the boiling bubble size and population can be a good are to be investigated.
iii. Wire-wire interaction has been studied in present work. As a future work it will be very interesting to study how they are interacting with each other wile boiling from a wire mesh and how nucleation is happening from the junctions of the wire mesh.

5.2.1 Internal Annular Boiling:

i. In present study annular flow boiling has been investigated numerically inside tube. In future study can also be done outside tube and comparison can be done how it is behaving differently than inside tube.
ii. Further extension of this work can be numerical study of boiling from rod bundle, which will be very much important for nuclear industry.

REFERENCES

Adamsson, C. and Le Corre, J.M., 2011. Modeling and validation of a mechanistic tool (MEFISTO) for the prediction of critical power in BWR fuel assemblies. *Nuclear Engineering and Design*, *241*(8), pp.2843-2858.

Barbosa Jr, J.R., Hewitt, G.F. and Richardson, S.M., 2003. High-speed visualisation of nucleate boiling in vertical annular flow. *International journal of heat and mass transfer*, *46*(26), pp.5153-5160.

Brackbill, J.U., Kothe, D.B. and Zemach, C., 1992. A continuum method for modeling surface tension. *Journal of computational physics*, *100*(2), pp.335-354.

Collier, J.G. and Thome, J.R., 1994. *Convective boiling and condensation*. Clarendon Press.

Das, A.K., Das, P.K. and Saha, P., 2009. Performance of different structured surfaces in nucleate pool boiling. *Applied Thermal Engineering*, *29*(17-18), pp.3643-3653.

Das, A.K., Das, P.K. and Saha, P., 2007. Effect of a rotating flow field on boiling heat transfer from a flat surface. *Journal of Enhanced Heat Transfer*, *14*(1).

Dhir, V.K., Duffey, R.B. and Catton, I., 1979. On the quenching of a four rod bundle. In *ASME Fluid Flow and Heat Transfer Over Rod or Tube Bundle, Winter Meeting* (pp. 231-238). American Society of Mechanical Engineers.

Di Marco, P. and Grassi, W., 2002. Motivation and results of a long-term research on pool boiling heat transfer in low gravity. *International journal of thermal sciences*, *41*(7), pp.567-585.

El-Genk, M.S. and Saber, H.H., 2001. Minimum thickness of a flowing down liquid film on a vertical surface. *International Journal of Heat and Mass Transfer*, *44*(15), pp.2809-2825.

Emonot, P., Souyri, A., Gandrille, J.L. and Barré, F., 2011. CATHARE-3: A new system code for thermal-hydraulics in the context of the NEPTUNE project. *Nuclear Engineering and Design*, *241*(11), pp.4476-4481.

Glück, M., 2007. Vertrauen und Legitimation durch Bürgerzufriedenheit. *Diss. Universität St. Gallen, Bern: Haupt Verlag*.

Haramura, Y. and Katto, Y., 1983. A new hydrodynamic model of critical heat flux, applicable widely to both pool and forced convection boiling on submerged bodies in saturated liquids. *International Journal of Heat and Mass Transfer*, *26*(3), pp.389-399.

Hendricks, T.J., Krishnan, S., Choi, C., Chang, C.H. and Paul, B., 2010. Enhancement of pool-boiling heat transfer using nanostructured surfaces on aluminum and copper. *International Journal of Heat and Mass Transfer*, *53*(15-16), pp.3357-3365.

Hewitt, G.F. and P.M.C. Lacey, 1965. The breakdown of the liquid film in annular two-phase flow. *International Journal of Heat and Mass Transfer*, *8*(5), pp.781-791.

Kumar, P., Das, A.K. and Mitra, S.K., 2016. Physical understanding of gas-liquid annular flow and its transition to dispersed droplets. *Physics of Fluids*, *28*(7), p.072101.

Lafaurie, B., Nardone, C., Scardovelli, R., Zaleski, S. and Zanetti, G., 1994. Modelling merging and fragmentation in multiphase flows with SURFER. *Journal of Computational Physics*, *113*(1), pp.134-147.

Lu, S.M. and Lee, D.J., 1989. Effects of heater and heating methods on pool boiling. *AI Ch. E. Journal (American Institute of Chemical Engineers);(USA)*, *35*(10).

Mukherjee, A. and Kandlikar, S.G., 2005. Numerical simulation of growth of a vapor bubble during flow boiling of water in a microchannel. *Microfluidics and Nanofluidics*, *1*(2), pp.137-145.

Nishikawa, K. and Yamagata, K., 1960. On the correlation of nucleate boiling heat transfer. *International Journal of Heat and Mass Transfer*, *1*(2-3), pp.219-235.

Nukiyama, S., 1966. The maximum and minimum values of the heat Q transmitted from metal to boiling water under atmospheric pressure. *International Journal of Heat and Mass Transfer*, *9*(12), pp.1419-1433.

Ong, R., King, A., Mullins, B., Cooper, T. and Caley, M., 2011. Computational fluid dynamics model of thermal microenvironments of corals. *MODSIM 2011*.

Pandey, V., Biswas, G., Dalal, A. and Welch, S.W., 2018. Bubble lifecycle during heterogeneous nucleate boiling. *Journal of Heat Transfer*, *140*(12), p.121503.

Plesset, M.S. and Zwick, S.A., 1954. The growth of vapor bubbles in superheated liquids. *Journal of applied physics*, *25*(4), pp.493-500.

Pryazhnikov, M.I. and Minakov, A.V., 2017, November. Study of pool boiling of distilled water on SiO2 nanoparticle-coated wire. In *Journal of Physics: Conference Series* (Vol. 925, No. 1, p. 012029). IOP Publishing.

Reimann, M. and Grigull, U., 1975. Wärmeübergang bei freier Konvektion und Filmsieden im kritischen Gebiet von Wasser und Kohlendioxid. *Wärme-und Stoffübertragung*, *8*(4), pp.229-239.

Rohsenow, W.M., 1951. *A method of correlating heat transfer data for surface boiling of liquids*. Cambridge, Mass.: MIT Division of Industrial Cooporation,[1951].

Samkhaniani, N. and Ansari, M.R., 2017A. Numerical simulation of superheated vapor bubble rising in stagnant liquid. *Heat and Mass Transfer*, *53*(9), pp.2885-2899.

Samkhaniani, N. and Ansari, M.R., 2017B. The evaluation of the diffuse interface method for phase change simulations using OpenFOAM. *Heat Transfer—Asian Research*, *46*(8), pp.1173-1203.

Semeria, R. and Martine, B., 1965, June. Paper 3: Calefaction Spots on a Heating Wall: Temperature Distribution and Resorption. In *Proceedings of the Institution of Mechanical Engineers, Conference Proceedings* (Vol. 180, No. 3, pp. 192-205). Sage UK: London, England: SAGE Publications.

Shatto, D.P. and Peterson, G.P., 1999. Pool boiling critical heat flux in reduced gravity. *Journal of heat transfer*, *121*(4), pp.865-873.

Son, G. and Dhir, V.K., 1997. Numerical simulation of saturated film boiling on a horizontal surface. *Journal of heat transfer*, *119*(3), pp.525-533.

Son, G. and Dhir, V.K., 2008. Numerical simulation of nucleate boiling on a horizontal surface at high heat fluxes. *International Journal of heat and Mass transfer*, *51*(9-10), pp.2566-2582.

Sugawara, S. and Miyamoto, Y., 1990. FIDAS: Detailed subchannel analysis code based on the three-fluid and three-field model. *Nuclear Engineering and Design*, *120*(2-3), pp.147-161.

Sugawara, S., Sakai, T., Watanabe, K. and Rummens, H.E.C., 1991. Subchannel analysis by the FIDAS code based on the three-fluid model. *Nuclear engineering and design*, *132*(2), pp.253-264.

Tanasawa, I., 1991. Advances in condensation heat transfer. In *Advances in heat transfer* (Vol. 21, pp. 55-139). Elsevier.

Tien, C.L., 1962. A hydrodynamic model for nucleate pool boiling. *International Journal of Heat and Mass Transfer*, *5*(6), pp.533-540.

Tokura, I., Hanaoka, Y., Suzuki, H., Hirata, H. and Yoneta, M., 1994. An experimental study of subcooled boiling from wires in micro-gravity. In *International Symposium on Space Technology and Science, 19 th, Yokohama, Japan* (pp. 629-633).

Tong, L.S., 2018. *Boiling heat transfer and two-phase flow*. Routledge.

Van Ouwerkerk, H.J., 1972. Burnout in pool boiling the stability of boiling mechanisms. *International Journal of Heat and Mass Transfer*, *15*(1), pp.25-34.

Valette, M., Pouvreau, J., Bestion, D. and Emonot, P., 2011. Revisiting large break LOCA with the CATHARE-3 three-field model. *Nuclear Engineering and Design*, *241*(11), pp.4487-4496.

Weller, H.G., Tabor, G., Jasak, H. and Fureby, C., 1998. A tensorial approach to computational continuum mechanics using object-oriented techniques. *Computers in physics*, *12*(6), pp.620-631.

Xie, Z., Hewitt, G.F., Pavlidis, D., Salinas, P., Pain, C.C. and Matar, O.K., 2017. Numerical study of three-dimensional droplet impact on a flowing liquid film in annular two-phase flow. *Chemical Engineering Science*, *166*, pp.303-312.

Yang, J., Narayanan, C. and Lakehal, D., 2017. Large Eddy & Interface Simulation (LEIS) of disturbance waves and heat transfer in annular flows. *Nuclear Engineering and Design*, *321*, pp.190-198.

Zuber, N., 1963. Nucleate boiling. The region of isolated bubbles and the similarity with natural convection. *International Journal of Heat and Mass Transfer*, *6*(1), pp.53-78.

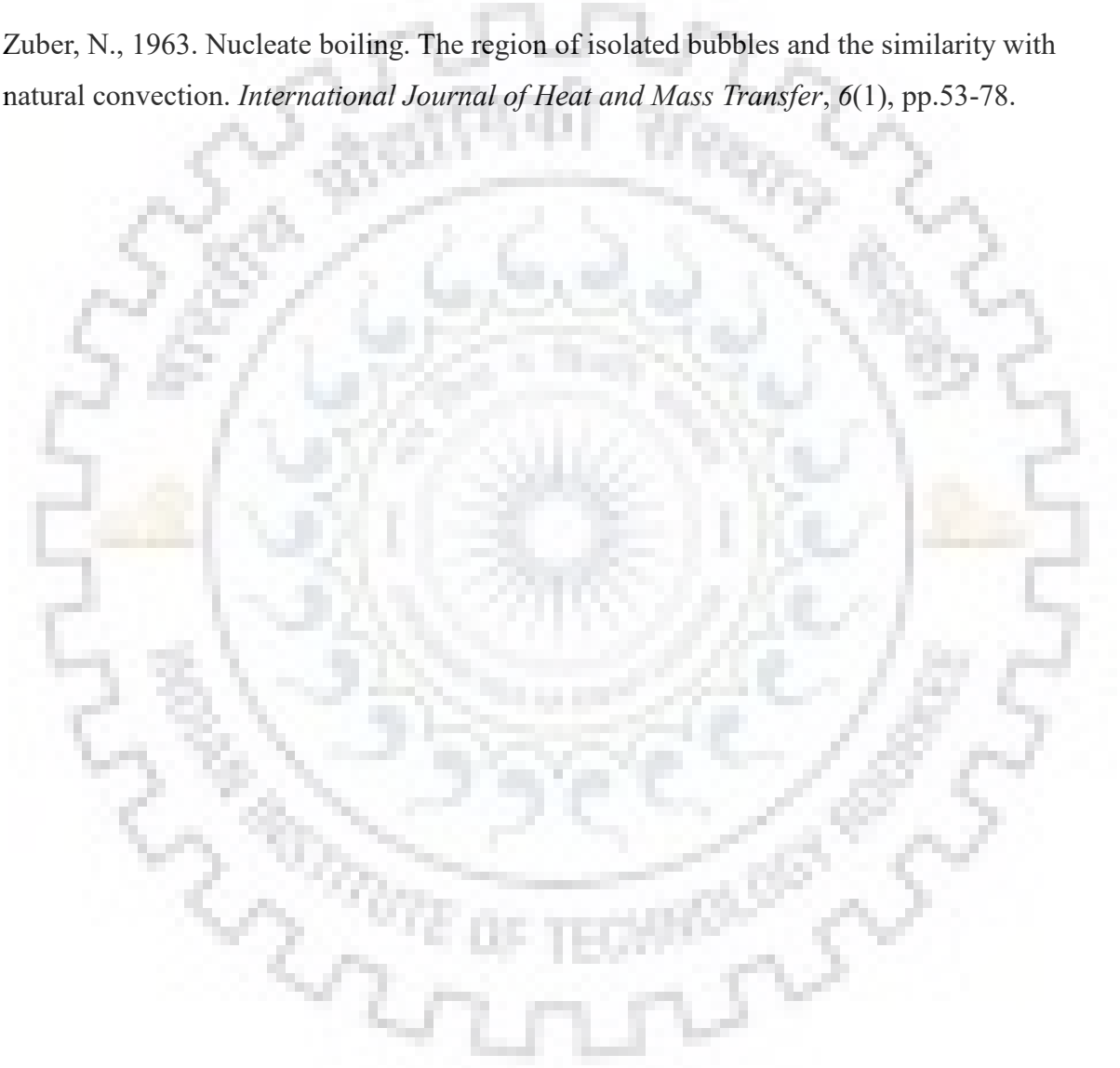

PUBLICATIONS

Relevant to Present Work

Journal

Published

Avik Saha, Arup Kumar Das (2019). "Numerical study of boiling around wires and influence of active or passive neighbours on vapour film dynamics", International Journal of Heat and Mass Transfer 130, 440-454, Impact factor **3.891**

Under Review

Liril D Silvi, **Avik Saha**, Dinesh K. Chandraker, Sumana Ghosh, Arup K. Das, "Numerical analysis of pre-dryout sequences through the route of interfacial evolution in annular gas-liquid two-phase flow with phase change", International Journal of Heat and Mass Transfer

Conference

Avik Saha, Chandan Swaroop Meena, Arup Kumar Das, "Numerical Analysis of Nukiyama's Experiment Around A Thin Wire", 5th International Conference on Computational Methods for Thermal Problems, THERMACOMP2018, July9-11, 2018, Indian Institute of Science, Bangalore, INDIA, 181-184

Avik Saha, Arup Kumar Das, "Boiling around Horizontal Wire in Presence of Neighbouring Active and Passive Wires: A Numerical Study", 7th International and 45th National Conference on Fluid Mechanics and Fluid Power (FMFP) December 10-12, 2018, IIT Bombay, Mumbai, India

Other Publication

Conference

Liril D Silvi, **Avik Saha**, Dinesh K. Chandraker, Sumana Ghosh, Arup K. Das, "Numerical Investigation of Dry-Out Phenomenon in Nuclear Fuel Rod Bundle Assembly", 14th International Conference on Heat Transfer, Fluid Mechanics and Thermodynamics, HEFAT 2019, July 22 – 24, 2019 (Full paper accepted for Oral presentation)